Gravitational Wave Data Analysis for Laser Interferometric Space Antenna

Project No. 2204-1

S.V. Dhurandhar* and Jean-Yves Vinet**

*Inter-University Centre for Astronomy and Astrophysics,
Post Bag No 4, Ganeshkhind,
Pune - 411 007,
INDIA.

**CNRS, Observatoire de la Côte d'Azur
UMR6162–ILGA (Interférométrie Laser pour la Gravitation et l'Astrophysique)
BP 4229 F-06304
Nice Cedex 4
FRANCE.

Contents

Introduction

1.1 Overview of LISA

Breakthroughs in modern technology have made possible the construction of extremely large interferometers both on ground and in space for the detection and observation of gravitational waves (GW). Several ground based detectors are being constructed around the globe; these are the projects, **LIGO**, **VIRGO**, **GEO**, **TAMA** and **AIGO** of building interferometers whose arm-lengths will be of the order of kilometers. These detectors will operate in the high frequency range of GW of $\sim$ 10 Hz to a few kHz. A natural limit occurs on decreasing the lower frequency cut-off of 10 Hz because it is not practical to increase the arm-lengths on ground and also because of the gravity gradient noise which is difficult to eliminate below 10 Hz. Thus, the ground based interferometers will not be sensitive below the limiting frequency of $\sim$ 10 Hz. But on the other hand, there exist in the cosmos, interesting astrophysical GW sources which emit GW below this frequency such as the galactic binaries, massive and super-massive blackhole binaries etc. If we wish to observe these sources, we need to go to lower frequencies. The solution is to build an interferometer in space, where such noises will be absent and allow the detection of GW in the low frequency regime. **LISA** - *Laser Interferometric Space Antenna* - is a proposed mission which will use coherent laser beams exchanged between three identical spacecraft forming a giant (almost) equilateral triangle of side 5×10^6 kilometers to observe and detect low frequency cosmic GW. The ground based detectors and LISA complement each other in the observation of GW in an essential way, analogous to the optical, radio, X-ray, γ-ray etc., observations do for the electromagnetic waves. As these detectors begin to operate, a new era of *Gravitational Astronomy* is on the horizon and a radically different view of the universe is expected to be revealed.

LISA consists of three spacecraft, flying five million kilometers apart, in an equilateral triangle. The space-crafts are maintained drag-free by a complex system of accelerometers and micro-propellers. Each spacecraft will carry two optical assemblies that contain the main optics and a free-falling inertial sensor. The light sent out by a laser in one space-craft is received by the telescope on the distant space-craft. The incoming light from

Figure 1.1: LISA orbital configuration around the Sun, describing a cone with 60° half opening angle. The centroid of the triangle follows an Earth-like orbit trailing 20 degrees behind.

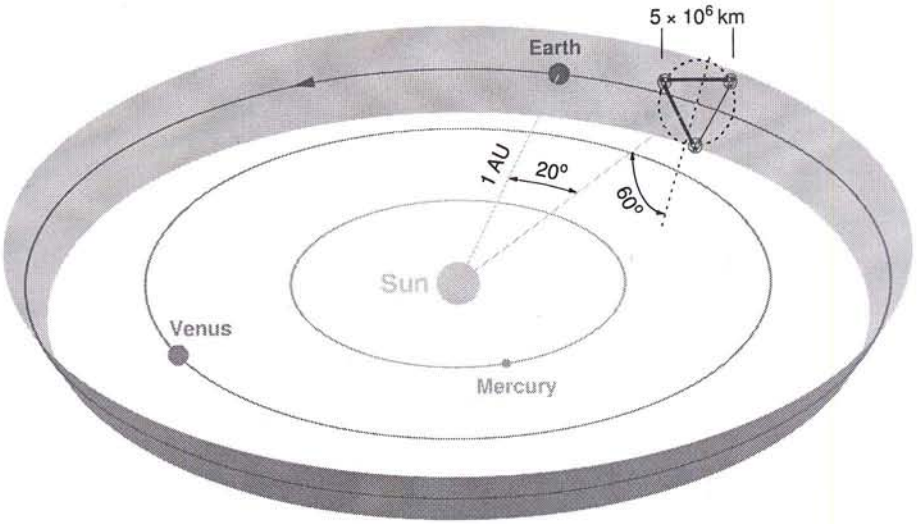

the distant space-craft is then mixed with the in-house laser and the differential phase is recorded. This defines one elementary data stream. There are thus six elementary data streams which are formed by going clockwise and anti-clockwise around the LISA triangle. Suitable combinations of these elementary data streams can be used to optimally extract the GW signal from the instrumental noise. In other words, LISA is basically a giant Michelson interferometer placed in space, with a third arm added to give independent information on the two gravitational wave polarisations, and for redundancy. The distance between the spacecraft - the interferometer arm-length - determines the frequency range in which LISA can make observations; it was carefully chosen to allow for the observation of most of the interesting sources of gravitational radiation. Each space-craft revolves in its own heliocentric orbit. The center of LISA's triangle will follow Earth's orbit around the Sun, trailing 20 degrees behind. It will maintain a distance of 1 AU (astronomical unit) from the Sun, the average distance between the Earth and the Sun (Fig. 1.1). The space-craft rotate in a circle drawn through the vertices of the triangle and the LISA constellation as a whole revolves around the Sun. LISA's operational position was chosen as a compromise between the need to minimise the effects on the spacecraft of changes in the Earth's gravitational field and the need to be close enough to the Earth for easy communication.

The primary objective of the LISA mission is to detect and observe gravitational waves

Figure 1.2: Comparison of frequency range of sources for ground-based and space-based gravitational wave detectors. The sources shown are in two clearly separated regimes: events in the range from 10 Hz to kHz (and only these will be detectable with terrestrial antennas such as LIGO), and a low-frequency regime 0.1 mHz to 0.1 Hz, accessible only with a space based detector such as LISA

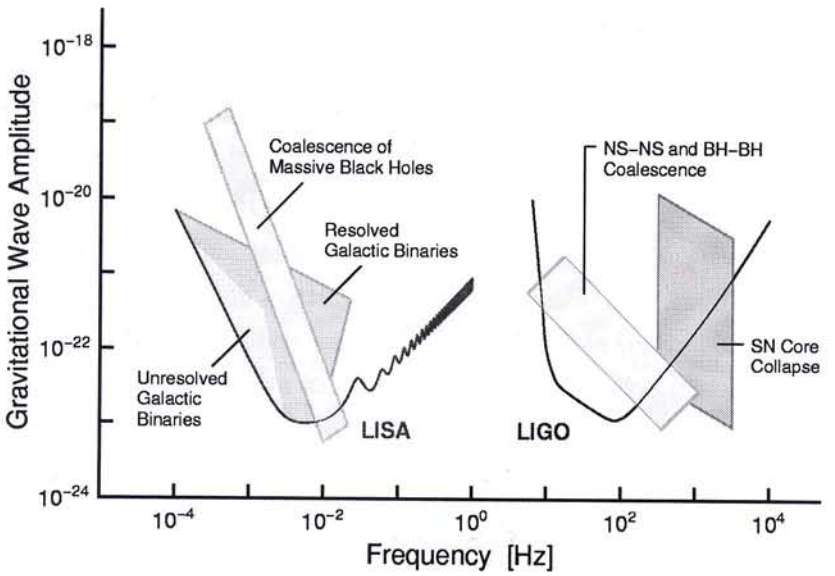

from massive black holes and galactic binaries in the frequency range 0.1 mHz to 0.1 Hz. Ground-based interferometers can observe the bursts of gravitational radiation emitted by galactic binaries during the final stages (minutes and seconds) of coalescence when the frequencies are high and both the amplitudes and frequencies increase quickly with time. At low frequencies, which are only observable in space, the orbital radii of the binary systems are larger and the frequencies are stable over millions of years. Coalescences of massive blackholes and super-massive blackholes are only observable from space. Both ground and space-based detectors will also search for a cosmological background of gravitational waves. Since both kinds of detectors have similar energy sensitivities their different observing frequencies are ideally complementary; their different observing frequency bands will provide crucial spectral information about the source. The astrophysical sources that LISA could observe include galactic binaries, extra-galactic super-massive blackhole binaries and coalescences, stochastic GW background from the early universe (See Fig. 1.2).

Coalescing binaries are one of important sources in the LISA frequency band. These include Galactic and extra galactic stellar mass binaries, massive and super massive blackhole binaries. The frequency of the GW emitted by such a system is twice its orbital frequency. The population synthesis studies indicate a large number of stellar mass binaries in the

frequency range below 2-3 mHz [1, 2]. In the lower frequency range ($\leq$ 1 mHz) there are a large number of such sources in each of the frequency bins. Since GW detectors are omnidirectional, it is impossible to resolve an individual source. These sources effectively form a stochastic GW background referred to as *binary confusion noise*. It has been also proposed that the galactic halo MACHOs such as white dwarfs and blackholes (with mass $\sim 0.5\ M_{\odot}$) can also produce stochastic GW background [3–11]. In a recent work, Tinto *et al.* [12] have used Doppler delayed beams for discriminating the stochastic background from the instrumental noise. The angular resolution of LISA is restricted because it is an all-sky monitoring detector with quadrupole beam pattern, however, the angular resolution can be achieved by the relative amplitude and phases of the two polarisations and Doppler modulation of the beams due to the motion of LISA around the sun [13, 14].

Blackhole binaries are also interesting both from the theoretical and astrophysical point of view. Super massive black hole binaries are strong emitters of GW and these spectacular events can be detectable beyond redshift of $z = 1$. These systems would help to determine the cosmological parameters independently. Such an event would confirm beyond doubt the existence of massive blackholes. From the fundamental physics point of view, the waveforms of signals from such objects at times near coalescence can provide extremely sensitive tests of general relativity for non-Newtonian conditions. Because the phase of the signals over thousands of cycles or longer can be tracked accurately for even fairly weak signals, very minor errors in the predictions of the theory would be detectable. By combining the amplitude, polarisation, and chirp-rate information from LISA's observations, we will be able to deduce the distance to the event. In cosmological terms, the distance measured will be the luminosity distance. The extremely high signal-to-noise ratios that are expected in some cases are remarkable. They mean that LISA will not just detect such events; it will be able to study them in detail. The frequency modulation of the observed signal over a period of 3 months or more will locate the event on the sky, and the amplitude modulation as the plane containing LISA rotates will determine the signal's polarisation.

Just as the cosmic microwave background is left over from the Big Bang, so too should there be a background of gravitational waves. If, just after the Big Bang, gravitational radiation were in thermal equilibrium with the other fields, then today its temperature would have been redshifted to about 0.9 K. This radiation peaks, as does the microwave radiation, at frequencies above 10^{10} Hz. At frequencies accessible to LISA, or indeed even to ground-based detectors, this radiation has negligible amplitude. So if LISA sees a primordial background, it will be non-thermal. Unlike electromagnetic waves, gravitational waves do not interact with matter after a few Planck times after the Big Bang, so they do not thermalize. Their spectrum today, therefore, is simply a redshifted version of the spectrum they formed with, and non-thermal spectra are probably the rule rather than the exception for processes that produce gravitational waves in the early universe.

Figure 1.3: LISA Sensitivity to binary star systems in our Galaxy and blackholes in distant galaxies. The heavy black curve shows the LISA detection threshold, giving the noise amplitude of 5 after a 1-year observation. At frequencies below 3 mHz, binaries in the Galaxy are so numerous that LISA will not resolve them, and they form a noise background; this is also indicated at its expected 5 level. The region where LISA should resolve thousands of binaries that are closer to the Sun than most or that radiate at higher frequencies. The signals expected from two known binaries are indicated by the triangles. Many other systems are known to be observable, but are not indicated here. The shaded area is where signals are expected from coalescences of massive blackholes in galaxies at redshifts of order $z = 1$. These signals are complex and may last less than 1 year, so the region is drawn to indicate the expected signal-to-noise ratio above the LISA instrumental noise. Two signals are indicated, for coalescences of binaries consisting of two 10^6 $M_\odot$ and two 10^4 $M_\odot$ blackholes. These show how sensitive LISA will be, reaching amplitude signal-to-noise ratios exceeding several thousand. While such events may occur only once per year, signals from small black holes falling into larger ones should be very common. Their strength is indicated by giving one example, where a 10 $M_\odot$ blackhole falls into a 10^6 $M_\odot$ black hole at $z = 1$.

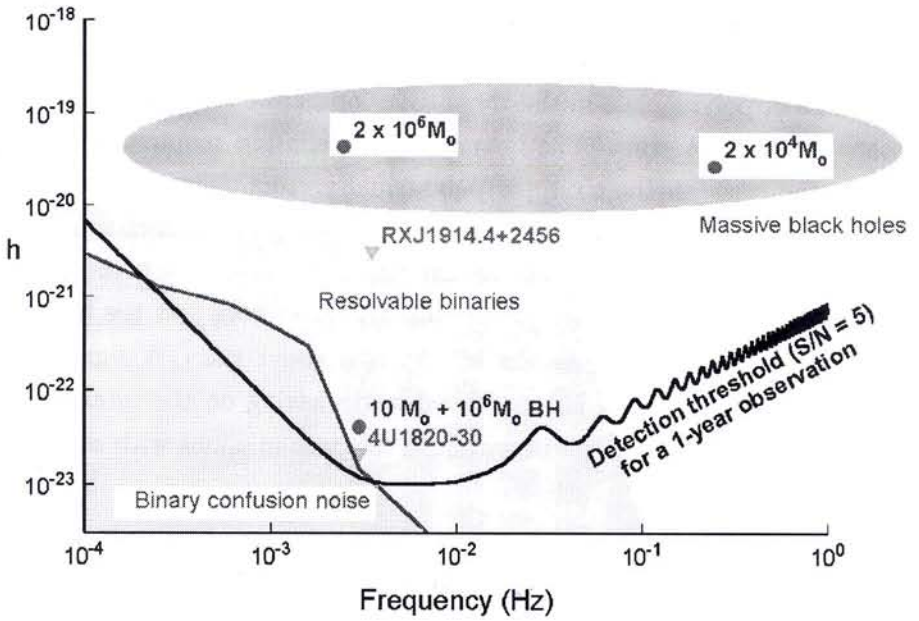

1.2 Laser Phase Noise Cancellation and Optimal Signal Extraction

LISA sensitivity is limited by several noise sources. A major noise source is the laser phase (frequency) noise which arises due to phase fluctuations of the master laser. Amongst the important noise sources, laser phase noise is expected to be several orders of magnitude larger than other noises in the instrument. The current stabilisation schemes estimate this noise to about $\Delta\nu/\nu_0 \simeq 3 \times 10^{-14}/\sqrt{\text{Hz}}$, where ν_0 is the frequency of the laser and $\Delta\nu$ the fluctuation in frequency. If the laser frequency noise can be suppressed then the noise floor is determined by the optical-path noise which fakes fluctuations in the lengths of optical paths and the residual acceleration of proof masses resulting from imperfect shielding of the drag-free system. The noise floor is then at an effective GW strain sensitivity $h \sim 10^{-21}$ or 10^{-22}. Thus, cancelling the laser frequency noise is vital if LISA is to reach the requisite sensitivity. Since it is impossible to maintain equal distances between space-craft, cancellation of laser frequency noise is a non-trivial problem. Several schemes have been proposed to combat this noise. In these schemes, the data streams are combined with appropriate time delays in order to cancel the laser frequency noise. **The main achievement of our work is the development of a systematic and rigorous method using commutative algebra which generates *all* the data combinations cancelling the laser frequency noise.**

The data combinations consist of the six suitably delayed data streams, the delays being integer multiples of the light travel times between spacecraft, which can be conveniently expressed in terms of polynomials in the three delay operators corresponding to the light travel time along the three arms. The laser noise cancellation requirement manifests as 'orthogonality' conditions on the six-tuple polynomial vectors. These data combinations or polynomial vectors form a module over a polynomial ring, well known in the literature, as the *first module of syzygies*. This module has four generators which can reproduce all the data combinations cancelling laser phase noise. Telemetering just the four generators to Earth is sufficient for obtaining all the information about the GW signal. Moreover, the telemetering can be done at a reduced band-width saving on the total cost. Finally, this approach is general in that it can be extended to space-missions with more than three spacecraft.

The access to all data combinations provides the necessary redundancy - different data combinations produce different transfer functions for GW and so certain data combinations could be optimal for given astrophysical source parameters in the sense of maximising signal-to-noise (SNR), detection probability, improving parameter estimates etc.

The foremost application is the maximisation of SNR for a given GW source. This problem is also addressed for an almost monochromatic source. The signal covariance

matrix is computed for binaries whose frequency changes at most adiabatically (the strictly monochromatic case is included) and for which the signal is averaged over polarisations and directions. Here adiabatic means that the signal response, the noise and hence the SNR change imperceptibly even if the GW source changes frequency during the observation time. Thus, even though the results are presented at each fixed frequency, the sources need not be strictly monochromatic, and thus the results apply to a wider class of sources. The signal covariance matrix has the same eigenvectors as those of the noise covariance matrix. Then it is shown that the SNR for any data combination in the module, lies between an upper and a lower bound. The upper and lower bounds of the SNR are functions of frequency which are just the SNR curves of the eigenvectors. The extremisation - both maximisation and minimisation - of SNR is important for different purposes; maximisation is important for the detection and parameter estimation of a GW source, while minimisation is important for the purpose of distinguishing the GW confusion noise from the instrumental noise. The improvement of SNR of the upper-bound over the Michelson combination goes up to 70 %, but only at high frequencies $\gtrsim 5$ mHz. At low frequencies $\lesssim 5$ mHz, both have the same sensitivity. Since the eigenvectors are orthogonal - orthogonality defined in terms of the scalar product given by the noise covariance matrix - they are statistically independent observables. Thus the sum of the squares of the eigenvectors produces a 'network' statistic whose SNR is improved by a factor between $\sqrt{2}$ and $\sqrt{3}$ over the maximum of SNRs of the individual eigenvectors. The improvement over the Michelson combination is about 40 % at low frequencies $\lesssim 3$ mHz and rises above 100 % at high frequencies.

The second application is *optimally* tracking a GW source fixed on the celestial sphere in the barycentric frame. Since the orientation of LISA will change during the observational period, the antenna pattern for any given data combination will change with time, which means that, even if at a given time a particular data combination yields the highest SNR, it will not remain optimal at other times. The basic idea is to continuously *switch* the data combinations so that the SNR at each moment remains maximum. This problem can be conveniently cast in terms of the formalism developed. Here too one can combine outputs from independent data combinations to form a 'network' statistic which can yield higher SNR than any one single data combination.

The following are the salient achievements of our work:

1. **We have given a general method based on commutative algebra for generating data combinations for cancelling laser phase noise in LISA:**

   (i) **The method can be applied to more general configurations,** *eg.* **LISA follow-on missions with more than three spacecraft. In fact the plan is to have four spacecraft in case of one of them fails.**

   (ii) **The mathematical theorems guarantee that** *ALL* **such data combinations are generated from a set of (four) generators.**

2. **Only four data streams (four generators) need to be telemetered to the earth instead of the six data streams.**

3. **The data needs to be sampled at lower rate; laser noise of higher frequency** (~ 30 **Hz**$/\sqrt{\text{Hz}}$) **is eliminated, and the sampling rate is governed by the highest detectable GW frequency 1 Hz. This and the previous point implies** *saving in the band-width* **while telemetering the data to earth.**

4. **This formulation allows simple expressions/notations which is important for numerical coding.**

5. **The method can be extended in a straight forward way for bench motion noise, Ultra Stable Oscillator (USO) noise. The cancellation of USO noise is easily apparent from our formalism.**

6. **The SNR can be maximised for monochromatic sources by diagonalising the noise covariance matrix.**

7. **LISA can be viewed as a network of independent detectors. One can square and add the outputs to yield higher SNR - factor of** $\sqrt{2}$ **or** $\sqrt{3}$ **depending on the mode of operation.**

8. **The combinations can be switched optimally when tracking a source. We find that the SNR can be improved upto 60% because of the optimal tracking.**

Time-Delay Interferometery and Noise Cancellation Schemes

In ground based detectors the arms are chosen to be of equal length so that the laser light experiences identical delay in each arm of the interferometer. This arrangement precisely cancels the laser frequency/phase noise at the photodetector. This cancellation of noise is crucial since the raw laser noise is orders of magnitude larger than other noises in the interferometer. The required sensitivity of the instrument can thus only be achieved by near exact cancellation of the laser frequency noise. However, in LISA it is impossible to achieve equal distances between spacecraft and the laser noise cannot be cancelled in an obvious manner. In LISA, six data streams arise from the exchange of laser beams between the three spacecraft - it is not possible to bounce laser beams between different spacecraft, as is done in ground based detectors; a scheme analogous to the RF transponder scheme is used as was done in the early experiments for detecting GW by Doppler tracking a spacecraft from Earth. Several schemes, some quite elaborate, have been proposed [16,17] which combine the recorded data by suitable time-delays corresponding to the three arm-lengths of the giant triangular interferometer. These schemes have data combinations of six or at most eight data points which give respectively a six and eight pulse response of GW and also show how other data combinations can be obtained by linear superposition. Here we present a *systematic method* based on modules over polynomial rings, which not only reproduces the previously obtained results, but guarantees *all* the data combinations which cancel the laser noise. The data combinations in the case of laser frequency noise consist of the six suitably delayed data streams, the delays being integer multiples of the light travel times between spacecraft, which can be conveniently expressed in terms of polynomials in the three delay operators E_1, E_2, E_3 corresponding to the light travel time along the three arms. The laser noise cancellation condition puts three constraints on the six polynomials of the delay operators corresponding to the six data streams. The problem therefore consists of finding six tuples of polynomials which satisfy the laser noise

cancellation constraints. These polynomial tuples form a module[1] called in the literature, the *module of syzygies*. A brief discussion on rings and modules is included in Appendix A. There exist standard methods for obtaining the module, by that we mean, methods for obtaining the generators of the module so that the linear combinations of the generators generate the entire module. Three constraints on six tuples of polynomials do not lead to three generators as naive reasoning might suggest. Here we are dealing with modules rather than vector spaces and the rules are different. The procedure first consists of obtaining a Groebner basis for the ideal generated by the coefficients appearing in the constraints. This ideal is in the polynomial ring in E_1, E_2, E_3 over the domain of rational numbers (or integers if one gets rid of the denominators). To obtain the Groebner basis for the ideal, one may use the Buchberger algorithm or use a package such as Mathematica. From the Groebner basis there is a standard way to obtain a generating set for the required module. All of this procedure has been described in the literature [18, 19]. We thus obtain seven generators for the module. However, the method does not guarantee a minimal set and we find that a generating set of 4 polynomial six tuples suffice to generate the required module. Alternatively, we can obtain generating sets by using the software Macaulay 2. It gives us a Groebner basis for the module consisting of five generators and another generating set consisting of six elements. The importance of obtaining more data combinations is evident: they provide the necessary redundancy - different data combinations produce different transfer functions for GW and so specific data combinations could be optimal for given astrophysical source parameters in the context of maximising SNR, detection probability, improving parameter estimates etc.

The scheme we have described above can also be extended in a straight forward way to include optical bench motions and the USO noise. In case of optical bench motion noise cancellation twelve Doppler streams of data are needed and we can apply the above scheme to cancel the noise due to optical bench drift and laser frequency noise. The six extra streams can be combined by subtracting one stream from the other to obtain three streams in which the frequency shifts in the optical fibers are cancelled. Thus we have only nine streams to contend with and now the module consists of nine tuples of polynomials on which six linear constraints are imposed. We show that the problem can be solved in the terms of the previous one where the three extra polynomials are written in terms of the six tuple polynomials which are solutions to the laser frequency noise cancellation problem. Thus the solution to the first problem extends easily to the second. Likewise we require six more data streams - 18 data streams in all - at a side band frequency in order to also cancel the USO noise in addition to the laser frequency and optical bench motion noises.

[1] A module is an abelian group over a *ring* as contrasted with a vector space which is an abelian group over a field. The scalars form a ring and just like in a vector space, scalar multiplication is defined. However, in a ring the multiplicative inverses do not exist in general for the elements, which makes all the difference!

Our scheme can be easily extended to cancel the USO noise.

2.1 Time-delayed Data

We label the spacecraft as 1,2 and 3. Let L_1, L_2, L_3 be the lengths of the arms (sides of the triangle) where L_3 is the distance between spacecraft 1 and 2; and so on by cyclic rotation of indices (see figure 2.4). Each spacecraft has a laser which is

- used to send beams to the other two spacecraft, and,
- used as a local oscillator to produce a beat signal with the incoming beams from the other two spacecraft.

The data are recorded as *fractional Doppler shifts*. These fractional Doppler shifts can occur due to the GW signal and the noise. Here we will be concerned with the laser frequency noise only. More precisely, if ν_0 is the central frequency of the laser and the frequency fluctuation of the laser on spacecraft i at time t is $\Delta\nu_i(t)$, then the fractional frequency fluctuation $C_i(t)$ is given by,

$$C_i(t) = \frac{\Delta\nu_i(t)}{\nu_0}. \tag{2.1}$$

The six streams of Doppler data are obtained from the $C_i(t)$ by combining them suitably with their time delayed copies, where the time delays are just the light travel times between the three spacecraft. We adopt the following notation for the six streams: we divide the six streams into two sets U^i and V^i where, $i = 1, 2, 3$ of three streams each. U^i and V^i can be regarded as 3 component vectors $\mathbf{U}$ and $\mathbf{V}$ respectively. Also we denote the time-delayed data in arm k, $k = 1, 2, 3$, by the shift operator E_k whose action on a function $f(t)$ is described by the equation:

$$E_k f(t) = f(t - L_k), \tag{2.2}$$

where we have chosen units in which the speed of light is unity. The six streams with terms containing *only* the laser frequency noise are:

$$\begin{aligned}
U^1 &= E_2C_3 - C_1, \\
U^2 &= E_3C_1 - C_2, \\
U^3 &= E_1C_2 - C_3, \\
V^1 &= C_1 - E_3C_2, \\
V^2 &= C_2 - E_1C_3, \\
V^3 &= C_3 - E_2C_1.
\end{aligned} \tag{2.3}$$

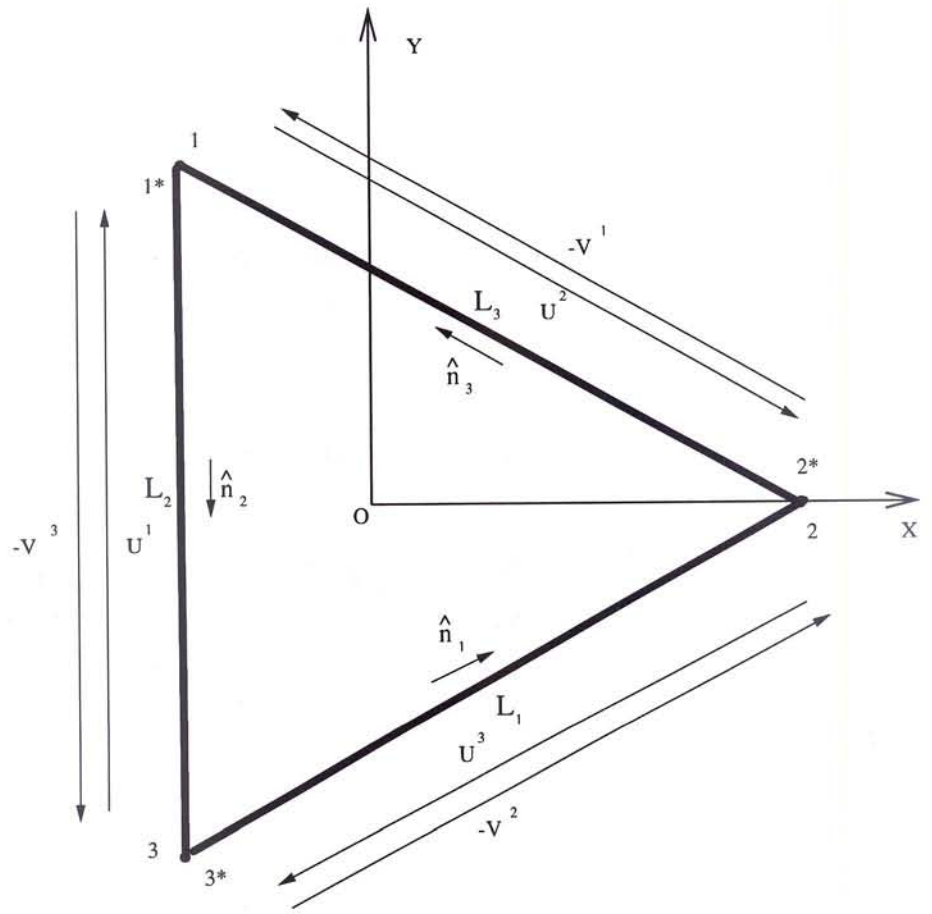

Figure 2.4: LISA Geometry: The LISA constellation consist of three spacecraft each carrying two optical bench systems i and $i^*, i = 1, 2, 3$. They exchange six laser beams which are represented by $U^i$and V^i in the figure. The noise cancellation data combinations are obtained by appropriately delaying these six beams across the length of arms L_i.

Thus explicitly we have, $U^1(t) = C_3(t - L_2) - C_1(t)$ etc. $U^1(t)$ is the data stream obtained by beating the laser beam transmitted by spacecraft 3 to spacecraft 1 measured at time t at spacecraft 1; and so on by cyclic rotation. Similarly $-V^1(t) = C_2(t - L_3) - C_1(t)$ is the laser beam emitted by spacecraft 2 and received and beaten with the laser at spacecraft 1 at time t. If we label the spacecraft in a counter-clockwise (positive sense) fashion, then the beams U^i travel in the positive sense while the beams V^i travel in the negative sense. Note that we have excluded intentionally from the beams additional frequency fluctuations due to other noises such as, optical-path noise, proof-mass noise etc, and the GW signal. Since our immediate goal is to cancel the laser frequency noise we have only kept the terms in the data streams relevant to the laser frequency noise. Combining the streams for cancelling the laser frequency noise will introduce transfer functions for the other noises and the GW

signal. This is important and will be discussed subsequently in the report.

The goal of the analysis is to add suitably delayed beams together so that the laser frequency noise terms add up to zero. This amounts to seeking data combinations which cancel the laser frequency noise. In the notation/formalism that we have invoked, the delay is obtained by applying the operators E_k to the beams U^i and V^i. A delay of $k_1L_1 + k_2L_2 + k_3L_3$ is represented by the operator $E_1^{k_1}E_2^{k_2}E_3^{k_3}$ acting on the data, where k_1, k_2 and k_3 are integers. In general a polynomial in E_k, which is a polynomial in three variables, applied to say U^1 combines the same data stream $U^1(t)$ with different time-delays of the form $k_1L_1 + k_2L_2 + k_3L_3$. This notation conveniently rephrases the problem. One must find six polynomials say $p_i(E_1, E_2, E_3)$, $q_i(E_1, E_2, E_3)$, $i = 1, 2, 3$ such that:

$$\sum_{i=1}^{3} p_i V^i + q_i U^i = 0. \tag{2.4}$$

Cancellation of the laser noise is implicit in the above equation.

2.2 The Difference Equation for Shift Operators

It is convenient to express Eq. (2.3) in matrix form. This allows us to obtain a matrix operator equation whose solutions are $\mathbf{p}$ and $\mathbf{q}$ where we have now written p^i and q^i as column vectors. We can similarly express U^i, V^i, C^i as column vectors $\mathbf{U}, \mathbf{V}, \mathbf{C}$ respectively. In matrix form Eq. (2.3) become:

$$\mathbf{V} = \mu^T\ \mathbf{C}, \qquad \mathbf{U} = -\mu\ \mathbf{C}, \tag{2.5}$$

where, μ is a 3×3 matrix given by,

$$\mu = \begin{pmatrix} 1 & 0 & -E_2 \\ -E_3 & 1 & 0 \\ 0 & -E_1 & 1 \end{pmatrix}. \tag{2.6}$$

The exponent 'T' represents the transpose of the matrix. The Eq. (2.4) becomes:

$$(\mu\mathbf{p} - \mu^T\mathbf{q})^T\ \mathbf{C} = 0\,. \tag{2.7}$$

where we have taken care to put $\mathbf{C}$ on the right of the operators. Since the above equation must be satisfied for arbitrary 'data' $\mathbf{C}$, we obtain a matrix equation for the shift operators:

$$\mu\mathbf{p} = \mu^T\mathbf{q}\,. \tag{2.8}$$

The solutions to Eq. (2.8) are $\mathbf{p}, \mathbf{q}$ which are column vectors of polynomials in the shift operators E_k. Note that since the E_k are just shift operators, they commute, so the order

in writing these operators is unimportant. In mathematical terms, the polynomials form a commutative ring.

We can formally solve for $\mathbf{p}$ since the matrix μ is invertible. However, $\det \mu = 1 - E_1E_2E_3$ appears in the denominator on the R.H.S., which leads to the division by polynomials in E_k. This may seem hard to interpret. But we can pull this factor to the L. H. S. to 'rationalise' the expressions. Then we obtain,

$$\Delta \mathbf{p} = \mathbf{A}\ \mathbf{q}, \tag{2.9}$$

where $\mathbf{A} = \mu_{adj}\mu^T$ and μ_{adj} is the adjoint of μ. The operator $\Delta = 1 - E_1E_2E_3$ is the usual difference operator that appears in finite differences and difference equations. The quantity $E_1E_2E_3$ plays a central role in determining the natural time-step for the problem, namely, $s = L_1 + L_2 + L_3$; which is nothing but the light travel time around the perimeter of the LISA triangle. Δ is just the difference corresponding to this time-step.

Explicitly, using (2.6) the matrix $\mathbf{A}$ is given by:

$$\mathbf{A} = \begin{pmatrix} 1 - E_2^2 & E_1E_2 - E_3 & E_2(1 - E_1^2) \\ (1 - E_2^2)E_3 & 1 - E_3^2 & E_2E_3 - E_1 \\ E_3E_1 - E_2 & E_1(1 - E_3^2) & 1 - E_1^2 \end{pmatrix}. \tag{2.10}$$

The equations display a cyclic symmetry in the indices $1, 2, 3$ which is also apparent in the matrix $\mathbf{A}$. The cyclic symmetry results from the nature of the problem since we are free to choose the labelling of the three space-crafts. In the matrix $\mathbf{A}$ we must also change the rows/columns consistently performing the cyclic change of the indices. The cyclic symmetry is further carried over to the solutions $(\mathbf{p}, \mathbf{q})$.

The integration of the Eq. (2.9) can be carried out in time-steps of s. The integration is immediate if we operate the Eq. (2.9) on $\mathbf{V}$. We first need to take the transpose of Eq. (2.9) and then operate on $\mathbf{V}$. We then obtain:

$$\begin{aligned} \Delta \mathbf{p}^T\mathbf{V} &= \mathbf{q}^T\mathbf{A}^T\ \mathbf{V} \\ &= \mathbf{q}^T(\mu_{adj}\mu^T)^T\ \mathbf{V} \\ &= \mathbf{q}^T\mu\Delta\ \mathbf{C} \\ &= -\Delta\mathbf{q}^T\ \mathbf{U}, \end{aligned} \tag{2.11}$$

which gives,

$$\Delta(\mathbf{p}^T\ \mathbf{V} + \mathbf{q}^T\ \mathbf{U}) = 0. \tag{2.12}$$

This equation immediately integrates to,

$$(\mathbf{p}^T\ \mathbf{V} + \mathbf{q}^T\ \mathbf{U})(t + ns) = (\mathbf{p}^T\ \mathbf{V} + \mathbf{q}^T\ \mathbf{U})(t), \tag{2.13}$$

where n is an integer. If we arbitrarily set $t = 0$ and if $(\mathbf{p}^T\ \mathbf{V} + \mathbf{q}^T\ \mathbf{U})(0) = 0$, then $(\mathbf{p}^T\ \mathbf{V} + \mathbf{q}^T\ \mathbf{U})(ns) = 0$.

It is not clear to us, how the above solution would be useful physically, but we present it as an interesting outcome. However, the main problem is of seeking solutions $(\mathbf{p}, \mathbf{q})$ to Eq. (2.8). This problem and its solution we discuss in the next section.

2.3 The Modules of Syzygies

Several solutions have been exhibited in [16, 17] to Eq. (2.8). The solutions have the characteristic property that the $\det \mu$ cancels on both sides leading to polynomial vectors $\mathbf{p}$ and $\mathbf{q}$. We reproduce here the solutions obtained in previous works. The solution ζ is given by $\mathbf{p}^T = \mathbf{q}^T = (E_1, E_2, E_3)$. The solution α is described by $\mathbf{p}^T = (1, E_3, E_1E_3)$ and $\mathbf{q}^T = (1, E_1E_2, E_2)$. The solutions β and γ are obtained from α by cyclically permuting the indices of $E_k, \mathbf{p}$ and $\mathbf{q}$. These solutions as realised in earlier works are important, because they consist of polynomials with lowest possible degrees and thus are simple. Other solutions containing higher degree polynomials can be generated conveniently from these solutions. Linear combinations of these solutions are also solutions to the given system of equations. But it is not clear that this procedure generates all the solutions. In particular, ζ cannot be generated from the set α, β and γ, where generating a data combination means writing it as a linear combination of the elements belonging to the generating set.

The basic reason, as mentioned earlier, is that we do not have a vector space here. Three independent constraints on a six tuple do not produce a space which is necessarily generated by three basis elements. This conclusion would follow if the solutions formed a vector space but they do not. The polynomial six-tuple $\mathbf{p}, \mathbf{q}$ can be multiplied by polynomials in E_1, E_2, E_3 (scalars) which do not form a field. So that the inverse in general does not exist within the ring of polynomials. We therefore have a module over the ring of polynomials in the three variables E_1, E_2, E_3.

In this section we present the general methodology for obtaining the solutions to (2.8). The method is illustrated by applying it to equations (2.8). In the next subsection we consider the more general problem of optical bench motion and the USO noise.

2.3.1 Cancellation of Laser Frequency Noise

There are three linear constraints on the polynomials given by the equations (2.8). Since the equations are linear the solutions space is a submodule of the module of six-tuples of polynomials. The module of six-tuples is a free module, i.e. it has six basis elements that not only generate the module but are linearly independent. A natural choice of the basis is $f_i = (0, ..., 1, ..., 0)$ with 1 in the i-th place and 0 everywhere else; i runs from 1 to 6. The definitions of generation (spanning) and linear independence are the same as that for vector spaces. A free module is essentially like a vector space. But our interest lies in its

submodule which need not be free and need not have just three generators as it would seem if we were dealing with vector spaces.

The problem at hand is of finding the generators of this submodule i.e. any element of the module should be expressible as a linear combination of the generating set. In this way the generators are capable of spanning the full module or generating the module. We examine the Eq. (2.8) explicitly componentwise:

$$\begin{aligned} p_1 - q_1 + E_3 q_2 - E_2 p_3 &= 0, \\ p_2 - q_2 + E_1 q_3 - E_3 p_1 &= 0, \\ p_3 - q_3 + E_2 q_1 - E_1 p_2 &= 0. \end{aligned} \tag{2.14}$$

The first step is to use Gaussian elimination to obtain p_1 and p_2 in terms of p_3, q_1, q_2, q_3. We then obtain:

$$\begin{aligned} p_1 &= q_1 - E_3 q_2 + E_2 p_3, \\ p_2 &= q_2 - E_1 q_3 + E_3 p_1 \\ &= E_3 q_1 + (1 - E_3^2) q_2 - E_1 q_3 + E_2 E_3 p_3, \end{aligned} \tag{2.15}$$

and then substitute these values in the third equation to obtain a linear implicit relation between p_3, q_1, q_2, q_3. We then have:

$$(E_1 E_2 E_3 - 1) p_3 + (E_1 E_3 - E_2) q_1 + E_1 (1 - E_3^2) q_2 + (1 - E_1^2) q_3 = 0. \tag{2.16}$$

Obtaining solutions to Eq. (2.16) amounts to solving the problem since the the remaining polynomials p_1, p_2 have been expressed in terms of p_3, q_1, q_2, q_3 in (2.15).

We will assume that the polynomials have rational coefficients *i.e* the coefficients belong to $\mathcal{Q}$ the field of the rational numbers. The set of polynomials form a ring - the polynomial ring in three variables which we denote by $\mathcal{R} = \mathcal{Q}[E_1, E_2, E_3]$. The polynomial vector $(p_3, q_1, q_2, q_3) \in \mathcal{R}^4$. The set of solutions to (2.16) is just the *kernel* of the homomorphism $\varphi : \mathcal{R}^4 \to \mathcal{R}$ where the polynomial vector (p_3, q_1, q_2, q_3) is mapped to the polynomial $(E_1 E_2 E_3 - 1) p_3 + (E_1 E_3 - E_2) q_1 + E_1 (1 - E_3^2) q_2 + (1 - E_1^2) q_3$. Thus the solution space $ker\varphi$ is a submodule of $\mathcal{R}^4$. It is called the *module of syzygies* in the literature. The generators of this module can be obtained from standard methods available in the literature. We briefly outline the method given in the books by Becker et al. [18] and Kreuzer and Robbiano [19] below. The details have been included in the appendix B.

2.3.2 Groebner Basis

The first step is to obtain the Groebner basis for the ideal $\mathcal{U}$ generated by the coefficients in Eq. (2.16):

$$u_1 = E_1 E_2 E_3 - 1, \quad u_2 = E_1 E_3 - E_2, \quad u_3 = E_1 (1 - E_3^2), \quad u_4 = 1 - E_1^2. \tag{2.17}$$

The ideal $\mathcal{U}$ consists of linear combinations of the form $\sum v_i u_i$ where v_i, $i = 1, ..., 4$ are polynomials in the ring $\mathcal{R}$. There can be several sets of generators for $\mathcal{U}$. A Groebner basis is a set of generators which is 'small' in a specific sense.

There are several ways to look at the theory of Groebner basis. One way is, suppose we are given polynomials $g_1, g_2, ..., g_m$ in one variable over say $\mathcal{Q}$ and we would like to know whether another polynomial f belongs to the ideal generated by the g's. A good way to decide the issue would be to first compute the gcd (greatest common divisor) g of $g_1, g_2, ..., g_m$ and check whether f is a multiple of g. One can achieve this by doing the long division of f by g and checking whether the remainder is zero. All this is possible because $\mathcal{Q}[x]$ is a Euclidean domain and also a principle ideal domain (PID) wherein any ideal is generated by a single element. Therefore we have essentially just one polynomial - the gcd - which generates the ideal generated by $g_1, g_2, \ldots, g_m$. The ring of integers or the ring of polynomials in one variable over any field are examples of PIDs whose ideals are generated by single elements. However, when we consider more general rings (not PIDs) like the one we are dealing with here, we do not have a single gcd but a set of several polynomials which generates an ideal in general. A Groebner basis of an ideal can be thought of as a generalisation of the gcd. In the univariate case, the Groebner basis reduces to the gcd.

Groebner basis theory generalises these ideas to multivariate polynomials which are neither Euclidean rings nor PIDs. Since there is in general not a single generator for an ideal, Groebner basis theory comes up with the idea of dividing a polynomial with a *set* of polynomials, the set of generators of the ideal, so that by successive divisions by the polynomials in this generating set of the given polynomial, the remainder becomes zero. Clearly, every generating set of polynomials need not possess this property. Those special generating sets that do possess this property (and they exist!) are called Groebner bases. In order for a division to be carried out in a sensible manner, an order must be put on the ring of polynomials, so that the final remainder after every division is strictly smaller than each of the divisors in the generating set. A natural order exists on the ring of integers or on the polynomial ring $\mathcal{Q}(x)$; the degree of the polynomial decides the order in $\mathcal{Q}(x)$. However, even for polynomials in two variables there is no natural order apriori (Is $x^2 + y$ greater or smaller than $x + y^2$?). But one can, by hand as it were, put an order on such a ring by saying $x >> y$, where $>>$ is an order, called the lexicographical order. We follow this type of order, $E_1 >> E_2 >> E_3$ and ordering polynomials by considering their highest degree terms. It is possible to put different orderings on a given ring which then produce different Groebner bases. Clearly, a Groebner basis must have 'small' elements so that division is possible and every element of the ideal when divided by the Groebner basis elements leaves zero remainder, *i.e.* every element modulo the Groebner basis reduces to zero.

In the literature, there exists a well-known algorithm called the the Buchberger algo-

rithm which may be used to obtain the Groebner basis for a given set of polynomials in the ring. So a Groebner basis of $\mathcal{U}$ can be obtained from the generators u_i given in Eq. (2.17) using this algorithm. It is essentially again a generalisation of the usual long division that we perform on univariate polynomials. More conveniently, we prefer to use the wellknown 'Mathematica' package. Mathematica yields a 3 element Groebner basis $\mathcal{G}$ for $\mathcal{U}$:

$$\mathcal{G} = \{E_3^2 - 1, E_2^2 - 1, E_1 - E_2 E_3\}\,. \tag{2.18}$$

One can easily check that all the u_i of Eq. (2.17) are linear combinations of the polynomials in $\mathcal{G}$ and hence $\mathcal{G}$ generates $\mathcal{U}$. One also observes that the elements look 'small' in the order mentioned above. However, one can satisfy oneself that $\mathcal{G}$ is a Groebner basis by using the standard methods available in the literature. One method consists of computing the S-polynomials (see Appendix A) for all the pairs of the Groebner basis elements and checking whether these reduce to zero modulo $\mathcal{G}$.

This Groebner basis of the ideal $\mathcal{U}$ is then used to obtain the generators for the module of syzygies.

2.3.3 Generating Set for the Module of Syzygies

The generating set for the module is obtained by further following the procedure in the literature [18, 19]. The details are given in Appendix B, specifically for our case. We obtain 7 generators for the module. These generators do not form a minimal set and there are relations between them; in fact this method does not guarantee a minimum set of generators. These generators can be expressed as linear combinations of $\alpha, \beta, \gamma, \zeta$ and also in terms of $X^{(1)}, X^{(2)}, X^{(3)}, X^{(4)}$ given below in Eq. (2.19). The importance in obtaining the 7 generators is that the standard theorems guarantee that these 7 generators do infact generate the required module. Therefore, from this proven set of generators we can check whether a particular set is infact a generating set. We present several generating sets below:

Alternatively, we may use a software package called *Macaulay 2* which calculates the generators given the the equations (2.14). Using *Macaulay 2*, we obtain six generators. Again, Macaulay's algorithm does not yield a minimal set; we can express the last two generators in terms of the first four. Below we list this smaller set of four generators in the order $X = (p_1, p_2, p_3, q_1, q_2, q_3)$:

$$\begin{aligned}
X^{(1)} &= (E_1E_3 - E_2, 0, E_3^2 - 1, 0, E_2E_3 - E_1, E_3^2 - 1),\\
X^{(2)} &= (E_1, E_2, E_3, E_1, E_2, E_3),\\
X^{(3)} &= (1, E_3, E_1E_3, 1, E_1E_2, E_2),\\
X^{(4)} &= (E_1E_2, 1, E_1, E_3, 1, E_2E_3).
\end{aligned} \tag{2.19}$$

Note that the last three generators are just $X^{(2)} = \zeta, X^{(3)} = \alpha, X^{(4)} = \beta$. But there is an extra generator $X^{(1)}$ needed to generate all the solutions.

Another set of generators which could be useful for further work is a Groebner basis of a module. The concept of a Groebner basis of an ideal can be extended to that of a Groebner basis of a submodule of $(K[x_1, x_2, ..., x_n])^m$ where K is a field, since a module over the polynomial ring can be considered as generalisation of an ideal in a polynomial ring. Just as in the case of an ideal, a Groebner basis for a module is a generating set with special properties. For the module under consideration we obtain a Groebner basis using *Macaulay 2* :

$$\begin{aligned}
G^{(1)} &= (E_1, E_2, E_3, E_1, E_2, E_3), \\
G^{(2)} &= (E_1E_3 - E_2, 0, E_3^2 - 1, 0, E_2E_3 - E_1, E_3^2 - 1), \\
G^{(3)} &= (E_1E_2, 1, E_1, E_3, 1, E_2E_3), \\
G^{(4)} &= (1, E_3, E_1E_3, 1, E_1E_2, E_2), \\
G^{(5)} &= (E_3(E_1^2 - 1), 1 - E_3^2, 0, 0, 1 - E_1^2, E_1(E_3^2 - 1)).
\end{aligned} \tag{2.20}$$

Note that in this Groebner basis $G^{(1)} = \zeta = X^{(2)}, G^{(2)} = X^{(1)}, G^{(3)} = \beta = X^{(4)}, G^{(4)} = \alpha = X^{(3)}$. Only $G^{(5)}$ is the new generator.

Another set of generators are just α, β, γ and ζ. This can be checked using *Macaulay 2* or one can relate α, β, γ and ζ to the generators $X^{(A)}, A = 1, 2, 3, 4$ by polynomial matrices. In Appendix C, we express the 7 generators we obtained following the literature, in terms of α, β, γ and ζ. Also we express α, β, γ and ζ in terms of $X^{(A)}$. This proves that all these sets generate the required module of syzygies.

The question now arises as to which set of generators we should choose which facilitates further analysis. The analysis is simplified if we choose a smaller number of generators. Also we would prefer low degree polynomials to appear in the generators so as to avoid cancellation of leading terms in the polynomials. By these two criteria we may choose, $X^{(A)}$ or $\alpha, \beta, \gamma, \zeta$.

2.4 Cancellation of Noise from Moving Optical Benches

There are two optical benches on each space-craft which have random velocities and are connected by optical fibers. The random velocities of the optical benches and the delay in the optical fibers are measured as further Doppler shifts apart from other noise and the GW signal. Since we are interested in the cancellation of laser frequency noise and motion of the optical benches, we write expressions for the beams containing only these quantities. The Doppler beams will of course contain other effects arising from shot noise, GW signal, motion of proof masses etc., but we will not write them in the expressions for the Doppler data because they are not relevant to the problem we are interested in. We follow the

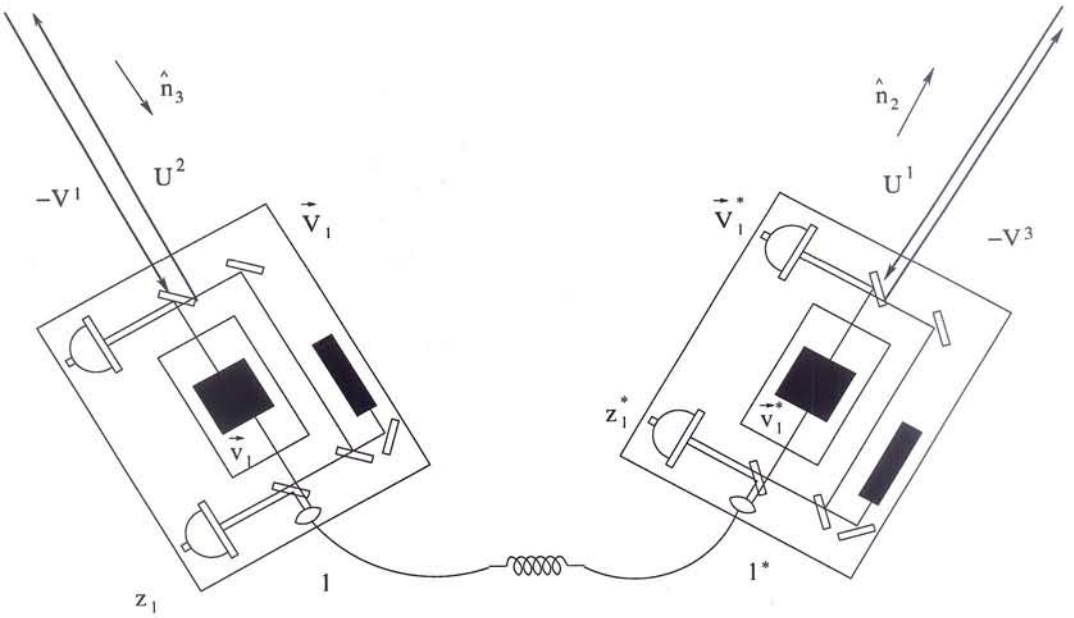

Figure 2.5: Optical bench arrangement in the spacecraft

notations of [16, 17]. The quantities pertaining to the left bench will be unstarred while that for the right bench are starred. There are now twelve Doppler data streams which need to be combined in an appropriate manner in order to cancel the noise from the laser as well as from the motion of the optical benches. The fractional frequency fluctuations of laser on the left optical bench i are denoted by C_i and on the right optical bench i^* by C_i^*, the random velocities of the benches $\mathbf{V}_i, \mathbf{V}_i^*$ and η_i the frequency shifts in the optical fibers connecting the optical benches in space-craft i. We then have the following expressions for the four data streams pertaining to space-craft 1:

$$\begin{aligned} U^1 &= E_2(C_3 - \hat{\mathbf{n}}_2 \cdot \mathbf{V}_3) - (\hat{\mathbf{n}}_2 \cdot \mathbf{V}_1^* + C_1^*), \\ V^1 &= -E_3(C_2^* + \hat{\mathbf{n}}_3 \cdot \mathbf{V}_2^*) + (C_1 - \hat{\mathbf{n}}_3 \cdot \mathbf{V}_1), \\ z_1 &= C_1 - C_1^* + \eta_1 - 2\hat{\mathbf{n}}_3 \cdot \mathbf{V}_1\,, \\ z_1^* &= C_1^* - C_1 + \eta_1 + 2\hat{\mathbf{n}}_2 \cdot \mathbf{V}_1^*\,. \end{aligned} \tag{2.21}$$

The other eight data streams on space crafts 2 and 3 are obtained by cyclic permutations of the indices in the above equations. Here $\hat{\mathbf{n}}_2$ denotes a unit vector in the direction from space-craft 1 to space-craft 3 and the remaining unit vectors $\hat{\mathbf{n}}_3$ and $\hat{\mathbf{n}}_1$ are obtained by cyclically permutating the indices.

We find that the twelve Doppler data streams depend only on the particular combinations $C_1 - \hat{\mathbf{n}}_3 \cdot \mathbf{V}_1$ and $C_1^* + \hat{\mathbf{n}}_2 \cdot \mathbf{V}_1^*$ and their cyclic permutations. We define these

combinations as $\tilde{C}_1$ and $\tilde{C}_1^*$ respectively, i.e.:

$$\begin{aligned} \tilde{C}_1 &= C_1 - \hat{\mathbf{n}}_3 \cdot \mathbf{V}_1 \,, \\ \tilde{C}_1^* &= C_1^* + \hat{\mathbf{n}}_2 \cdot \mathbf{V}_1^* \,, \end{aligned} \tag{2.22}$$

and also their cyclic permutations. Then the expressions for the data streams simplify considerably. We write the expressions for the data streams corresponding to space-craft 1. Others are obtained as before by cyclic permutations:

$$\begin{aligned} U^1 &= E_2\tilde{C}_3 - \tilde{C}_1^* \,, \\ V^1 &= -E_3\tilde{C}_2^* + \tilde{C}_1 \,, \\ Z^1 &= \frac{1}{2}(z_1 - z_1^*) \\ &= \tilde{C}_1 - \tilde{C}_1^* \,. \end{aligned} \tag{2.23}$$

The new variables Z^i have been defined which automatically cancel the η_i. Also we note that the U^i, V^i have the same form as in Eq. (2.3), except that the C_i are replaced by the $\tilde{C}_i$ which account for the motions of the optical benches.

The noise cancellation condition now becomes:

$$p_i V^i + q_i U^i + r_i Z^i = 0 \,, \tag{2.24}$$

where r_i are polynomials in E_1, E_2, E_3. Since the above equations should hold for any $\tilde{C}_i, \tilde{C}_i^*$, we obtain the following equations the polynomials p_i, q_i, r_i must satisfy:

$$\begin{aligned} p_1 + E_3 q_2 + r_1 &= 0 \,, \\ E_2 p_3 + q_1 + r_1 &= 0 \,, \\ p_2 + E_1 q_3 + r_2 &= 0 \,, \\ E_3 p_1 + q_2 + r_2 &= 0 \,, \\ p_3 + E_2 q_1 + r_3 &= 0 \,, \\ E_1 p_2 + q_3 + r_3 &= 0 \,. \end{aligned} \tag{2.25}$$

We now have a nine component polynomial vector. The solutions to Eq. (2.25) form another module of syzygies which is related in a simple way to the module obtained in just laser noise cancellation. Eliminating r_i from Eq. (2.25) we obtain the same equations for p_i and q_i as in (2.14). This enables us to extend the previously obtained generating sets to this module. Thus, thanks to the mapping of $C_i, (C_i^*) \longrightarrow \tilde{C}_i, (\tilde{C}_i^*)$, the two modules are isomorphic. We just state the remaining three entries (r_1, r_2, r_3) of the generating sets keeping the same notation. The first set of 4 generators in the order (r_1, r_2, r_3) are:

$$X^{(1)} = (E_2(1 - E_3^2), E_1(1 - E_3^2), 1 - E_3^2) \,,$$

$$\begin{aligned} X^{(2)} &= -(E_1 + E_2E_3, E_2 + E_1E_3, E_3 + E_1E_2)\,, \\ X^{(3)} &= -(1 + E_1E_2E_3, E_1E_2 + E_3, E_1E_3 + E_2)\,, \\ X^{(4)} &= -(E_1E_2 + E_3, 1 + E_1E_2E_3, E_1 + E_2E_3)\,. \end{aligned} \tag{2.26}$$

In the other generating set, namely, the Groebner basis we need to specify just G_5 since the other elements are in the previous generating set. Thus,

$$G^{(5)} = (0, (E_1^2 - 1)(1 - E_3^2), 0). \tag{2.27}$$

2.5 Ultra Stable Oscillator Noise

One proposed design of LISA envisages having six independent lasers, two on each space-craft having central frequencies ν_i and $\nu_i^*, i = 1, 2, 3$. These frequencies could well differ by several hundred MHz. The outputs of the photodetectors therefore will have a large fringe rate and must be down-converted (heterodyned) to the GW frequency band. For the down-conversion each space-craft comes with an onboard clock - the Ultra Stable Oscillator (USO). We will assume that each USO has a frequency f_i, which brings along with it clock-jitter with frequency fluctuations ξ_i. The frequency fluctuations ξ_i bring in another source of noise - the USO noise. It has been realised recently, that the ultra stable oscillator (USO) is an important source of noise, which could be two or three orders of magnitude above the shot and optical path noise. Thus the USO noise will determine the noise floor if the laser phase noise and the noise due to the motion of the optical benches is cancelled. Suppressing the USO noise is crucial for the data analysis of LISA. One way is to attempt reducing the USO noise in the hardware. However, given our powerful data analysis methods involving commutative algebra, it is possible to tackle this question in the data analysis - that is, look for data combinations which can also suppress the USO noise. Recently Tinto et al [22] have made a case that time-delay interferometric methods may be employed successfully for cancelling the USO noise. Our methods of commutative algebra make it obvious how this noise can be cancelled.

The six data elementary data streams now also include the USO terms. We just mention the data stream U^1:

$$U^1 = (\nu_3 - \nu_1^* - a_{21}f_1) + E_2C_3 - C_1^* - a_{21}\xi_1 + \text{other noise} + \text{GW signal}, \tag{2.28}$$

where a_{21} is a down-conversion factor. We may choose a_{21} such that $\nu_3 - \nu_1^* - a_{21}f_1 = 0$ so that the first term vanishes and we are left with just the USO noise term $U_\xi^1 = -a_{21}\xi_1$. Similarly, the rest of the 5 data streams are given by $V_\xi^1 = -a_{31}\xi_1$ and their cyclic permutations.

Six more data streams - called correction data - obtained at side-band frequencies $\nu_i + f_i$, $\nu_i^* + f_i$ are needed for cancelling the USO noise. Both the main frequency data

as well as the side-band data contain the USO clock-jitter noise. This redundancy in the data is used to eliminate the USO noise. Since just the side-band is used, the module cancelling USO noise is identical (isomorphic) to the laser frequency noise cancellation module. Writing only the USO noise part, we denote these correction data streams by U'^i_ξ, V'^i_ξ. These are given by:

$$U'^1_\xi = E_2\xi_3 - \xi_1 - b_{21}\xi_1, \quad V'^1_\xi = \xi_1 - E_3\xi_2 - b_{31}\xi_1 \tag{2.29}$$

where b_{21} and b_{31} are down-conversion factors for the correction data. The coefficient b_{21} satifies the equation $(\nu_3 + f_3 - (\nu_1^* + f_1) - b_{21}f_1 = 0$ (likewise b_{31} satifies a similar equation). After elementary algebra one finds that the quantity:

$$\Delta U^1 = \frac{U'^1_\xi - U^1_\xi}{f_3} = E_2Q_3 - Q_1, \tag{2.30}$$

where $Q_i = \xi_i/f_i$. ΔU^1 has the same form as in the case of laser frequency noise or optical bench motion noise (See Eq. (2.3) and (2.23)). Similarly,

$$\Delta V^1 = \frac{V'^1_\xi - V^1_\xi}{f_2} = Q_1 - E_3Q_2\,. \tag{2.31}$$

The other such data streams can be obtained from cyclic permutations. This implies that we again obtain the same (isomorphic) module, as in the previous cases. These data streams can be used to eliminate the USO noise. For example, the USO part of the Michelson combination is given by:

$$X_\xi = -a_{21}(1 - E_2^2)f_1Q_1 + a_{31}(1 - E_2^2)f_1Q_1 + a_{32}E_3(1 - E_2^2)f_2Q_2 - a_{23}(1 - E_3^2)E_2f_3Q_3. \tag{2.32}$$

The first term can be cancelled by adding to X_ξ the combination:

$$(-\Delta U^1 + E_2\Delta V^3)a_{21}f_1 = a_{21}f_1(1 - E_2^2)Q_1$$

and so on.

Thus by using identical techniques the USO noise can also be cancelled.

2.6 Conclusion

We have presented a rigorous and systematic procedure for obtaining data combinations which cancel the laser frequency noise based on algebraic geometrical techniques and commutative algebra. The data combinations cancelling the laser noise have the structure of a module called the module of syzygies. The module is over a ring of polynomials in three variables, corresponding to the three time delays along the three arms of the interferometer. Our formalism can be extended in a straightforward way to cancel optical bench motion noise as well as USO noise.

Each of the noise cancelling data combinations have different response to the GW signal. Also, the noises such as acceleration noise of proof-mass and the optical-path noises are not cancelled out in this scheme. In the sections that follow, we compute the GW responses and the transfer functions for the noise for the data combinations in the module.

Detector response and Sensitivity to GW

The ripples produced in the spacetime by the gravitational waves are recorded by LISA as fractional Doppler shifts of the laser frequency. The data will contain the total frequency shift from the various noises and the GW signal. In the previous sections we have found the data combinations of beams cancelling the laser phase noise, optical bench motion noise and USO noise. In following sections we investigate the response of the detector for these data combinations, the transfer functions for the generators and also their linear combinations. The laser phase noise, optical bench motion noise and USO noise is then also cancelled for the linear combinations. However, noises such as the shot noise and the acceleration noise of the proof masses do not cancel out. In the following subsections we set up the coordinate system adapted to the LISA geometry and then go on to compute the response of LISA.

3.1 Parameterisation of the Interferometer

The Figure 2.4 describes the LISA geometry. We choose a coordinate system in which the LISA triangle is at rest. Although this coordinate system is in motion relative to the usual coordinate systems normally encountered, we will find such a system of coordinates convenient for further analysis, such as computing SNR's of monochromatic sources etc.

The unit vector $\hat{w}$ (Fig 3.6) connecting the origin and the source is parameterised by the source angular location $(\theta,\ \phi)$, so that

$$\hat{w} = \begin{pmatrix} \sin\theta\ \cos\phi \\ \sin\theta\ \sin\phi \\ \cos\theta \end{pmatrix}, \tag{3.33}$$

the transverse plane is spanned by the unit transverse vector $\hat{\theta}$ and $\hat{\phi}$, defined by

$$\hat{\theta} = \frac{\partial\hat{w}}{\partial\theta}, \quad \hat{\phi} = \frac{1}{\sin\theta}\frac{\partial\hat{w}}{\partial\phi}. \tag{3.34}$$

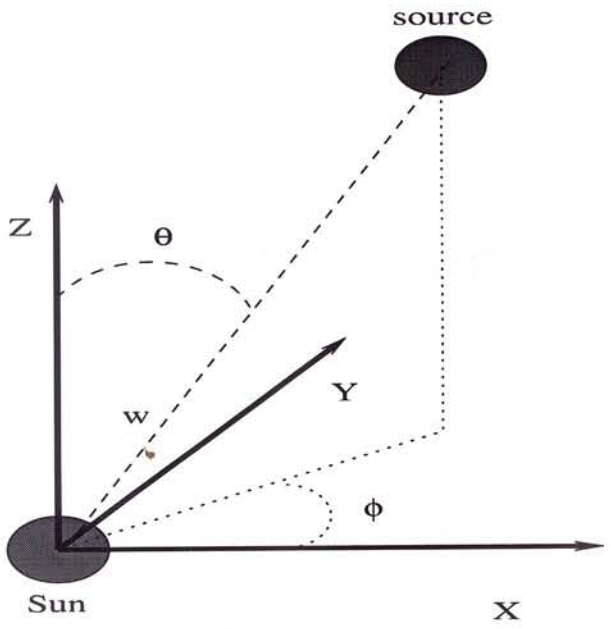

Figure 3.6: Source and detector orientation

As the wave propagates through the LISA triangle, the components of the gravitational perturbation can be written as

$$h_{ij}(t,\vec{r}) \;=\; h_+\left(t-\hat{w}\cdot\vec{r}\right)\left(\theta_i\theta_j-\phi_i\phi_j\right) \;+\; h_\times\left(t-\hat{w}\cdot\vec{r}\right)\left(\theta_i\phi_j+\theta_j\phi_i\right)\,, \tag{3.35}$$

where $h_+(t)$ and $h_\times(t)$ are arbitrary functions describing the two GW amplitudes.

We consider the effect of this perturbation on the light beam travelling between two points A and B. From this we obtain the complete response. Let $\vec{r}_A$ and $\vec{r}_B$ be the position vectors of points A and B respectively (as shown in Fig. (3.7). Then the line element of the spacetime along the beam null ray obeys,

$$0 \;=\; dt^2-dx^2-dy^2-dz^2+h_{ij}dx^idx^j, \tag{3.36}$$

where the i,j run over space indices only. If $\hat{n}$ is the unit vector directed from A to B, we have

$$dx^i \;=\; n^i d\lambda\,, \tag{3.37}$$

where λ is the Euclidean length. The equations (3.36) can be expressed as,

$$0 \;=\; dt^2-d\lambda^2\left[1-h_{ij}n^in^j\right]\,, \tag{3.38}$$

or equivalently

$$d\lambda \;=\; dt\left[1+\frac{1}{2}h\left(t-\hat{w}\cdot\vec{r}\right)\right]\,. \tag{3.39}$$

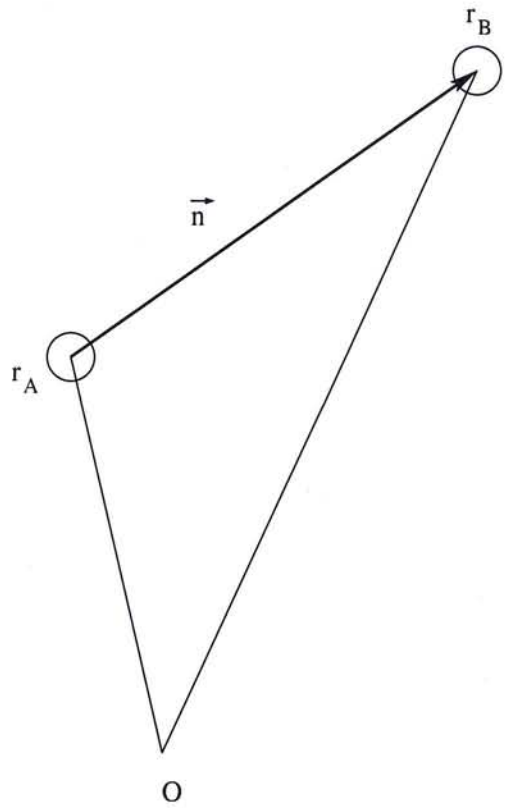

Figure 3.7: Light propagation along single arm

From Eq. (3.35) we get

$$h(t) = h_+(t)\xi_+(\theta,\phi) + h_\times(t)\xi_\times(\theta,\phi)\,, \tag{3.40}$$

$$\begin{cases} \xi_+ = (\hat{\theta}\cdot\hat{n})^2 - (\hat{\phi}\cdot\hat{n})^2 \\ \xi_\times = 2(\hat{\theta}\cdot\hat{n})(\hat{\phi}\cdot\hat{n}) \end{cases} . \tag{3.41}$$

3.2 *h*-Sensitivity of One Arm

We now apply the above analysis to compute the Doppler response of the laser beam along one arm of the LISA detector. Let the beam start at $t = t_0$ from the point $\vec{r}_A$ and travel towards the point $\vec{r}_B$ and reach it at $t = t_1$. Then,

$$\vec{r}(t) = \vec{r}_A + (t - t_0)\hat{n}, \quad \vec{r}(t_1) = \vec{r}_B\,. \tag{3.42}$$

The line element along this path satisfies the equation,

$$d\lambda = dt\left\{1 + \frac{1}{2}h\left[(1 - \hat{w}\cdot\hat{n})t - \hat{w}\cdot\vec{r}_A + t_0\hat{w}\cdot\hat{n}\right]\right\}. \tag{3.43}$$

The global travel time $t_1 - t_0$ is given by the integral :

$$L = t_1 - t_0 + \frac{1}{2}\int_{t_0}^{t_1} h\left[t(1-\hat{w}\cdot\hat{n}) - \hat{w}\cdot\vec{r}_A + t_0\hat{w}\cdot\hat{n}\right] dt\,. \tag{3.44}$$

It is convenient for many purposes to pursue our analysis in the Fourier domain. We Fourier transform the GW amplitude h:

$$h(t) = \int d\Omega\ \tilde{h}(\Omega) exp(-i\Omega t)\,, \tag{3.45}$$

and the travel time can be expressed as,

$$t_1 - t_0 = L - \frac{1}{2}\int d\Omega\tilde{h}(\Omega)\ \int_{t_0}^{t_1} exp\left[-i\Omega\left(1-\hat{w}\cdot\hat{n}\right)t\right] exp\left[i\Omega\hat{w}\cdot\vec{r}_A\right] exp\left[-i\Omega t_0\hat{w}\cdot\hat{n}\right] dt\,. \tag{3.46}$$

In the zeroth order of the integral, we have $t_1 - t_0 = L$, and we obtain:

$$\begin{aligned} t_1 - t_0 &= L - \frac{1}{2}\int d\Omega\tilde{h}(\Omega)\ exp\left(i\Omega\hat{w}\cdot\vec{r}_A\right) exp\left(-i\Omega t_1\right) \\ &\times \frac{exp\left(i\Omega L\hat{w}\cdot\hat{n}\right) - exp(i\Omega L)}{-i\Omega(1-\hat{w}\cdot\hat{n})}\,. \end{aligned} \tag{3.47}$$

The phase change over that time interval is $\Phi = \omega(t_1 - t_0)$, where $\omega = 2\pi\nu_{opt}$ is the optical circular frequency. We can assume that the time t_1 is the current time and t_0 the retarded time, so that the phase is $\Phi(t) = \omega(t - t_0)$:

$$\begin{aligned} \Phi(t) &= \omega L - \frac{\omega}{2(1-\hat{w}\cdot\hat{n})}\int d\Omega\tilde{h}(\Omega)\ exp\left(i\Omega\hat{w}\cdot\vec{r}_A\right) exp\left(-i\Omega t\right) \\ &\times \frac{exp\left(i\Omega L\hat{w}\cdot\hat{n}\right) - exp(i\Omega L)}{-i\Omega}\,. \end{aligned} \tag{3.48}$$

By taking the time derivative, we get the instantaneous frequency,

$$\frac{\delta\nu(t)}{\nu_{opt}} = \frac{1}{\omega}\frac{d\Phi(t)}{dt}\,. \tag{3.49}$$

In the time domain and using $\vec{r}_A + L\hat{n} = \vec{r}_B$ we finally get,

$$\frac{\delta\nu(t)}{\nu_{opt}} = \frac{-1}{2(1-\hat{w}\cdot\hat{n})}\left[h\left(t-\hat{w}\cdot\vec{r}_B\right) - h\left(t-\hat{w}\cdot\vec{r}_A - L\right)\right]. \tag{3.50}$$

In the Fourier domain we may express this result as:

$$\widetilde{\frac{\delta\nu(\Omega)}{\nu_{opt}}} = \frac{\tilde{h}(\Omega)}{2(1-\hat{w}\cdot\hat{n})} exp\left[i\Omega(L+\hat{w}\cdot\vec{r}_A)\right]\left(1 - exp\left[-i\Omega L(1-\hat{w}\cdot\hat{n})\right]\right)\,. \tag{3.51}$$

3.3 *h*-Sensitivity of Elementary Data Streams

In this section we compute the expression for the transfer function for the six elementary streams given in the Eq. (2.3). These data streams are combined with suitable time delays for cancelling laser phase noise. These operations lead to different GW transfer functions for data combinations in the module.

The Doppler shift being expressed in the Fourier domain as,

$$\widetilde{\frac{\delta\nu(\Omega)}{\nu_{opt}}} = \tilde{h}_+(\Omega)F_+(\Omega) + \tilde{h}_\times(\Omega)F_\times(\Omega)\,, \tag{3.52}$$

where $F_{+,\times}(\Omega)$ are transfer functions. We can compute the transfer functions for the combinations U_i, V_i. We just give below $F_{U_1;+,\times}$ and $F_{V_1;+,\times}$; the others are obtained by cyclic permutations:

$$\begin{aligned} F_{U_1;+,\times} &= \frac{e^{i\Omega(\hat{w}\cdot\vec{r}_3+L_2)}}{2\,(1+\hat{w}\cdot\hat{n}_2)}\left(1-e^{-i\Omega L_2(1+\hat{w}\cdot\hat{n}_2)}\right)\xi_{2;+,\times}\,, \\ F_{V_1;+,\times} &= -\frac{e^{i\Omega(\hat{w}\cdot\vec{r}_2+L_3)}}{2\,(1-\hat{w}\cdot\hat{n}_3)}\left(1-e^{-i\Omega L_3(1-\hat{w}\cdot\hat{n}_3)}\right)\xi_{3;+,\times}\,, \end{aligned} \tag{3.53}$$

where,

$$\xi_{i;+} = (\hat{\theta}\cdot\hat{n}_i)^2 - (\hat{\phi}\cdot\hat{n}_i)^2 \qquad \xi_{i;\times} = 2(\hat{\theta}\cdot\hat{n}_i)(\hat{\phi}\cdot\hat{n}_i)\,. \tag{3.54}$$

To implement the cancellation of laser phase noise these elementary beams must be combined with suitable time-delays. We notice that in the Fourier domain the delay operators get replaced by simple multiplicative factors as the following computations show. This is one of the advantages of the Fourier analysis. The delay operators introduced earlier are E_i such that for any function of time $f(t)$, we have

$$E_i * f(t) = f(t-L_i)\,, \tag{3.55}$$

which in the Fourier domain in nothing but

$$\widetilde{E_i * f(\Omega)} = e_i(\Omega)\tilde{f}(\Omega)\,, \tag{3.56}$$

where the e_i are simple multiplicative factors:

$$e_i = e^{i\Omega L_i}\,. \tag{3.57}$$

Thus operator polynomials in E_i become actual polynomials in e_i in the Fourier domain. This particularly simple fact can be used to advantage for the simple but astrophysically important sources, namely the monochromatic sources considered in the next section.

Below in the figures 3.8(a) and 3.8(b) we present the transfer functions F_{V_1} for both polarisations: The other transfer functions show similar characteristics.

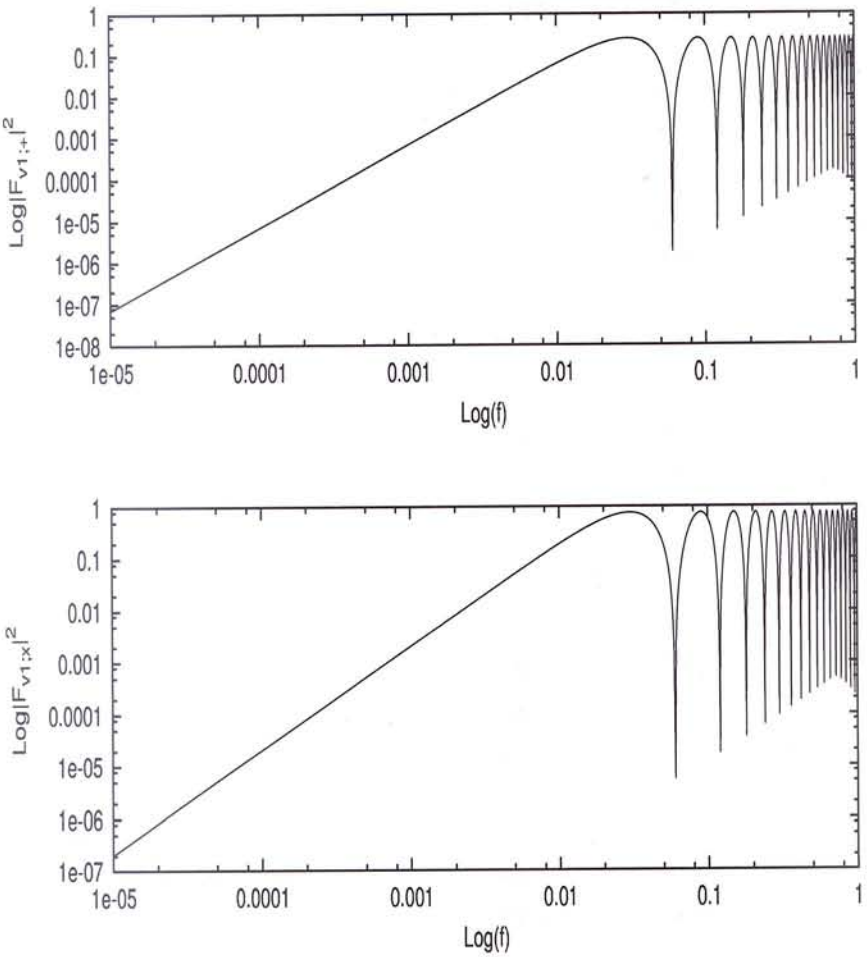

Figure 3.8: Log Log plot of the *PSD* $|F_{V_{1;+}}|^2$ and $|F_{V_{1;\times}}|^2$, of the corresponding transfer function are displayed in (a) and (b) respectively, as a function of frequency for $\theta = 0$, $\phi = 0$.

3.4 Noise

We recall that the laser frequency noise and optical bench motion noise can be cancelled by taking appropriate combinations of the beams. In this scheme the noises that do not cancel out in the module of *syzygies* are the acceleration noise of the proof masses and the shot noise. These then form the bulk of noise spectrum which we obtain below for any given data combination X. We compute the noise power spectral densities for the generators $X^{(A)}$.

The beam with the signal and the various noises can be written as,

$$U^1 = E_2\tilde{C}_3 - \tilde{C}_1^* + 2\hat{n}_2 \cdot \vec{v}_1^* + h_{U1} + Y_{U1}^{opt} \tag{3.58}$$

$$V^1 = -E_3\tilde{C}_2^* + \tilde{C}_1 + 2\hat{n}_3 \cdot \vec{v}_1 - h_{V1} - Y_{V1}^{opt} \tag{3.59}$$

$$Z^1 = \left(\frac{1}{2}\right)(z_1 - z_1^*) + \hat{n}_3 \cdot \vec{v}_1 + \hat{n}_2 \cdot \vec{v}_1^* \,. \tag{3.60}$$

The other beams can be obtained by taking cyclic permutations. Here $\vec{v}_1$ and $\vec{v}_1^*$ are the random velocities of the proof masses, in the left and right branches respectively, in space craft 1.

Let the noise cancelling combination X be given by,

$$X = p_i V^i + q_i U^i + r_i Z^i \,, \tag{3.61}$$

where the 9-tuple (p_i, q_i, r_i) is in the module of syzygies. Using Eq. (3.61) we obtain the power spectral density of X for the two noises,

$$< X^2 >^{pf} = \sum_{i=1}^{3} \left(|2p_i + r_i|^2 + |2q_i + r_i|^2\right) S^{pf} \,, \tag{3.62}$$

$$< X^2 >^{opt} = \sum_{i=1}^{3} \left(|p_i|^2 + |q_i|^2\right) S^{opt} \,, \tag{3.63}$$

where S^{pf} is obtained from $\vec{v}_i$ and $\vec{v}_j^*$ and denotes the proof mass noise; S^{opt} denotes the optical path noise which includes shot noise, beam pointing noise etc. We take $S^{pf}(f) = 2.5 \times 10^{-48}\,[f/1\,Hz]^{-2}\,Hz^{-1}$ and $S^{opt}(f) = 1.8 \times 10^{-37}\,[f/1\,Hz]^2\,Hz^{-1}$ following the literature [17].

For the purpose of computing the GW response and the noise, we make a simplifying assumption that the arm-lengths are equal ie. $L_1 = L_2 = L_3 = L$. This assumption is justified because the GW wavelength is much larger than the differences between the actual arm-lengths. Thus we have,

$$e_1 = e_2 = e_3 \equiv e^{i\Omega L}.$$

In the particular cases of the generators $X^{(A)}, A = 1, 2, 3, 4$ we obtain,

$$\begin{aligned} S_{X^{(1)}}(f) &= \left[16\sin^2(2\pi f L) + 32\sin^4 \pi f L)\right] S^{pf} \\ &+ \left[8\sin^2(\pi f L) + 8\sin^2(2\pi f L)\right] S^{opt} \end{aligned} \tag{3.64}$$

$$S_{X^{(2)}}(f) = 24\sin^2(\pi f L) S^{pf} + 6S^{opt} \tag{3.65}$$

$$S_{X^{(3)}}(f) = \left[16\sin^2(\pi f L) + 8\sin^2(3\pi f L)\right] S^{pf} + 6S^{opt} \tag{3.66}$$

$$S_{X^{(4)}}(f) = \left[16\sin^2(\pi f L) + 8\sin^2(3\pi f L)\right] S^{pf} + 6S^{opt} \tag{3.67}$$

The plots of these noise spectra are shown in the figure 3.9.

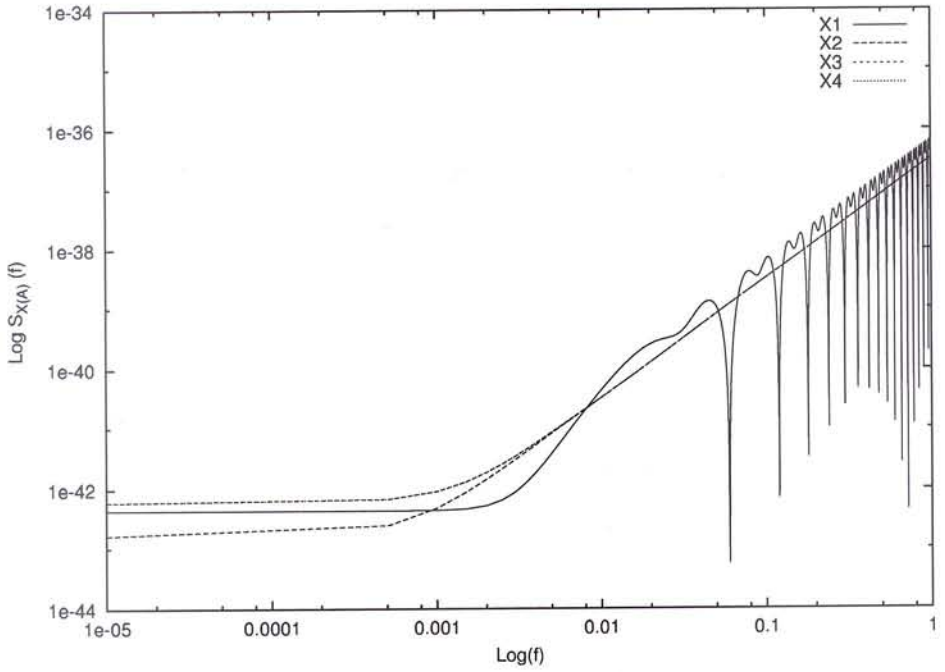

Figure 3.9: Log Log plot of the noise spectra for the generators $X^{(A)}$. The curves for $X^{(3)}$ and $X^{(4)}$ coincide in the figure.

3.5 Monochromatic Sources

Monochromatic sources are simplest among the gravitational wave sources. There are a number of important objects such as pulsars, rotating neutron stars, coalescing-binaries with sufficiently low mass may be considered as emitting monochromatic GW radiation. We will call those sources to be monochromatic which even if they change a little in frequency in a given observation time, the fractional change in SNR for the optimal data combination does not fall below a pre-assigned limit. We could take this limit to be few percent, but for concreteness we fix the limit at 1 %. The observation time T we take to be one year.

For binary stars, the relevant quantity which decides the evolution in the GW frequency at a given frequency f_0 is the so called chirp mass $\mathcal{M} = \mu^{3/5} M^{2/5}$, where μ is the reduced mass and M is the total mass of the binary system. We assume a Newtonian evolution for the binary system which gives the rate of change of GW frequency f as,

$$\dot{f} = \frac{3}{8} \frac{f_0}{\tau_c}, \tag{3.68}$$

where τ_c is the Newtonian coalescence time measured from the epoch when the GW fre-

quency is f_0 and the 'dot' denotes derivative with respect to time. The τ_c is given by,

$$\tau_c \sim 2.15 \times 10^6 \left[\frac{\mathcal{M}}{M_\odot}\right]^{-\frac{5}{3}} \left[\frac{f_0}{1\text{mHz}}\right]^{-\frac{8}{3}} \text{years}, \tag{3.69}$$

where $M_\odot$ is the solar mass.

A limit on the rate of change of frequency can obtained by considering the total change in the frequency Δf during the period of observation T. That is,

$$\Delta f = \dot{f} T. \tag{3.70}$$

Inverting the above equations we obtain a limit on the chirp mass $\mathcal{M}$:

$$\mathcal{M} \leq 175 \left[\frac{f_0}{1\text{mHz}}\right]^{-\frac{11}{5}} \left[\frac{\Delta f}{1\mu Hz}\right]^{\frac{3}{5}} M_\odot. \tag{3.71}$$

In our investigation we take the bandwidth Δf by allowing SNR to change by 1% at the frequency f_0. Numerically, we estimate Δf for various values of f_0. The table below shows the upper bound for $\mathcal{M}$ at various frequencies f_0:

f_0 in mHz	Δf in μ Hz for 1% change in SNR	$\frac{\mathcal{M}}{M_\odot}$
0.1	1.0	27705
1	9.9	691
2	22	243
10	1130	74

Here our goal is to seek a data combination which optimises the SNR for a monochromatic source with given polarisation parameters and direction information. A convenient set of polarisation parameters are the angles ϵ and ψ describing the orientation of the angular momentum vector in space. The direction to the source is described by the polar angles θ and ϕ in the coordinate system tied to LISA. For a monochromatic source the wave form can be written as,

$$\begin{aligned} h_+(t) &= H\left[\frac{1+\cos^2\epsilon}{2}\cos 2\psi\,\cos\Omega t + \cos\epsilon\,\sin 2\psi\,\sin\Omega t\right], \\ h_\times(t) &= H\left[-\frac{1+\cos^2\epsilon}{2}\sin 2\psi\,\cos\Omega t + \cos\epsilon\,\cos 2\psi\,\sin\Omega t\right], \end{aligned} \tag{3.72}$$

where the angles (ϵ, ψ) describe the orientation of the binary orbit (ϵ, ψ could be the direction angles of the orbital angular momentum vector) and H the overall amplitude which depends on the masses, the distance and the frequency f as given below:

$$H = 1.188 \times 10^{-22} \cdot \left[\frac{\mathcal{M}}{1000\,M_\odot}\right]^{\frac{5}{3}} \cdot \left[\frac{R}{1\,\text{Gpc}}\right]^{-1} \cdot \left[\frac{f}{1\,\text{mHz}}\right]^{2/3}, \tag{3.73}$$

where R is the distance to the source, $f = \Omega/2\pi$ is the GW frequency of the source and $\mathcal{M} = (\mu^3 M^2)^{\frac{1}{5}}$ the chirp-mass, where μ and M are respectively the reduced and the total mass of the binary. For the typical parameters taken above the frequency evolves very slowly, so much so that the time for the system to coalesce is more than 20 years. For an observational time of the order of an year, the frequency of the binary changes very little so that the source can be practically taken to be monochromatic.

Since we deal with essentially monochromatic sources, the Fourier domain is appropriate for further analysis. In the Fourier domain we have,

$$\begin{aligned} h_+(\Omega) &= H\left[\frac{1+\cos^2\epsilon}{2}\cos 2\psi - i\cos\epsilon\sin 2\psi\right], \\ h_\times(\Omega) &= H\left[-\frac{1+\cos^2\epsilon}{2}\sin 2\psi - i\cos\epsilon\cos 2\psi\right]. \end{aligned} \tag{3.74}$$

The response for the signal at the detector can now be written as,

$$h_X = \sum_{i=1}^{3}\left[p_i\left(F_{Vi;+}h_+ + F_{Vi;\times}h_\times\right) + q_i\left(F_{Ui;+}h_+ + F_{Ui;\times}h_\times\right)\right], \tag{3.75}$$

where p_i's and q_i's are in the module of syzygies. From Eq. (3.62) and (3.63) we can compute the total noise spectrum for the generators and it can be written as,

$$S_X(f) = \sum_{i=1}^{3}\left[\left(|2p_i + r_i|^2 + |2q_i + r_i|^2\right)S^{pf} + \left(|p_i|^2 + |q_i|^2\right)S^{opt}\right]. \tag{3.76}$$

The expression for the signal to noise ratio (SNR) for the monochromatic source simplifies to,

$$SNR = \left\{\frac{|h_X|}{\sqrt{S_X(f)}}\right\}. \tag{3.77}$$

We plot the sensitivities of the generators $X^{(A)}$ as function of f in figures 4.11(a) and 4.12(a) for fixed direction θ and ϕ. It is also important to understand the angular dependence of the sensitivity of generators, which are plotted in the figures 3.10(a)-3.10(d) at a frequency of $f = 1$ mHz. The sensitivity S is defined following [23],

$$S = 5\frac{\sqrt{S_X B}}{|h_X|}, \tag{3.78}$$

where $B = 1/T$, where T is the observation time which we take to be one year. The number 5 corresponds to an SNR of 5.

In this section we have found the GW response and the noise power spectral densities (PSD) for the various data combinations. We have given simple and elegant expressions for obtaining the same. In the next section we use these results to compute the SNR for the data combinations in the module and then optimise the average SNR and sensitivity.

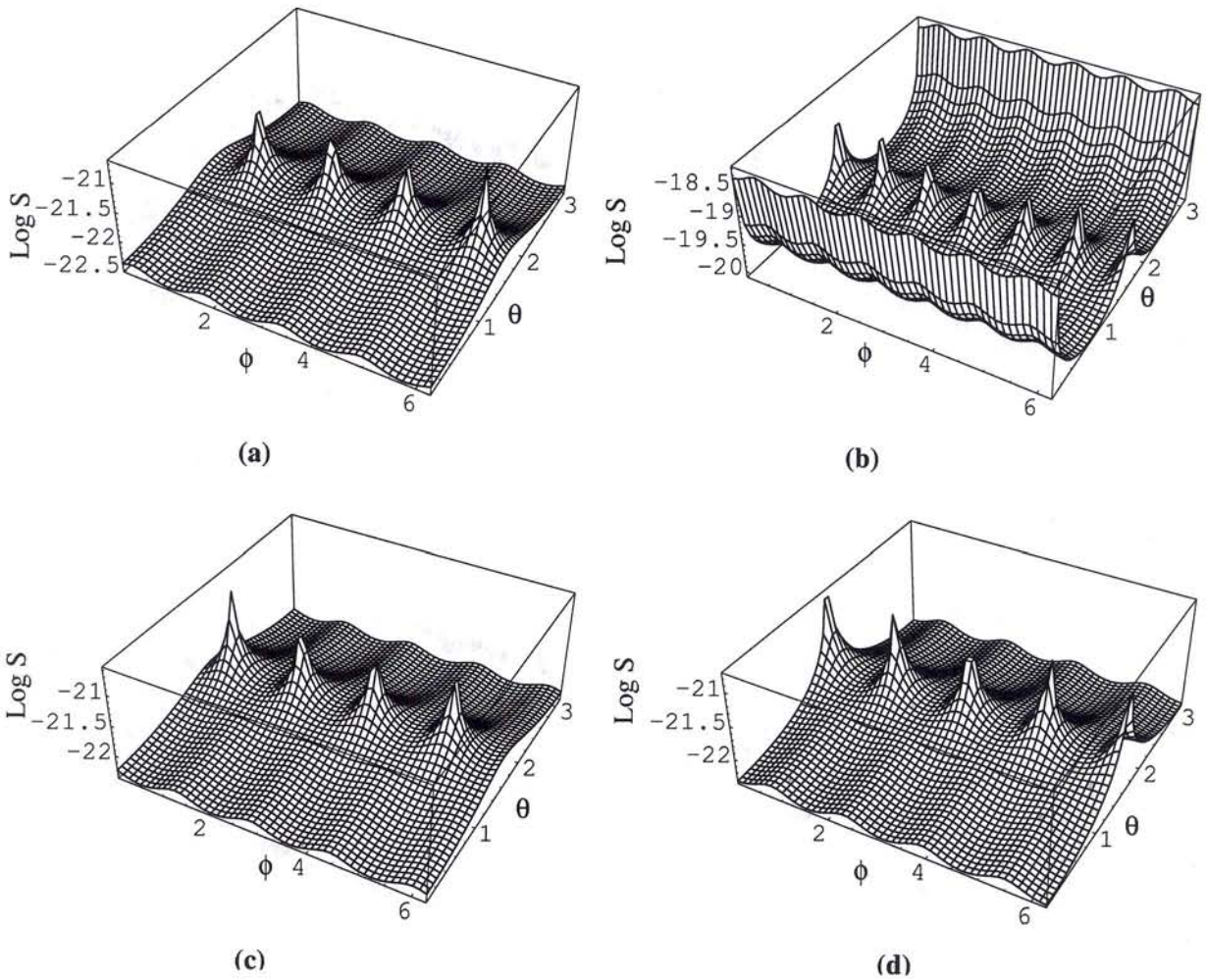

Figure 3.10: Plots of log S of the generators $X^{(A)}, A = 1, 2, 3, 4$, are displayed in (a), (b), (c) and (d), respectively, as function of θ and ϕ for $f = 1$ mHz and SNR $= 5$.

Optimising SNR

4.1 Introduction

We start this section with the formalism for extremising the SNR. The noise and signal pertaining to the data streams can be construed of as vectors. Our formalism makes the discussion lucid, elegant and convenient for further analysis. We compute the noise covariance matrix, which is an outer product of the noise vector with its Hermitian conjugate and obtain its eigenvectors and eigenvalues. The signal matrix (again outer product of the signal vector with its Hermitian conjgate) is computed for binaries whose frequency changes at most adiabatically (the monochromatic case is included) and for which the signal is averaged over polarisations and directions. Here adiabatic means that the signal response, the noise and hence the SNR change imperceptibly even if the GW source changes frequency during the observation time. We find that the signal matrix has the same eigenvectors as the noise covariance matrix which results in computational simplification. We show that the SNR at each frequency for any data combination in the module, lies between an upper and a lower bound, the upper and lower bounds of the SNR being those of the eigenvectors. The extremisation - both maximisation and minimisation - of SNR is important for different purposes; maximisation is important for the detection and parameter estimation of a GW source, while minimisation is important for the purpose of distinguishing the GW confusion noise from the instrumental noise [21]. We further show that the bounding SNR curves have multiple intersections within the band-width of LISA (10^{-4} Hz - 0.1 Hz). The improvement of SNR of the upper-bound over the Michelson combination, goes upto 70% , but only at high frequencies $\gtrsim 5$ mHz. At low frequencies $\lesssim 5$ mHz, both have the same sensitivity. Since the eigenvectors are independent random variables, a 'network' SNR of independent detectors [24] can be constructed from the likelihood considerations which gives an improvement between $\sqrt{2}$ and $\sqrt{3}$ over the maximum of SNRs of the eigenvectors. The improvement over the Michelson combination is about 40% at low frequencies $\lesssim 3$ mHz and rises above 100% at high frequencies.

For the purpose of extremising the SNR, we choose the set of generators: α, β, γ and ζ (notation followed from [16, 17, 25]). The α, β, γ are cyclic permutations of each other. This symmetry comes in useful when computing scalar products between them and also

in diagonalising the noise, and signal covariance matrices defined in the next section. We list this generating set as 9-tuples of polynomials $(p_i,\, q_i,\, r_i)$. Recall that the polynomials $(p_i,\, q_i,\, r_i)$ are polynomials in the variables E_i and act on the data streams $\left(V^i,\, U^i,\, Z^i\right)$ respectively. These generators of the module are given by:

$$\begin{aligned}
\alpha &= (1, E_3, E_1E_3, 1, E_1E_2, E_2, -(1+E_1E_2E_3), -(E_1E_2+E_3), -(E_1E_3+E_2)),\\
\beta &= (E_1E_2, 1, E_1, E_3, 1, E_2E_3, -(E_1E_2+E_3), -(1+E_1E_2E_3), -(E_1+E_2E_3)),\\
\gamma &= (E_2, E_2E_3, 1, E_3E_1, E_1, 1, -(E_2+E_1E_3), -(E_1+E_2E_3), -(1+E_1E_2E_3)),\\
\zeta &= (E_1, E_2, E_3, E_1, E_2, E_3, -(E_1+E_2E_3), -(E_2+E_1E_3), -(E_3+E_1E_2)).
\end{aligned} \tag{4.79}$$

Note that these sets of generators are not linearly independent. In particular, the set of generators $\{\alpha, \beta, \gamma, \zeta\}$ [16] obey the following condition :

$$(1 - E_1E_2E_3)\zeta = (E_1 - E_2E_3)\alpha + (E_2 - E_1E_3)\beta + (E_3 - E_1E_2)\gamma\,. \tag{4.80}$$

When maximising the SNR in the Fourier space, this relation allows us to eliminate one of the generators at almost all frequencies, except when the product $E_1E_2E_3 = 1$. Note that $E_1E_2E_3$ is just the total time-delay $L_1 + L_2 + L_3$ around the LISA triangle. Here, we assume that all the arms of LISA are of equal length *i.e* $L_1 = L_2 = L_3 = L$. In the Fourier domain, *i.e,* $E_1 = E_2 = E_3 = E = e^{i\Omega L}$ and the operator polynomials become actual polynomials. One can then solve for ζ in terms of α, β, γ, *except* at the frequencies Ω, when $e^{3i\Omega L} = 1$. Taking $L \sim 5 \times 10^6$ km, the smallest such frequency $f = \Omega/2\pi$ is ~ 20 mHz. Thus,

$$\zeta = \frac{E}{1 + E + E^2}\,(\alpha + \beta + \gamma)\,, \tag{4.81}$$

and can be effectively eliminated while extremising SNR, except at the singular frequencies. Since SNR computation can be successfully carried out for frequencies arbitrarily close to the singular frequencies, for the computation, the singularities do not seem to be important. In the analysis that follows, we use only the three generators $\{\alpha,\, \beta,\, \gamma\}$.

We show further that the SNR can be improved with respect to the Michelson combination X, (notation of [16,17,25]), for monochromatic sources whose signals are averaged over directions and polarisations. The Michelson combination X is given by the polynomial vector,

$$\begin{aligned}
X &= \left(1 - E_2^2, 0, E_2\left(E_3^2 - 1\right), 1 - E_3^2, E_3\left(E_2^2 - 1\right), 0,\right.\\
&\quad \left. E_2^2 + E_3^2 - E_2^2E_3^2 - 1, 0, 0\right).
\end{aligned} \tag{4.82}$$

This combination is used to plot the standard LISA sensitivity curve [23]. From cyclic symmetry, the combinations Y and Z can be obtained which exhibit the same frequency response.

4.2 Strategies for Improving the Effective Sensitivity of LISA

In this section, we show that the set of generators $\{\alpha, \beta, \gamma\}$ can be combined into a new set, consisting of 'orthogonal' eigenvectors. The noise covariance matrix naturally defines a positive definite, non-degenerate bilinear form, which serves as a scalar product or a metric. Orthogonality between eigenvectors is defined in terms of this metric. Physically this means that the noises of the eigenvectors are uncorrelated with each other. The eigenvectors are easily obtained by diagonalising the noise covariance matrix. The averaged signal matrix that we consider here has the same form as the noise covariance matrix and consequently has the same eigenvectors. Thus this set of eigenvectors simultaneously diagonalises both matrices constituting the SNR and simplifies the analysis that follows. An important observation here is that the eigenvectors are independent observables. They represent therefore statistically independent detectors (so far as instrumental noises are concerned), and they can be treated as a network of detectors. Furthermore, they can be combined in a root mean square fashion to yield a 'detector network statistic' [24] to yield a much improved sensitivity.

4.2.1 The Formalism

In this subsection our goal is to maximise the SNR for a given monochromatic source over the set of noise cancelling combinations. These combinations can be generated by the generators given in the Eq. (2.19) and (2.20). The SNR corresponding to the each of the generators ($X^{(A)}$, $A = 1$ to 4) as a function of frequency are shown in the figure. However one must maximise the SNR over an arbitrary linear combination of $X^{(A)}$. This goal is difficult to achieve since it involves a maximisation over a space of six tuples of polynomials which is essentially a function space. In order to make the problem tractable and still achieve adequate results we restrict the polynomials to be constants. This approach does not fully optimise the SNR but it comes quite close to the optimal solution. Our approach can be thought of as a zero'th order approximation.

A linear combination of the generators can be written as

$$X = \sum_{A=1}^{4} \alpha_{(A)} X^{(A)}, \tag{4.83}$$

here, $\alpha_{(A)}$ (for A= 1 to 4) are a set of real numbers. Since a scalar multiple of X will not yield anything new, we set one of the α's, say, $\alpha_{(1)} = 1$. Thus the SNR now becomes a function of three parameters $\alpha_{(i)}, i = 2, 3, 4$, which are just real numbers and our objective is to maximise the SNR with respect to $\alpha_{(i)}$.

In order to carry out the analysis efficiently and elegantly we find that it is useful to

define complex noise vectors $N^{(A)}$ pertaining to $X^{(A)}$ as follows:

$$N^{(A)} = \left(\sqrt{S^{pf}}(2p_i^{(A)} + r_i^{(A)}), \sqrt{S^{pf}}(2q_i^{(A)} + r_i^{(A)}), \sqrt{S^{opt}}p_i^{(A)}, \sqrt{S^{opt}}q_i^{(A)}\right), \quad (4.84)$$

where, $p_i^{(A)}$, $q_i^{(A)}$ and $r_i^{(A)}$ corresponding to generators $X^{(A)}$ are given in the Eq. (2.19) and (2.26) and S^{pf} and S^{opt} are the proof-mass noise and the optical path noise given in section (3.4). We have $N^{(A)} \in C^{12}$ the 12 dimensional complex space and the usual scalar product C^{12} induces a norm; $N^{(A)} \cdot N_{(A)}{}^* \equiv ||N^{(A)}||^2$ gives the noise PSDs corresponding to the basis $X^{(A)}$.

In a similar fashion one can also write the signal corresponding to a particular basis element. We first define the polynomial 6-tuple for each generator $X^{(A)}$ as follows:

$$P^{(A)} = \left(p_i^{(A)}, q_i^{(A)}\right), \quad (4.85)$$

and the GW signal 6-tuple as,

$$H^* = (F_{V_i;+}h_+ + F_{V_i;\times}h_\times,\ F_{U_i;+}h_+ + F_{U_i;\times}h_\times). \quad (4.86)$$

The signal for a specific generator $X^{(A)}$ is then written as,

$$h^{(A)} = P^{(A)}.H^* \quad (4.87)$$

and the corresponding SNR is given by,

$$SNR^{(A)} = \frac{|h^{(A)}|}{||N^{(A)}||} = \sqrt{\frac{(P^{(A)} \cdot H^*)(P^{(A)} \cdot H^*)^*}{N^{(A)} \cdot N_{(A)}{}^*}}. \quad (4.88)$$

For an arbitrary linear combination X (Eq. (4.83)) the noise vector and the signal vector can be expressed as

$$N = \alpha_{(A)}N^{(A)}, \qquad P = \alpha_{(A)}P^{(A)}, \quad (4.89)$$

where summation convention has been used. The signal is just the scalar product $h = P.H^* = \alpha_{(A)}h^{(A)}$. We omit subscripts X on these quantities.

In this notation the SNR of the combination (4.83) can be written as,

$$SNR = \frac{|h|}{||N||}. \quad (4.90)$$

Writing out explicitly the sums in the scalar products,

$$(SNR)^2 = \frac{\alpha_{(A)}\alpha^{(B)*}h^{(A)}h_{(B)}{}^*}{\alpha_{(A)}\alpha^{(B)*}N^{(A)} \cdot N_{(B)}{}^*}. \quad (4.91)$$

Maximisation with respect to $\alpha_{(2)}, \alpha_{(3)}, \alpha_{(4)}$ leads to the following three conditions which must be obeyed by $\alpha_{(i)}$ in order to yield the maximum SNR for X:

$$\frac{\Re(hh_{(i)}{}^*)}{|h|^2} = \frac{\Re(NN_{(i)}{}^*)}{||N||^2}, \quad (4.92)$$

where $\Re(x)$ denotes the real part of the quantity x.

To demonstrate the usefulness of the formalism, we consider just two generators $X^{(1)}$ and $X^{(2)}$. We take the $\alpha_{(1)} = 1, \alpha_{(2)} = \alpha$ and other two α s zero. Then,

$$X = X^{(1)} + \alpha X^{(2)} . \tag{4.93}$$

The Eq. (4.91) reduces to the form,

$$\mathcal{S} = \frac{a_1 + 2b_1\alpha + c_1\alpha^2}{a_2 + 2b_2\alpha + c_2\alpha^2} , \tag{4.94}$$

where,

$$\begin{aligned} a_1 = |h^1|^2, \quad b_1 = \Re(h^1 h_2^*), \quad c_1 = |h^2|^2 , \\ a_2 = |N^1|^2, \quad b_2 = \Re(N^1 N_2^*), \quad c_2 = |N^2|^2 . \end{aligned} \tag{4.95}$$

The condition for the optimisation (4.92) simplifies to

$$(b_1a_2 - a_1b_2) + (c_1a_2 - a_1c_2)\alpha + (c_1b_2 - b_1c_2)\alpha^2 = 0 . \tag{4.96}$$

The two roots of the Eq. (4.96) can be obtained. Here, α is a function of the parameters f, θ, ϕ, ϵ and ψ. One of the solutions of the Eq. (4.96) correspond to the maximum and other correspond to the minimum of the SNR. In a similar fashion one can maximise the SNR by taking any two of the four generators given in the Eq. (2.19) and by taking appropriate $\alpha_{(i)}$ in the Eq. (4.83). We have seen in several cases that maximising over just two generators yields remarkably good results.

This simple case demonstrates that one can use the solutions given in the Eq. (2.19) to get a better SNR. However, to get full advantage one needs to maximise the SNR over the three α's. In order to optimise the SNR given by the general combination we resort to numerical methods since there is no straight forward method for solving the coupled algebraic equations given by (4.92). We use the Powell's method as given in [26] for maximising the SNR over the parameters $\alpha_{(A)}$. The sensitivity S for the generators $X^{(A)}$ and for the maximal SNR combination of $X^{(A)}$'s denoted by [X1,X2,X3,X4] as a function of frequency f has been plotted in figures 4.11(a) and 4.12(a). The corresponding values of $\alpha_{(A)}$ are shown in figures 4.11(b) and 4.12(b).

This simple example demonstrates how one can maximise SNR over the module. However in order to gain the physical insight it is important have analytical procedure for maximisation. We show later that this goal can be achieved by diagonalising the noise covariance matrix and the signal matrix. The extremisation can be carried out *algebraically* because of the special nature of the noise and signal matrices.

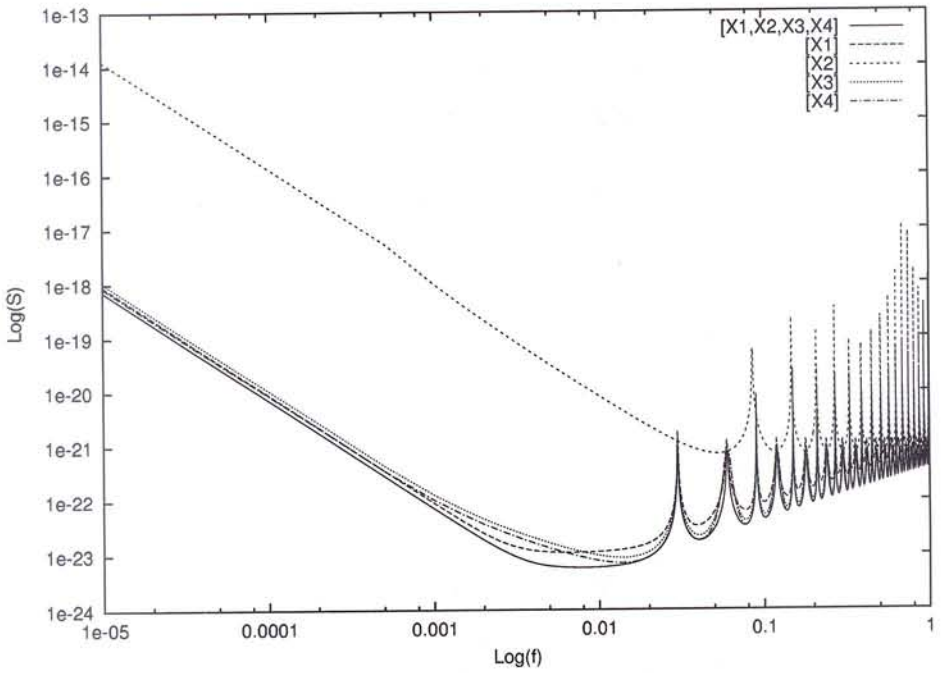

Figure 4.11(a). Log Log plot of the sensitivity S for the generators $X^{(A)}$ as function of f for $\theta = 0$, $\phi = 0$ over one year observation period for SNR = 5. The curve [X1,X2,X3,X4] depicts the sensitivity of the linear combination of four generators $X^{(A)}$, which gives maximum SNR.

4.2.2 The Noise Covariance Matrix

We define noise vectors in the Fourier domain $N^{(I)}$, $I = 1, 2, 3$ for each of the generators $\{\alpha, \beta, \gamma\}$ respectively, over the 12 dimensional complex space $\mathcal{C}^{12}$,

$$N^{(I)} = \left(\sqrt{S^{pf}}(2p_i^{(I)} + r_i^{(I)}), \sqrt{S^{pf}}(2q_i^{(I)} + r_i^{(I)}), \sqrt{S^{opt}}p_i^{(I)}, \sqrt{S^{opt}}q_i^{(I)}\right) . \tag{4.97}$$

The polynomials $(p_i^{(I)}, q_i^{(I)}, r_i^{(I)})$, (now actual polynomials in the Fourier domain) corresponding to the generators α, β and γ are given in the equation (4.79). The noise covariance matrix for the generators $\{\alpha, \beta, \gamma\}$ is defined as $\mathcal{N}_{(J)}^{(I)} = N^{(I)} \cdot N_{(J)}^{*}$ and takes the simple form,

$$\mathcal{N}_{(J)}^{(I)} = \begin{bmatrix} n_d & n_o & n_o \\ n_o & n_d & n_o \\ n_o & n_o & n_d \end{bmatrix} . \tag{4.98}$$

We note that because of the cyclic symmetry, the diagonal elements $N^{(I)} \cdot N_{(I)}^{*}$ are equal to each other - denoted by n_d. Similarly, all the off-diagonal elements $N^{(I)} \cdot N_{(J)}^{*}$, for $I \neq J$ are also equal to each other and which we denote by n_o. This was the reason a generating

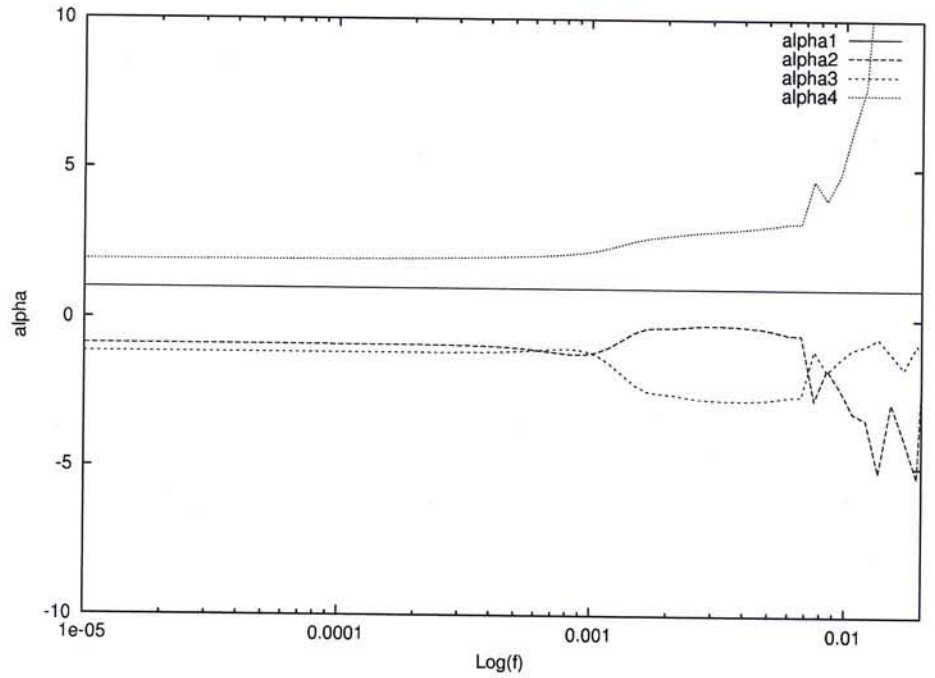

FIG. 4.11(b). Plot of coefficients $\alpha_{(A)}$ which gives the maximum SNR for linear combinations of all the four $X^{(A)}$ as function of f for $\theta = 0$ and $\phi = 0$.

set possessing symmetry properties was chosen in the first place. A matrix with this form has two degenerate eigenvalues. Thus, the eigenvalues of the noise covariance matrix are given by,

$$n_1 = n_2 = n_d - n_o \qquad \text{and} \qquad n_3 = n_d + 2n_o\,. \tag{4.99}$$

Since two of the eigenvalues are degenerate we need to systematically adopt a procedure for choosing the linearly independent and orthonormal set of eigenvectors. This choice is not unique. One such choice gives the following matrix $\mathcal{M}$

$$\mathcal{M} \;=\; \begin{bmatrix} \frac{1}{\sqrt{6}} & \frac{1}{\sqrt{6}} & -\sqrt{\frac{2}{3}} \\ -\frac{1}{\sqrt{2}} & \frac{1}{\sqrt{2}} & 0 \\ \frac{1}{\sqrt{3}} & \frac{1}{\sqrt{3}} & \frac{1}{\sqrt{3}} \end{bmatrix}, \tag{4.100}$$

which diagonalises the noise matrix $\mathcal{N}^{(IJ)}$, that is $\mathcal{M}\cdot\mathcal{N}\cdot\mathcal{M}^{-1}$ is diagonal, with eigenvalues as diagonal elements. The eigenvectors are:

$$\begin{aligned} Y^{(1)} &= \frac{1}{\sqrt{6}}\left(\alpha+\beta-2\gamma\right), \\ Y^{(2)} &= \frac{1}{\sqrt{2}}\left(\beta-\alpha\right), \\ Y^{(3)} &= \frac{1}{\sqrt{3}}\left(\alpha+\beta+\gamma\right). \end{aligned} \tag{4.101}$$

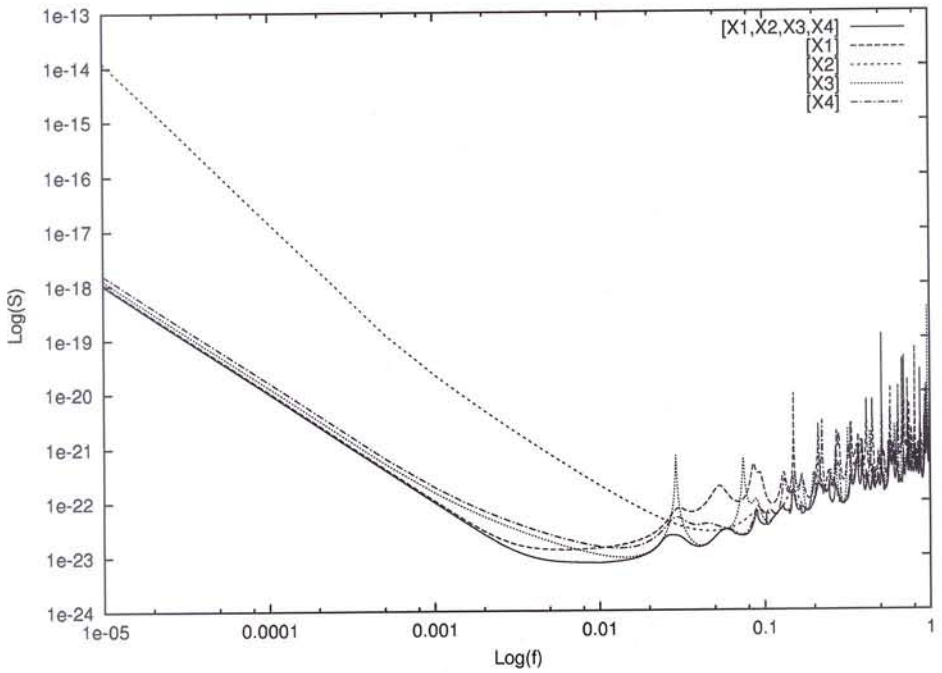

Figure 4.12:(a). Log Log plot of the sensitivity S for the generators $X^{(A)}$ as function of f for $\theta = \pi/4$, $\phi = \pi/4$ over one year observation period for SNR = 5. The curve [X1,X2,X3,X4] depicts the sensitivity of the linear combination of four generators $X^{(A)}$ which gives maximum SNR.

We find that the data combination $Y^{(3)}$ is proportional to the symmetric Sagnac combination ζ and has the same SNR as that of ζ.

4.2.3 The Signal Matrix

The response of a GW signal for a given data combination computed earlier is conveniently expressed in the Fourier domain by,

$$h(\Omega) = \sum_{i=1}^{3} \left[p_i \left(F_{V_{i;+}} h_+ + F_{V_{i;\times}} h_\times \right) + q_i \left(F_{U_{i;+}} h_+ + F_{U_{i;\times}} h_\times \right) \right] (\Omega) \,. \tag{4.102}$$

Here, $F_{V_{i;+/\times}}$ and $F_{U_{i;+/\times}}$ are the antenna pattern functions. We note that the signal depends only on the first six entries (p_i, q_i) of the 9-tuple describing a data combination. So while dealing with the signal response, we only consider the 6-tuple $P = (p_i, q_i)$ of the 9-tuple describing a data combination. We apply this formalism to a binary source which may be adiabatically changing in frequency. The two GW amplitudes of such a source at frequency Ω are given by the equation (3.74).

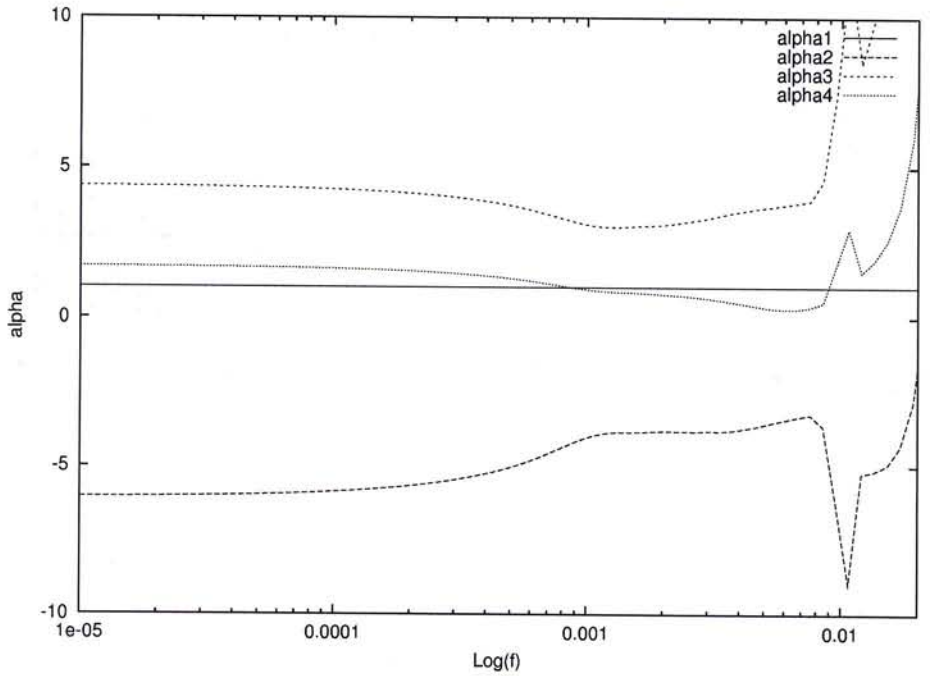

FIG. 4.12(b). Plot of coefficients $\alpha_{(A)}$ which gives the maximum SNR for linear combinations of all the four $X^{(A)}$ as function of f for $\theta = \pi/4$ and $\phi = \pi/4$.

In order to organise the calculations, we also define the detector response 6-tuple as,

$$R = \left(F_{V_{i;+}} h_+ + F_{V_{i;\times}} h_\times,\ F_{U_{i;+}} h_+ + F_{U_{i;\times}} h_\times\right) . \tag{4.103}$$

Both P and R will be considered as row vectors for the purpose of defining matrix products. In order to analyse the signal covariance matrix, it is useful to define a scalar product. For two data combinations P and Q (considered as row vectors), we define the scalar product as follows:

$$\ll P, Q \gg = P \cdot \mathcal{R} \cdot Q\dagger , \tag{4.104}$$

where, $\mathcal{R} = R^\dagger \cdot R$ is a Hermitian matrix of detector responses and the 'dot' denotes the matrix product. The norm of the vector P is then given by,

$$\|P\|^2 = \ll P, P \gg . \tag{4.105}$$

The norm of P is the GW response for the data combination described by P.

The signal matrix for any generating set $X^{(I)}$ (and corresponding $P^{(I)}$) is then defined as,

$$\mathcal{H}^{(I)}_{(J)} = \langle h^{(I)} h^*_{(J)} \rangle_{\epsilon\psi\theta\phi} = \left\langle \ll P^{(I)}, P^{(J)} \gg \right\rangle_{\epsilon\psi\theta\phi} , \tag{4.106}$$

where, $h^{(I)} = P^{(I)} \cdot R^\dagger$ and the bracket $\langle\ \rangle_{\epsilon\psi\theta\phi}$ represents the average over the polarisations and directions. Taking α, β and γ as the generators, the cyclic symmetry between

Figure 4.13: Noise Spectra of combinations $Y^{(I)}$

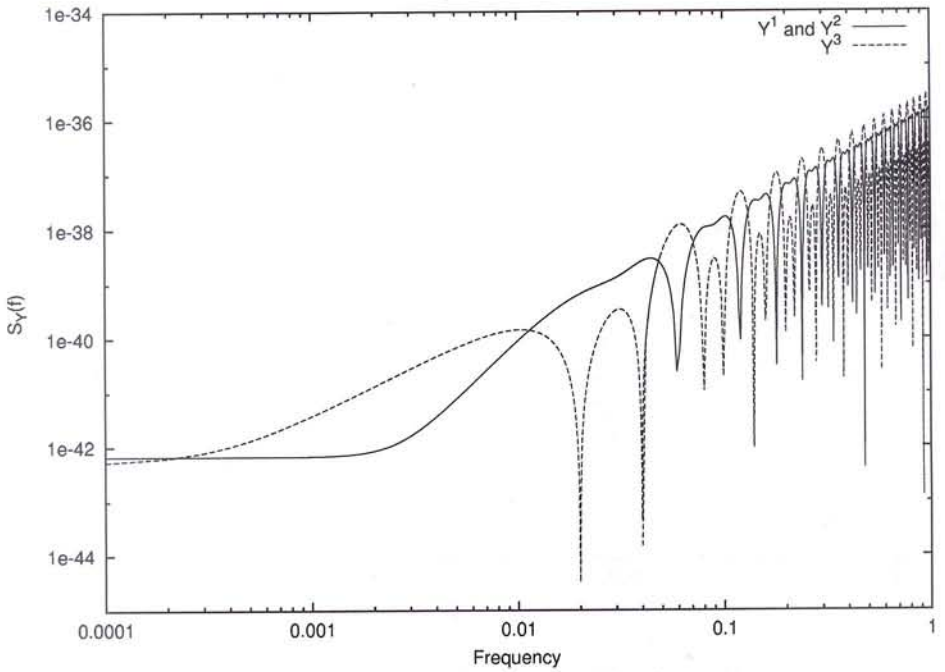

them gives rise to a signal covariance matrix $\mathcal{H}^{(I)}_{(J)}$ which has the same form as the noise covariance matrix $\mathcal{N}^{(I)}_{(J)}$ given in equation (4.98). In this case the n_d and n_o are replaced by $h_d = \langle h^{(I)} h^*_{(I)} \rangle$ and $h_o = \langle h^{(I)} h^*_{(J)} \rangle$ respectively. Thus $\mathcal{H}$ is diagonalised by the similarity transformation $\mathcal{M}$ and has the *same* eigenvectors $Y^{(I)}$. The eigenvalues of $\mathcal{H}^{(I)}_{(J)}$ are given by,

$$h_1 = h_2 = h_d - h_o, \qquad h_3 = h_d + 2h_o\,. \tag{4.107}$$

This simultaneous diagonalisation of both signal and noise matrices is important from the point of extremisation of SNR. This forms the content of the next subsection. However, we may note that in the formalism developed by Prince *et al* [27], the optimisation is performed without averaging over the source directions and polarisations, which results in the GW source matrix of rank 1. Since, the source directions are not known in general, we average over these parameters which results in a signal matrix of rank 3.

4.2.4 Extremising the SNR

An arbitrary data combination can be written as $Y = \alpha_{(I)} Y^{(I)}$, where $\alpha_{(I)}$ are polynomials in E. The SNR for this combination is given by,

$$SNR^2 = \frac{k_1 h_1 + k_3 h_3}{k_1 n_1 + k_3 n_3}\,, \tag{4.108}$$

Figure 4.14: Log Log plot of sensitivity S, curve as function of f after averaging over polarisation and source directions for a observation period of one year and SNR =5.

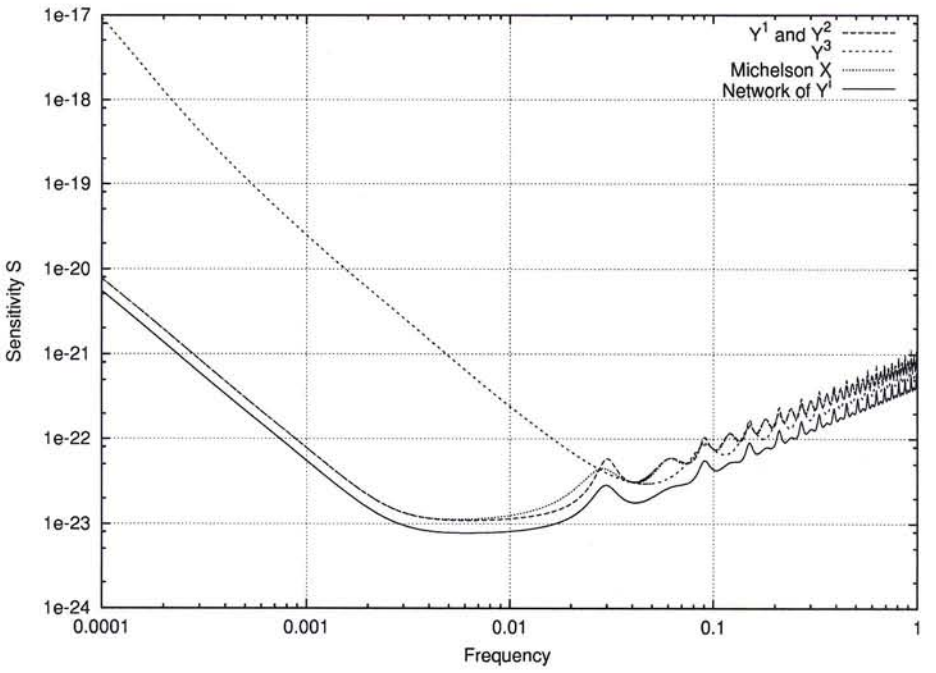

where, $k_1 = |\alpha_1|^2 + |\alpha_2|^2$ and $k_3 = |\alpha_3|^2$, and the ranges of k_1, k_3 are from 0 to ∞. The simplicity of this expression is because of using the new set of the orthogonal generators $Y^{(I)}$. It enables us to easily solve the extremisation problem. The maximum and the minimum of this expression is governed by the quantity η where,

$$\eta(f) = \frac{SNR^2_{(1)}}{SNR^2_{(3)}} = \frac{h_1/n_1}{h_3/n_3}, \tag{4.109}$$

where $SNR_{(I)}$ denotes the SNR of $Y^{(I)}$. When $\eta(f) \neq 1$, the SNR is a strictly monotonic function of the ratio k_1/k_3. If $\eta(f) > 1$ then the SNR of the generator $Y^{(1)}$ or $Y^{(2)}$ is greater than that of $Y^{(3)}$. Then for these frequencies $Y^{(1)}$ or $Y^{(2)}$ (or any linear combination of them) yields the maximum SNR while $Y^{(3)}$ yields minimum SNR. When $\eta(f) < 1$, the opposite is true: $Y^{(1)}$ or $Y^{(2)}$ (or any linear combination of them) yield the minimum SNR while $Y^{(3)}$ yields maximum SNR. The remaining case, when $\eta(f) = 1$ all the $Y^{(I)}$ have the same SNR. Since the extremum values of SNR are only attained by the eigenvectors, the corresponding SNR curves constitute the bounding curves for any linear combination of $Y^{(I)}$ s. So our results determine the limiting sensitivities of data combinations cancelling laser frequency noise and optical bench motion noise. It is interesting to note that at the frequencies where the bounding curves intersect, *all* the data combinations belonging to the module have the same SNR.

Figure 4.15: Plot of parameter η as a function of f. The points $\eta = 1$ correspond to the frequencies at which all the data combinations have the same SNR. $\eta > 1$ corresponds to the region in which data combination $Y^{(1)}$and $Y^{(2)}$ are more sensitive than $Y^{(3)}$ and vice versa.

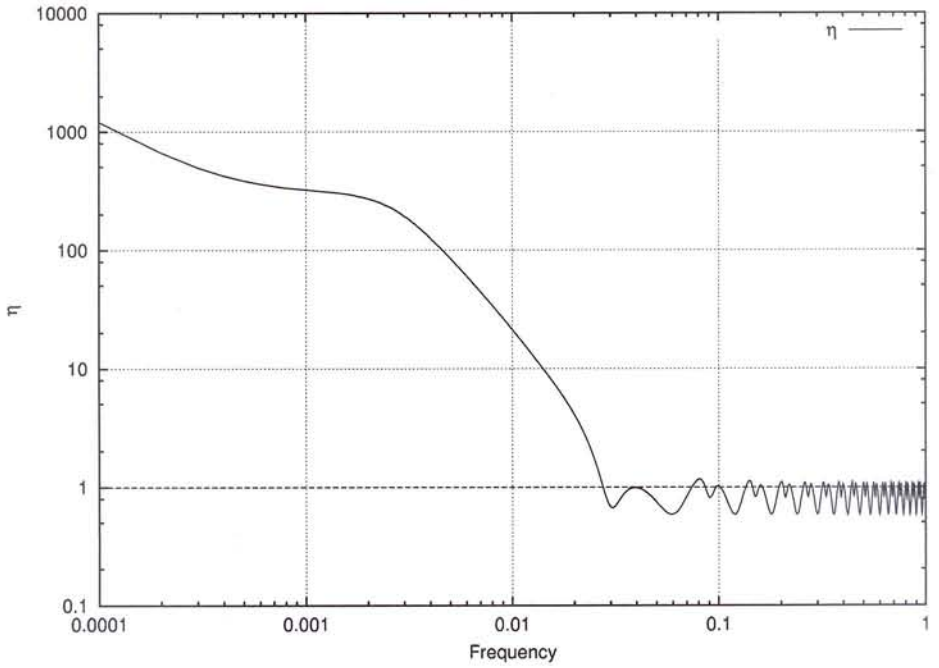

In the lower frequency range ($f \lesssim 15$ mHz), the combination $Y^{(3)}$(same as that of the combination ζ) has a very low sensitivity to the gravitational wave signal and the generators $Y^{(1)}$ (or $Y^{(2)}$) has maximum sensitivity to the signal. However, at high frequencies, the sensitivity curves of $Y^{(1)}$ and $Y^{(3)}$ intersect at several frequencies eg. $\sim$ 27 mHz, 39 mHz etc. While computing $\mathcal{H}^{(I)}_{(J)}$ and the average sensitivity, we assume a uniform distribution of sources over polarisations and source directions in the sky. Averaging over the polarisations is performed analytically and the averaging over source directions performed using the Monte Carlo method. The sensitivity, S is defined as, $S = 5\sqrt{\frac{B}{SNR}}$ (see Eq. 3.78), where, $B = \frac{1}{T}$ and T is the observation time which we take to be one year. In the Figure 4.14, we show the plots of S for the basis elements $Y^{(I)}$, for comparison, we also plot the sensitivity for the Michelson combination X. In the Figure 4.15, we plot the ratio η as a function of the frequency f. The points at which η intersects the line $y = 1$ corresponds to the points where all the data combinations in the module have the same value of SNR.

4.2.5 Operating LISA in a Network Mode

In the preceding sections, we have shown that either $Y^{(1)}, Y^{(2)}$ or $Y^{(3)}$ maximise the SNR and they are orthogonal *i.e.* they are independent random variables. The sensitivity of LISA can be further improved because, each of these generators can be realised as independent gravitational wave detectors. Here we obtain the network SNR by taking $Y^{(I)}$ as independent outputs of a network of three detectors. We assume that the underlying noise is Gaussian [24] and the $Y^{(I)}$ follow the standard normal distribution.

As shown in [24], if the noise of the individual detectors is uncorrelated then the network likelihood ratio is just the product of individual likelihood ratios; the log network likelihood ratio is the sum of the individual log likelihood ratios. Moreover, if the noise in the individual detectors is Gaussian, the surrogate statistic of the network, yields the network SNR as,

$$SNR^2_{network} = \sum_{I=1}^{3} SNR^2_{(I)} = 2\frac{h_1}{n_1} + \frac{h_3}{n_3}. \tag{4.110}$$

The corresponding sensitivities are shown in the Figure 4.14. At low frequencies $f \lesssim 15$ mHz, the improvement of the network SNR over the maximum of $Y^{(I)}$ is slightly greater than $\sqrt{2}$. This is because at low frequencies the data combination $Y^{(3)}$ is not very sensitive in comparison with $Y^{(1)}$. The best improvement in the relative SNR is achieved at frequencies where all the data combinations are equally sensitive, that is, when $\eta = 1$. A gain of a factor of $\sqrt{3}$ is achieved at these points. In the Figure 4.16, we have plotted the relative improvements in the network SNR with respect to the Michelson combination and the maximum of $Y^{(1)}$ and $Y^{(3)}$.

4.3 Residual Laser Phase Noise

It is indeed very difficult to maintain constant distance between the three space-crafts. In general, the three arm-lengths will be different. The actual length L_i' can only be estimated upto a certain accuracy. Let the estimated arm-length be L_i with an error ΔL_i such that the actual length is $L_i' = L_i + \Delta L_i$. Because of this uncertainty in the measurement of exact arm length, the laser phase noise can not be completely cancelled for a given laser noise-free data stream. If we demand that this residual laser phase noise level should be below the combined noise from proof mass S^{pf} and the optical path noise S^{opt} then this puts an upper limit on the laser stabilisation requirement $\widetilde{\Delta\nu}$ and is given by

$$\widetilde{\Delta\nu} = \frac{\nu_0}{\Omega\Delta L}\left[\frac{S^{pf} + S^{opt}}{\sum |p_i|^2 + |q_i|^2}\right]^{1/2}. \tag{4.111}$$

For Nd-YAG laser, $\nu_0 = 3\times10^{14}$ Hz and the inaccuracy in length is assumed to be $\Delta L \sim 200$ m, the upper limit on the laser stabilisation requirement is plotted for data combinations

Figure 4.16: Plots showing the relative improvements (ratios) of SNRs for the three cases: (i) Network SNR over the Michelson data combination (solid line). (ii) Network SNR over the maximum of Max $[Y^{(1)}, Y^{(3)}]$ (dotted line). (iii) Max $[Y^{(1)}, Y^{(3)}]$ over the Michelson (dashed line). Here Max $[Y^{(1)}, Y^{(3)}]$ is the maximum of the SNR of $Y^{(1)}$ and $Y^{(3)}$ over the bandwidth of LISA.

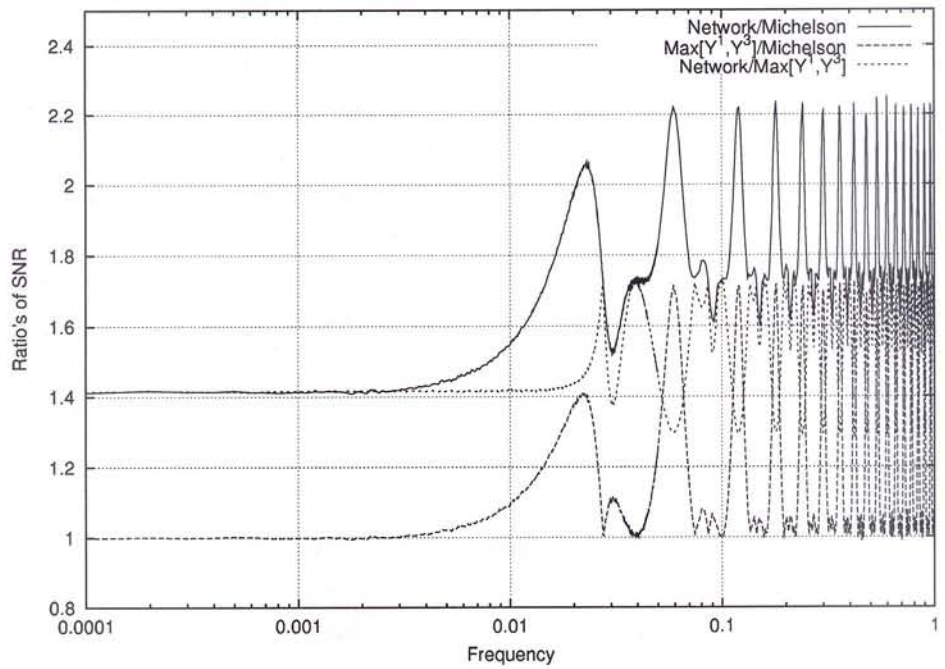

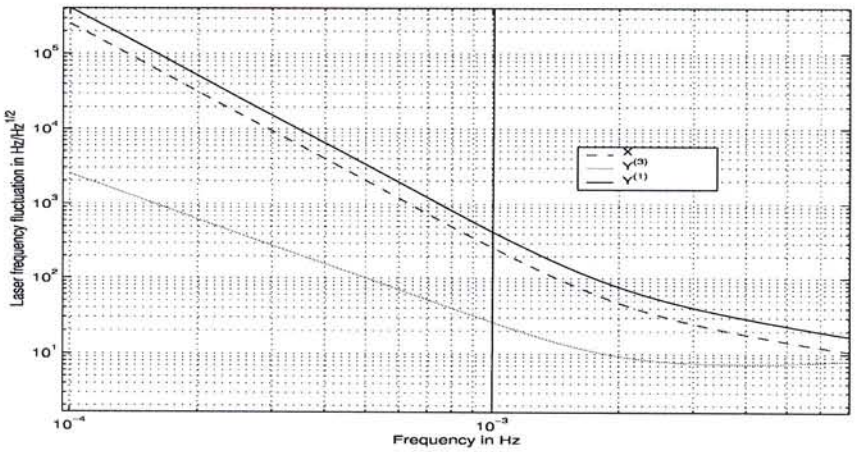

Figure 4.17: Laser frequency stabilisation $\widetilde{\Delta\nu}$ in $\mathrm{Hz}/\sqrt{\mathrm{Hz}}$ as function of frequency for $Y^{(1)}$, $Y^{(3)}$ and Michelson X combinations, for $\Delta L = 200$ m.

$Y_{(I)}$ in Fig. 4.17. For this assumed inaccuracy in arms, the $Y^{(3)}$ combination demands that the laser frequency stabilisation be at least as good as $\widetilde{\Delta\nu} \sim 25\ \mathrm{Hz}/\sqrt{\mathrm{Hz}}$ at 1 mHz. While for $Y^{(1)}$, the requirement is much less stringent on frequency stabilisation. The laser stabilisation requirement scales linearly with the assumed arm-length inaccuracy.

4.4 Conclusion

In this section we have used the results of the previous sections for optimising the sensitivity of LISA by analysing the noise and signal covariance matrices. Maximisation of the SNR is important for the detection and parameter estimation of a GW source. We have shown that the SNR for any data combination in the module, then lies between an upper and a lower bound. The upper and lower bounds of the SNR are functions of frequency and they correspond to the eigenvectors of the noise and signal covariance matrices. We have obtained the following results for the improvement in SNR: The improvement of SNR of the upper-bound over the Michelson combination goes upto 70% , at high frequencies $\gtrsim 5$ mHz, however, at low frequencies $\lesssim 5$ mHz, both have the same sensitivity. Since the eigenvectors are independent random variables, a 'network' SNR of independent detectors [24] has been constructed from likelihood considerations which gives an improvement between $\sqrt{2}$ and $\sqrt{3}$ over the maximum of SNRs of the eigenvectors. The improvement of the network SNR over the Michelson combination is about 40% at low frequencies $\lesssim 3$ mHz and rises above 100% at high frequencies.

Optimising the Directional Sensitivity of LISA

5.1 Introduction

The analysis of the emission of GW from known binaries could be extremely useful firstly for, direct determination of distances, and secondly, possible small general relativistic effects, if the SNR is large enough. For this reason, we focus on optimising the sensitivity of LISA for a given astrophysical source with known direction. Note that this optimisation is different from the one in the previous section where the direction of the source was not assumed to be known. The averaging then was performed also over the directions. Now we do *not* average over directions.

The sensitivity of LISA can be improved by solving technological problems, but it can also be improved by employing certain optimal data analysis strategies. Here, we show how algebraic methods previously developed in [25], can be used to design optimal strategies for combining data with appropriate time-delays. We first consider the simple case of a toy model where LISA rotates only in a plane. The reason for this analysis is to get some idea of the improvement in sensitivity without performing complex calculations. Later, we treat the case of the real orbit of LISA.

In the real orbit case, we show that it is possible to maintain the optimality during the year by continuously updating the parameters of the combination or simply by switching to optimal data combinations as the source appears to move in the LISA frame, as it moves in its complex orbit around the sun. The problem of optimisation of SNR, in this context, has been addressed before in [27] and [28]. In [27] optimisation has been carried out before averaging over the directions and polarisations, while in [28], the averaging is done first and then the optimisation. Given this situation, the averaging over the polarisations is performed first and then the SNR is optimised for the average signal for a given direction over the relevant data combinations - those data combinations cancelling laser frequency noise. Thus in this optimisation, the direction of source is assumed to be known, but not its polarisation. This would be the case for several binaries in our galaxy. We analyse two

observables in this context: (i) optimal data combination in the module which yields the maximum SNR for a given direction and (ii) a 'network' observable which is obtained by squaring and adding the SNRs of two independent (orthogonal) data combinations one of them being the optimal combination mentioned in (i) and another orthogonal to it. The network observable in general yields higher SNR. We analyse how these SNRs depend on direction of the source. For an integration time of one year, we compare our results by plotting sensitivity curves with those obtained from, (a) the Michelson combination X [29], which has been used for obtaining the standard sensitivity curve for LISA, and (b) the observable $X_{\rm switch}$ obtained by switching the three Michelson combinations optimally. We find that for sources lying in the ecliptic plane, the network sensitivity at low frequencies is about 34% more than the optimally switched Michelson combinations which rises to nearly 90% at 20 mHz. Finally we compute the optimal SNRs for six known binary systems in our galaxy, whose SNRs are significantly high, for an integration time of one year. We show that if at low frequencies the two SNRs of the orthogonal data combinations can be measured, then it is possible to estimate the inclination angle of the binary's orbit.

As before it is sufficient to consider LISA as an equilateral triangle; we ignore the deviations arising from this assumption. This simplifies the expressions for the noise and further also for the signal. The eigenvectors now contain overall common factors which are polynomials in E. These common factors make no difference to the computation of SNR as they cancel out from the numerator and denominator which comprise of the signal and the noise respectively. The unnormalised eigenvectors (with common factors cancelled) of the noise covariance matrix is the set $\{Y^{(I)}\}$ which we list below:

$$\begin{aligned} Y^{(1)} &= (1-E,\, 1+2E,\, -2-E,\, 1+2E,\, 1-E,\, -2-E)\,, \\ Y^{(2)} &= (-E-1,\, 1,\, E,\, -1,\, 1+E,\, -E)\,, \\ Y^{(3)} &= (1,\, 1,\, 1,\, 1,\, 1,\, 1)\,. \end{aligned} \tag{5.112}$$

We adopt the following terminology: we refer to a single element of the module as a data *combination*; while a function of the elements of the module, such as taking the maximum over several data combinations in the module or squaring and adding data combinations belonging to the module, is called as an *observable*. The important point to note is that the laser frequency noise is also suppressed for the observable although it may not be an element of the module.

5.2 The GW Signal from Binaries and the Signal Matrix

Since binaries will be important sources for LISA the analysis of such sources is relevant. One such class is of massive or super massive binaries whose individual masses could range

from $10^3 M_\odot$ to $10^8\ M_\odot$ and which could be around a Gpc away. Another class of interest are known binaries within our own galaxy whose individual masses are of the order of a solar mass but are just at a distance of a few kpc or less. Here we will assume the direction of the source to be known, which is justified for known binaries in our galaxy; but even for the former case of distant binaries, it amounts to 'looking' in a specific direction. For a binary that is not chirping, and hence monochromatic with frequency Ω, the two polarisation amplitudes $h_+(t)$ and $h_\times(t)$ [25] are given by the Eq.(3.74).

The GW response for a generator $Y^{(I)} = (p_j^{(I)}, q_j^{(I)})$ is,

$$h^{(I)}(\Omega) = F_+^{(I)}(\Omega) h_+(\Omega) + F_\times^{(I)}(\Omega) h_\times(\Omega)\,, \tag{5.113}$$

where,

$$\begin{aligned} F_+^{(I)}(\Omega) &= \sum_{i=1}^{3} \left(p_i^{(I)} F_{Vi;+} + q_i^{(I)} F_{Ui;+} \right)(\Omega)\,, \\ F_\times^{(I)}(\Omega) &= \sum_{i=1}^{3} \left(p_i^{(I)} F_{Vi;\times} + q_i^{(I)} F_{Ui;\times} \right)(\Omega)\,, \end{aligned} \tag{5.114}$$

where we have expressed the response of the two polarisations in terms of the responses of the elementary data streams for each of the polarisations. These are given in Eq. (3.53) and (3.54).

The signal matrix $h_{(J)}^{(I)}$ is given as follows:

$$\begin{aligned} h_{(J)}^{(I)} &= h^{(I)} h^*_{(J)}, \\ &= \left(F_+^{(I)} h_+ + F_\times^{(I)} h_\times \right) \left(F_{+(J)} h_+ + F_{\times(J)} h_\times \right)^* . \end{aligned} \tag{5.115}$$

In general we may not have any knowledge of the polarisation of the GW binary source. We therefore average over the polarisations and assume that the direction of the orbital angular momentum of the binary is uniformly distributed over the sphere. The orientation of the binary (its orbital angular momentum vector) has been described in terms of the angles ϵ and ψ in Eq.(3.74). Thus we carry out the averaging of $h_{(J)}^{(I)}$ over (ϵ, ψ) which results in an overall factor of $2/5$. The averaged matrix we denote by $\mathcal{H}_{(J)}^{(I)}$. In the Fourier domain it is given by,

$$\mathcal{H}_{(J)}^{(I)}(\Omega) = H^2 \left(\frac{2}{5} \right) \left(F_+^{(I)} F^*_{+(J)} + F_\times^{(I)} F^*_{\times(J)} \right)(\Omega)\,. \tag{5.116}$$

The signal matrix so averaged has the following properties:

- $\mathcal{H}$ is the sum of outer products of two vectors: $F_+^{(I)}$ with its complex conjugate and $F_\times^{(I)}$ with its complex conjugate. Thus the natural basis for expressing $\mathcal{H}$ consists of the two vectors $F_+^{(I)}$ and $F_\times^{(I)}$. In the analysis that follows we will use this fact.

- Because we average over the polarisations, $\mathcal{H}$ is constructed out of two vectors. Its rank is two, everywhere except on the $\theta = \frac{\pi}{2}$ plane where it is one when $F_{\times}^{(I)}$ goes identically to zero. Earlier, we had obtained a signal matrix of rank three because there we had averaged over the directions as well.

For simplicity first we describe a toy model, in which LISA rotates in a plane. In this analysis, we estimate the improvement in the LISA sensitivity, when we switch from one data combination to another in order to maintain optimality.

5.3 SNR Maximisation for a Toy Model of the LISA Triangle Rotating in a Plane

For simplicity we first consider a toy-model in which we assume that LISA rotates in the plane of the triangle formed by the spacescraft. This amounts to taking one motion into account, which is the rotation of LISA about an axis orthogonal to the plane containing the three space-craft. We ignore the other motion of LISA around the Sun. We note that the transfer functions of the beams U^i, V^i are computed in the frame of LISA. Hence, for the actual motion of LISA, a given GW source which is fixed on the celestial sphere will appear to follow a complex trajectory in this frame. Since LISA has a non-uniform directional response, it is a non-trivial problem to track the apparent motion of a 'fixed' GW source in the LISA frame and then compute its SNR. In the toy model this detail and complexity is bypassed, but at the same time the results are not too much compromised.

We choose the $X - Y$ plane to coincide with the plane formed by the three space-craft constituting the LISA triangle. The origin is chosen at the centre of the equilateral triangle (for computing the response, we take all the arms to be of equal length). The positive X-axis passes through space-craft 2. Figure 1 shows how the $X - Y$ axes have been chosen. The Z-axis is orthogonal to this plane with the positive direction given by the right-handed convention. Under these assumptions, the source would appear to move in the sky in a circular trajectory about the Z-axis with a period of one year. In terms of polar coordinates (θ, ϕ), the motion of such a source is uniform along ϕ with a constant value of θ. If one tracks a source with a single data combination, say $Y^{(1)}$, because the directional sensitivity of $Y^{(1)}$ is non-uniform, it does not track the source optimally. Figure (5.18) displays the 3-dimensional sensitivity plots of $Y^{(1)}$ and $Y^{(2)}$ as a function of the angles (θ, ϕ) for a monochromatic source at the GW frequency of 1 mHz and the signal uniformly averaged over the polarisations (this average is computed analytically). It is obvious from these plots that the sensitivity is a highly non-uniform function of source direction. We consider here the case when the source with GW frequency 1 mHz lies in the plane of the LISA triangle, that is, the GW source lies in the $\theta = \frac{\pi}{2}$ plane. We choose this value because,

Figure 5.18: Plot of log S, of the $Y^{(1)}$ and $Y^{(2)}$, are displayed in (a) and (b) respectively, as a function of θ and ϕ for $f = 1$ mHz and SNR=5 over a observation period of one year.

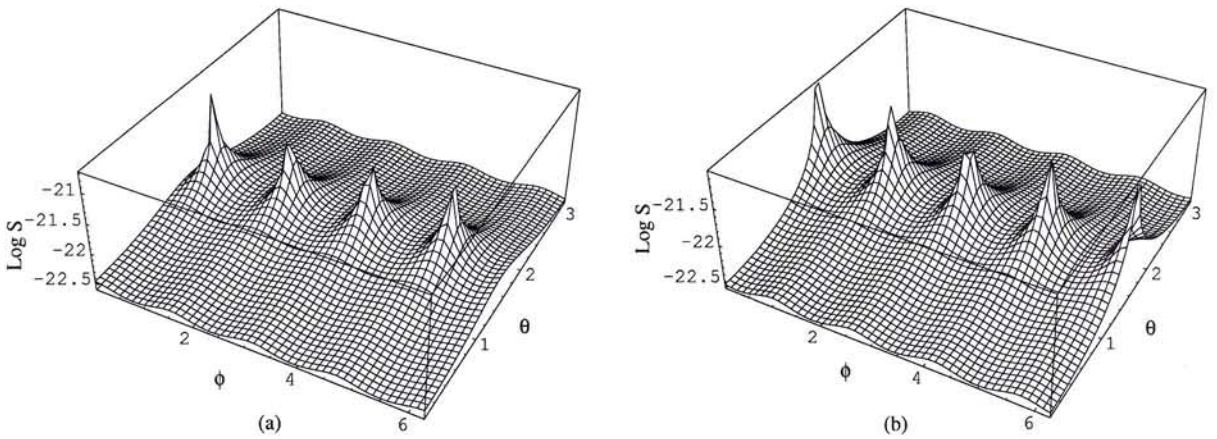

in the plane of LISA, the variations in the sensitivity are maximum for the combinations $Y^{(1)}$ and $Y^{(2)}$. From the Figures (5.18) and (5.19), we note that the generators $Y^{(I)}$ have zero sensitivity at few values of ϕ. This implies that no single data combination, even if it is a linear combination of these, can give optimal sensitivity. To obtain best results, one needs to maximise the SNR over the linear combinations $\alpha_{(I)}Y^{(I)}$.

We analyse two strategies for optimising the sensitivity:

(a) We consider the cyclic permutations of $Y^{(1)}$ and compute the maximum sensitivity using these three data combinations.

(b) We take the maximum of the linear combinations $\alpha_{(I)}Y^{(I)}$ where $\alpha_{(I)}$ are complex numbers. At each value of ϕ, a different linear combination of $Y^{(I)}$ is optimal. Thus the $\alpha_{(I)}$ for which the SNR is maximised are, in general, functions of ϕ.

The results of these analyses are described in Figure (5.21). For the strategy (a), the improvement in sensitivity averaged over ϕ is $\sim 49\%$; while for the strategy (b), the improvement in sensitivity averaged over ϕ is $\sim 59\%$. In addition Figure (5.20) shows the plots of $\alpha_{(I)}$ as function of ϕ, which maximise the SNR.

The strategy (a) does not give the best SNR as it maximises the response over only a set of three data combinations. On the other hand, strategy (b) maximises the SNR over the module and is therefore superior. It is interesting to note that the maximised SNR is constant as a function of ϕ and is the same as the SNR of $Y^{(1)}$ maximised over ϕ. We remark that the strategy (b) gives only marginal improvement over strategy (a), and also strategy (a) is easier to implement requiring relatively fewer computations.

Figure 5.19: Plot of sensitivity as a function angle ϕ at $\theta = \frac{\pi}{2}$ and $f = 1$ mHz after averaging over the polarisations.

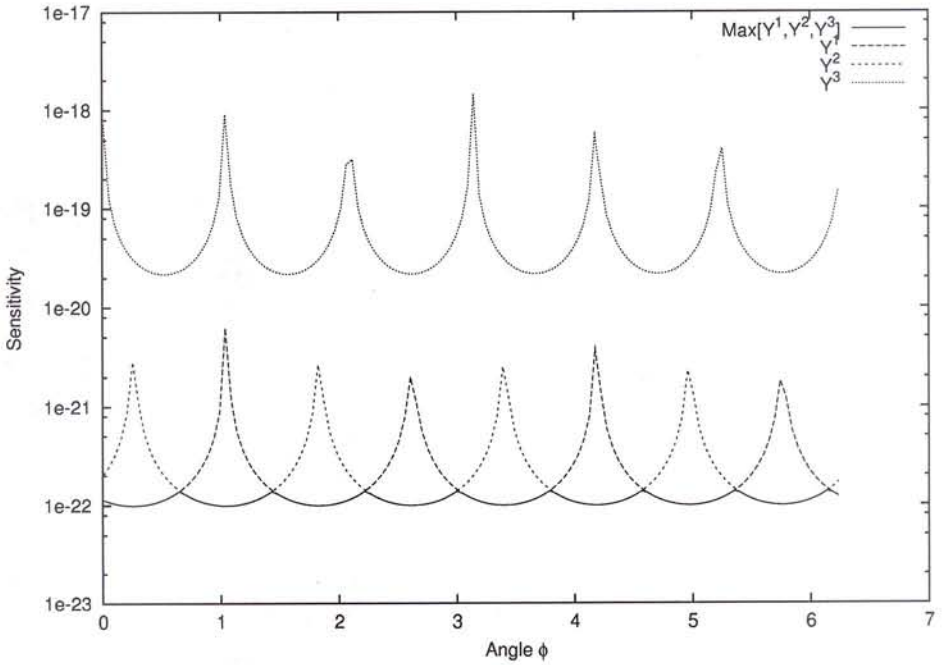

Figure 5.20: The coefficients $\alpha_{(I)}$ maximising the SNR of the combination $\alpha_{(I)}Y^{(I)}$ are plotted as functions of ϕ for the frequency 1 mHz and $\theta = \pi/2$.

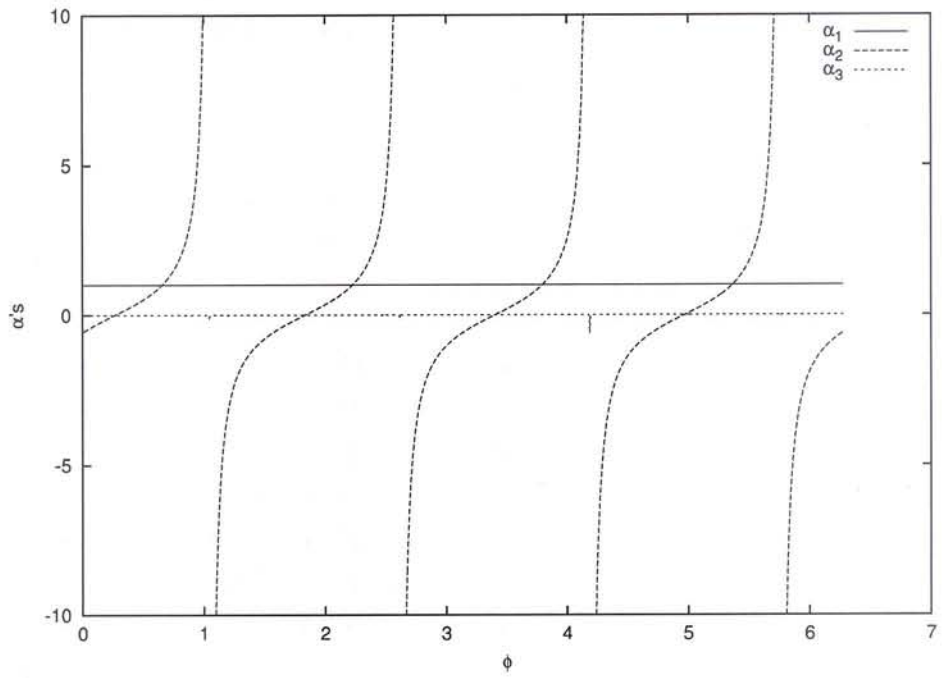

Figure 5.21: Sensitivity curves for the toy model of LISA are given as functions of ϕ at $f = 1$ mHz. The curves represented by broken lines correspond to the $Y^{(1)}$ and its cyclic permutations. The solid line curves represent the sensitivities for the two strategies: (a) taking the maximum of $Y^{(1)}$ and its cyclic permutations (thin solid line); (b) taking maximum over the linear combinations of $Y^{(I)}, I = 1, 2, 3$ (thick solid line).

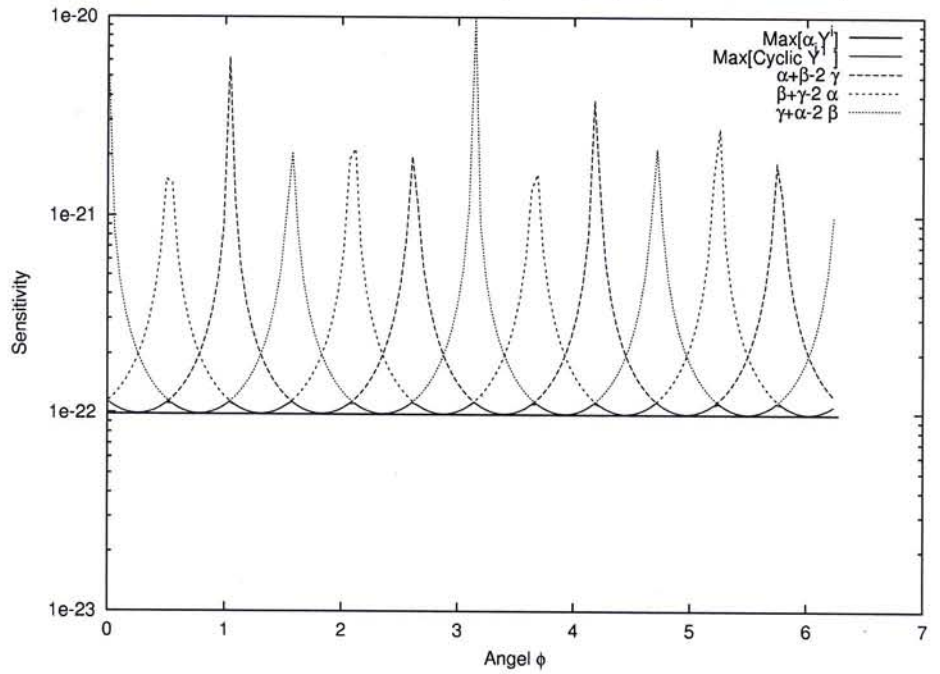

Figure 5.22: Plot of sensitivity S as a function of frequency, for the toy model.

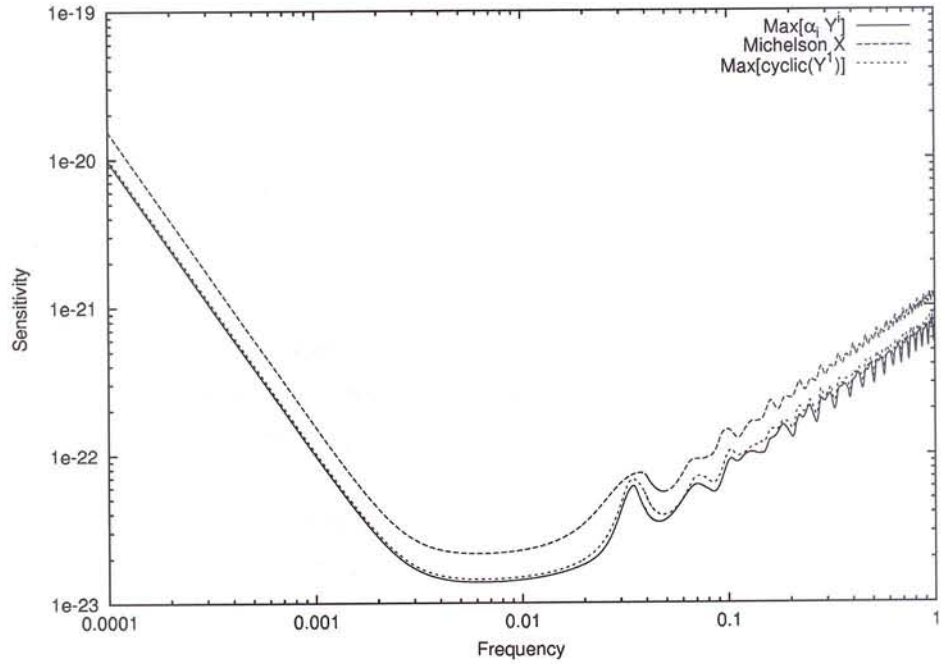

As seen for a GW source with a frequency of 1 mHz, strategy (b) gives a constant value for the maximum sensitivity over ϕ (see Figure (5.21)). Thus the maximum sensitivity is independent of ϕ for a given frequency. We further extend this analysis to other frequencies over the band-width of LISA, and obtain analogous results to the case of 1 mHz. This maximum sensitivity however depends on the frequency. In Figure (5.22), we present the maximum sensitivity curves as functions of frequency. For comparison, we perform analogous computations for the Michelson data combination X and the maximum of the cyclic permutations of $Y^{(1)}$. In all these cases, the GW amplitude is first averaged over the polarisations and then for a fixed frequency, the sensitivity as a function of ϕ is computed and then averaged over ϕ. Finally, this exercise is carried out for frequencies across the LISA band-width.

The 1 mHz case is representative of the low frequency regime $\lesssim 3$ mHz where the improvement in sensitivity is about 49% for strategy (a) and 59% for strategy (b). These improvements scale up at higher frequencies at say, ~ 15 mHz, to 56% and 67%, respectively, for the two strategies (a) and (b).

Using the simple toy model we have demonstrated that, if the source direction is known, the sensitivity can be increased by optimally switching the data combinations. This toy model can be further generalised for any given source direction and for realist orbital motion of the LISA triangle which is presented in the next section.

5.4 Optimising SNR the Actual Motion of LISA

In the rest of the section we now consider the real motion of LISA and optimise the SNR and sensitivity. This problem is more complex than the one considered in the previous section and much more analysis is necessary. Because LISA moves in a complicated orbit, a GW source which is fixed on the celestial sphere appears to move in the LISA frame. For optimising the directional sensitivity it is thus necessary to track the source by judiciously switching data combinations. We first optimise the SNR for a given direction by using the method of Lagrange multipliers and then integrate the optimal SNR over the observation period. For doing this the data combinations must necessarily be switched. We also treat the low frequency case separately, since it is of considerable astrophysical importance.

For a generic data combination $\alpha_{(I)}Y^{(I)}$ where $\alpha_{(I)}$ are polynomials in E, the SNR is given by:

$$SNR^2 = \frac{\alpha_{(I)}\alpha^{(J)*}\mathcal{H}^{(I)}_{(J)}}{\alpha_{(I)}\alpha^{(J)*}N^{(I)}_{(J)}}. \tag{5.117}$$

If the PSD is given in units of Hz^{-1} then the above equation yields the square of the SNR integrated over one second. Because one second is short compared to the various time-scales envisaged in the problem we call this SNR the *instantaneous* SNR. Since we are dealing with monochromatic sources, $E = e^{i\Omega L}$, the coefficients $\alpha_{(I)}$ reduce to just complex numbers. Also in the generating set $\{Y^{(I)}\}$ the noise covariance matrix is diagonal with diagonal elements $n^2_{(I)}$. However, we find $n_{(1)} = n_{(2)}$ in our case, so that the first two eigenvectors correspond to the same eigenvalue. Thus, the denominator of Eq.(5.117) simplifies to a sum of squares $|\alpha_{(1)}|^2 n_1^2 + |\alpha_{(2)}|^2 n_1^2 + |\alpha_{(3)}|^2 n_3^2$ which we can set equal to unity because the SNR does not depend on the normalisation of the data combination. Moreover, it is convenient to define coefficients β which are scaled by the noise, $\beta_{(1)} = \alpha_{(1)}n_1$, $\beta_{(2)} = \alpha_{(2)}n_2$, $\beta_{(3)} = \alpha_{(3)}n_3$ so that the $\beta_{(I)}$ satisfy,

$$|\beta_{(1)}|^2 + |\beta_{(2)}|^2 + |\beta_{(3)}|^2 = 1. \tag{5.118}$$

The expression for SNR simplifies to,

$$SNR^2 \;=\; \alpha^T \cdot \mathcal{H} \cdot \alpha \;= \beta^T \cdot \rho \cdot \beta, \tag{5.119}$$

where we define a SNR matrix ρ by,

$$\rho^{(I)}_{(J)} = \frac{\mathcal{H}^{(I)}_{(J)}}{n_{(I)}n_{(J)}}. \tag{5.120}$$

In the above equations the α, β are construed of as 3×1 column matrices and $\mathcal{H}$ and ρ as 3×3 square matrices.

The extremisation of SNR is now carried out with the method of Lagrange multipliers because of the normalisation constraint on β. This procedure yields an eigenvalue equation with the Lagrange multiplier appearing as an eigenvalue:

$$\rho \cdot \beta = \lambda \beta \,. \tag{5.121}$$

Since $\mathcal{H}$ has atmost rank 2, one eigenvalue is necessarily zero. We now proceed to compute the other two eigenvalues. The analysis is simplified if we go to the basis consisting of the two vectors $\vec{f_+}$ and $\vec{f_\times}$:

$$f_+^{(I)} = h_0 \frac{F_+^{(I)}}{n_{(I)}}, \quad f_\times^{(I)} = h_0 \frac{F_\times^{(I)}}{n_{(I)}}, \tag{5.122}$$

where $h_0 = (\sqrt{2/5})H$ is the amplitude of the GW averaged over the polarisation states at frequency Ω. We can then write the matrix ρ as a tensor product in terms of these two vectors:

$$\rho = \vec{f_+} \otimes \vec{f_+}^{\,*} + \vec{f_\times} \otimes \vec{f_\times}^{\,*} . \tag{5.123}$$

In general the vectors $\vec{f_+}$ and $\vec{f_\times}$ are not orthogonal.

The action of the matrix ρ on any vector $\vec{v}$ is given by,

$$\rho.\vec{v} \;=\; (\vec{f_+} \otimes \vec{f_+^*} + \vec{f_\times} \otimes \vec{f_\times^*}) \cdot \vec{v} \;=\; (\vec{f_+^*} \cdot \vec{v})\vec{f_+} + (\vec{f_\times^*} \cdot \vec{v})\vec{f_\times} \,. \tag{5.124}$$

For the eigenvalue problem, we have the eigenvalue equation,

$$(\vec{f_+^*} \cdot \vec{v})\vec{f_+} + (\vec{f_\times^*} \cdot \vec{v})\vec{f_\times} \;=\; \lambda \vec{v} \,. \tag{5.125}$$

Expressing the eigenvector $\vec{v}$ as a linear combination of $\vec{f_+}$ and $\vec{f_\times}$, $\vec{v} \;=\; c_+\vec{f_+} + c_\times \vec{f_\times}$, and from the linear independence of $\vec{f_+}$ and $\vec{f_\times}$ (they are linearly independent in general) we obtain the system of equations for c_+ and $c_\times$ as:

$$\begin{cases} (|\vec{f_+}|^2 - \lambda)c_+ + (\vec{f_+^*} \cdot \vec{f_\times})c_\times \;=\; 0 \\ (\vec{f_+} \cdot \vec{f_\times^*})c_+ + (|\vec{f_\times}|^2 - \lambda)c_\times \;=\; 0 \,. \end{cases} \tag{5.126}$$

Setting the determinant of this system to zero, we obtain eigenvalue equation:

$$\lambda^2 - (|\vec{f_+}|^2 + |\vec{f_\times}|^2)\lambda + |\vec{f_+} \times \vec{f_\times}|^2 = 0 \,, \tag{5.127}$$

which can be solved to yield the eigenvalues:

$$\lambda_\pm = \frac{1}{2}(|\vec{f_+}|^2 + |\vec{f_\times}|^2 \pm \sqrt{\Delta}), \tag{5.128}$$

where,

$$\begin{aligned} \Delta \;&=\; (|\vec{f_+}|^2 + |\vec{f_\times}|^2)^2 - 4|\vec{f_+} \times \vec{f_\times}|^2 \\ &=\; (|\vec{f_+}|^2 - |\vec{f_\times}|^2)^2 + 4|\vec{f_+} \cdot \vec{f_\times}^{\,*}|^2 . \end{aligned} \tag{5.129}$$

In the low frequency limit as we shall find $\vec{f_+} \cdot \vec{f_\times}^* \approx 0$ so that the positive square root of Δ is just $|\vec{f_+}|^2 - |\vec{f_\times}|^2$ and the eigenvalues are just $|\vec{f_+}|^2$ and $|\vec{f_\times}|^2$ (infact the eigenvalue equation factorises into linear factors) with $\vec{f_+}$ and $\vec{f_\times}$ as eigenvectors respectively. This can also be directly inferred from the structure of ρ. So it may be appropriate to call λ_- as $\lambda_\times$ even in the general case. In the general case the eigenvectors can be easily determined from Eq.(5.126):

$$\begin{aligned} \vec{v}_+ &= (\lambda_+ - |\vec{f_\times}|^2)\vec{f_+} + (\vec{f_\times}^* \cdot \vec{f_+})\vec{f_\times}\,, \\ \vec{v}_\times &= (\vec{f_\times} \cdot \vec{f_+}^*)\vec{f_+} + (\lambda_\times - |\vec{f_+}|^2)\vec{f_\times}\,, \end{aligned} \tag{5.130}$$

where $\vec{v}_{+,\times}$ are eigenvectors belonging to the eigenvalues $\lambda_{+,\times}$ respectively. Since ρ is Hermitian the eigenvectors are orthogonal, $\vec{v}_+ \cdot \vec{v}_\times^* = 0$ as can be verified also directly from the expressions of the eigenvectors. These eigenvectors are not normalised.

The eigenvalues $\lambda_{+,\times}$ are the squares of the instantaneous SNRs for the two data combinations described by the two corresponding eigenvectors. The data combinations are $\vec{v}_{+(I)}Y^{(I)}$ and $\vec{v}_{\times(I)}Y^{(I)}$, which we will call eigen-combinations or alternatively eigen-observables, and which give the instantaneous SNRs: $\mathrm{SNR}^2_{+,\times} \equiv \lambda_{+,\times}$ respectively. For a given direction (θ, ϕ) in the LISA frame, SNR_+ is the maximum instantaneous SNR among all data combinations. While $\mathrm{SNR}_\times$ is the minimum instantaneous SNR among data combinations that are linear combinations of $\vec{v}_+$ and $\vec{v}_\times$; those which lie in the 'plane' of $\vec{v}_+$ and $\vec{v}_\times$. However, $\mathrm{SNR}_\times$ is not zero in general and therefore not the absolute minimum; the absolute minimum SNR is zero corresponding to the third eigenvalue which is zero. Moreover, the eigenvectors are orthogonal, which means they yield statistically independent observables. Thus these observables can be combined in quadratures to form a network observable with instantaneous $\mathrm{SNR}_{\mathrm{network}}$ given by:

$$\begin{aligned} \mathrm{SNR}^2_{\mathrm{network}} &= \mathrm{SNR}^2_+ + \mathrm{SNR}^2_\times, \\ &= \lambda_+ + \lambda_\times = |\vec{f_+}|^2 + |\vec{f_\times}|^2. \end{aligned} \tag{5.131}$$

The third eigenvector is $\vec{f_+}^* \times \vec{f_\times}^*$; it is orthogonal to $\vec{f_+}$ and $\vec{f_\times}$ with eigenvalue zero[2]. This means that the data combination corresponding to this vector gives zero response in that particular direction, which may be important if one wishes to 'switch off' the GW coming from that direction.

5.5 Tracking a GW Source with LISA

In general the amplitude of the GW source will be small and it would be necessary to track or follow the source for a considerable period of time in order to accumulate an adequate

[2]While defining the vector cross product of two complex vectors, we require its scalar product with both vectors to vanish. Since the scalar product is defined by taking the complex conjugate of the second vector, complex conjugates appear in the cross product.

SNR. This period of time could range from few days to a year or even years - the life of the LISA experiment. The LISA configuration performs a complex motion due to which the source will appear to move in the LISA frame even if it is stationary in the barycentric frame. For the purposes of this analysis, we will take the observation time to be a year and integrate the SNR for this period of time. It is possible that some GW sources may be sufficiently powerful that SNR integration for an year is not required. In that case it is easily possible to limit the integration to the required period of observation and obtain useful results. We will also assume that the source is stationary in the barycentric frame, that is, its direction remains constant during the observation period. In this section we will present the transformations connecting the barycentric frame and the LISA frame and hence obtain the apparent motion in the LISA frame for a GW source fixed in the barycentric frame.

The LISA constellation trails the Earth in its orbit by 20° around the sun. The plane of LISA makes an angle of 60° with the plane of the ecliptic and the LISA triangle rotates in its own plane completing one rotation in a year. We describe the barycentric frame by the Cartesian coordinates $\{x_B, y_B, z_B\}$. The $x_B - y_B$ plane coincides with the orbital plane of LISA. The z_B-axis is orthogonal to this plane forming a right-handed coordinate system. The transformation from the barycentric frame to LISA frame is given as follows [23]: A vector $\mathbf{r_B} = (x_B, y_B, z_B)^T$ is transformed to $\mathbf{r_L} = (x_L, y_L, z_L)^T$ by the matrix $\mathcal{R}$ as,

$$\mathbf{r_L} = \mathcal{R} \cdot \mathbf{r_B}, \tag{5.132}$$

where $\mathcal{R}$ is a product of the three matrices containing Euler angles:

$$\mathcal{R} = \mathcal{C} \cdot \mathcal{B} \cdot \mathcal{A}, \tag{5.133}$$

where the matrices $\mathcal{A}$, $\mathcal{B}$ and $\mathcal{C}$ are given by,

$$\begin{aligned}
\mathcal{A} &= \begin{pmatrix} \cos\psi_a & \sin\psi_a & 0 \\ -\sin\psi_a & \cos\psi_a & 0 \\ 0 & 0 & 1 \end{pmatrix}, \\
\mathcal{B} &= \begin{pmatrix} 1 & 0 & 0 \\ 0 & \frac{1}{2} & \frac{\sqrt{3}}{2} \\ 0 & -\frac{\sqrt{3}}{2} & \frac{1}{2} \end{pmatrix}, \\
\mathcal{C} &= \begin{pmatrix} \cos\psi_c & \sin\psi_c & 0 \\ -\sin\psi_c & \cos\psi_c & 0 \\ 0 & 0 & 1 \end{pmatrix}.
\end{aligned} \tag{5.134}$$

Here $\psi_a = \omega t + \alpha_0$, $\psi_c = -\omega t + \beta_0$ and $\omega = 2\pi/T_\odot$. $T_\odot$ is the orbital period of LISA which we take to be of one year duration. The α_0 and β_0 are constants fixing initial conditions

when the observation begins. The matrix $\mathcal{R}$ is time-dependent and is a product of two time-dependent matrices.

The unit vector $\hat{w}_B$ of the source direction described by the angles (θ_B, ϕ_B) in the barycentric frame is given by $\hat{w}_B = (\sin\theta_B \cos\phi_B, \sin\theta_B \sin\phi_B, \cos\theta_B)$. The corresponding vector $\hat{w}_L$ in the LISA frame is then, $\hat{w}_L = \mathcal{R}(t) \cdot \hat{w}_B$. From this vector we can explicitly work out the angles (θ_L, ϕ_L):

$$\begin{aligned} \theta_L &= \cos^{-1}\left(\frac{1}{2}\cos\theta_B - \frac{\sqrt{3}}{2}\sin\theta_B \sin(\phi_B - \psi_a)\right), \\ \phi_L &= \tan^{-1}\left(\frac{w_L^2}{w_L^1}\right), \end{aligned} \tag{5.135}$$

where,

$$\begin{aligned} w_L^1 &= \cos\psi_c \sin\theta_B \cos(\phi_B - \psi_a) \\ &\quad + \frac{1}{2}\sin\psi_c \sin\theta_B \sin(\phi_B - \psi_a) \\ &\quad + \frac{\sqrt{3}}{2}\sin\psi_c \cos\theta_B, \\ w_L^2 &= -\sin\psi_c \sin\theta_B \cos(\phi_B - \psi_a) \\ &\quad + \frac{1}{2}\cos\psi_c \sin\theta_B \sin(\phi_B - \psi_a) \\ &\quad + \frac{\sqrt{3}}{2}\cos\psi_c \cos\theta_B. \end{aligned} \tag{5.136}$$

For a fixed source direction (θ_B, ϕ_B) in the barycentric frame, the apparent source direction depends on time in the LISA frame; θ_L, ϕ_L are functions of time; the source appears to move in the LISA frame. Thus a given data combination even if it is optimal initially, will not continue to remain optimal subsequently. Our strategy is then to *switch* the data combinations continuously so that the SNR remains optimal at all times. In this way we can optimally track the source and accumulate maximum SNR. The following figures show the apparent trajectory of the source for one year in the LISA frame when (i) the source lies at the pole of the barycentric frame - it is just a circle in the LISA frame: $\theta_L = \pi/3$ (See Fig.5.23) and (ii) the source lies in plane of the LISA orbit - a figure of 8 is described by the source (See Fig.5.24).

5.6 Optimising the Directional Sensitivities

For optimal tracking of the source, we switch the data combinations so that the SNRs yielded are optimal at all times. Three SNRs are of interest; $SNR_{+,\times}$ and $\mathrm{SNR}_{\mathrm{network}}$, that is, the two eigenvalues and their sum. The eigenvalues are functions of θ_L, ϕ_L which

Figure 5.23: Apparent position of the source in the sky as seen from LISA frame for ($\theta_B = 0$, $\phi_B = 0$). The track of the source for a period of one year is shown on the unit sphere in the LISA frame.

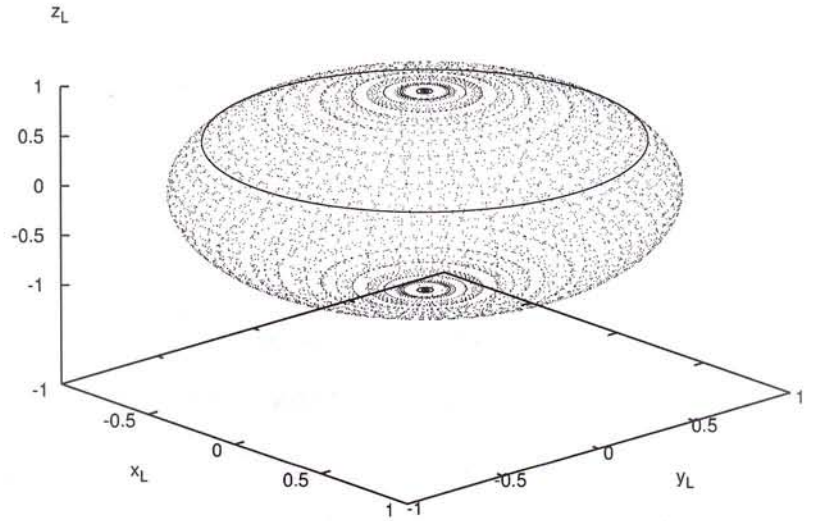

Figure 5.24: Apparent position of the source in the sky as seen from LISA frame for ($\theta_B = \frac{\pi}{2}$, $\phi_B = 0$). The track of the source for a period of one year is shown on the unit sphere in the LISA frame.

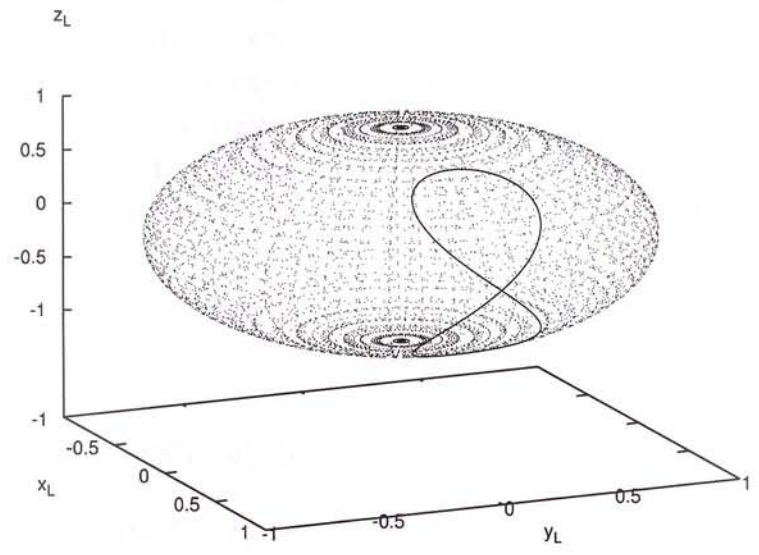

are in turn functions of t as the GW source describes its apparent motion in the LISA frame. The three integrated SNRs are given by:

$$\begin{aligned} \mathrm{SNR}^2_{+,\times}(\hat{w}_B) &= \int_0^T \lambda_{+,\times}(\theta_L(t;\hat{w}_B),\phi_L(t;\hat{w}_B))dt, \\ \mathrm{SNR}^2_{\mathrm{network}}(\hat{w}_B) &= \mathrm{SNR}^2_{+}(\hat{w}_B) + \mathrm{SNR}^2_{\times}(\hat{w}_B), \end{aligned} \tag{5.137}$$

where we have taken the total observation time to be T and the initial time of observation to be zero. If we integrate for a complete year, we can set the initial observation time to be zero without loss of generality and at the same time set the constants α_0, β_0 to be zero. However, if we make observations for times that are not integral number of years, the constants α_0, β_0 must be chosen appropriately in the transformation matrix $\mathcal{R}$.

An important point is that, since LISA moves in an heliocentric orbit, a Doppler phase depending on the position vector of the LISA projected on to the direction to the source $\hat{w}_B$ and the GW frequency will be added to the phase of the GW signal. This Doppler phase will be a function of time which will be added to the monochromatic part of the phase Ωt of the signal. We assume in this analysis that this phase has been accounted for when integrating the signal. One way is to 'stretch' the time-coordinate so that the signal appears monochromatic (a technique well-known to radio astronomers) [30, 31].

5.6.1 The Low Frequency Limit

An important case arises when we consider GW of low frequencies, say below 3 mHz. For this case it is possible to obtain analytical expressions for the optimal SNRs. A large fraction of the sources for LISA fall into this category, for example, massive/supermassive blackhole binaries, several galactic and extragalactic binaries which contribute to the 'confusion noise'.

We need to compute the $\vec{f_+}$ and $\vec{f_\times}$ in order to compute the SNR matrix ρ and then obtain its eigenvalues. Integrating the eigenvalues for the period of observation will yield the relevant SNRs. To this end, we expand $F_{Ui;+,\times}$ and $F_{Vi;+,\times}$ to the lowest order in the dimensionless frequency ΩL:

$$\begin{aligned} F_{U1;+,\times} &= i\frac{\Omega L}{2}\left(1 + i\Omega L\,\tau_2\right)\xi_{2;+,\times}, \\ F_{V1;+,\times} &= -i\frac{\Omega L}{2}\left(1 + i\Omega L\,\tau_3\right)\xi_{3;+\times}, \end{aligned} \tag{5.138}$$

where,

$$\begin{aligned} \tau_m &= \frac{1}{2}\left(1 - \frac{\hat{w}\cdot\hat{r}_m}{\sqrt{3}}\right), \\ \xi_{m;+} &= \frac{\left(1+\cos^2\theta\right)}{2}\cos\left(2\phi - (2m-1)\frac{\pi}{3}\right) - \frac{1}{2}\sin^2\theta, \\ \xi_{m;\times} &= -\cos\theta\sin\left(2\phi - (2m-1)\frac{\pi}{3}\right), \end{aligned} \tag{5.139}$$

where, $\hat{r}_m$ is the unit vector in the direction of m-th spacecraft and $m = 1, 2, 3$ and the angles θ, ϕ refer to the LISA frame (as before we have dropped the subscript 'L'). The transfer functions for the four other elementary data streams are obtained by cyclic permutations. In order to get the $\vec{f_+}, \vec{f_\times}$ we must operate on the U^i, V^i with the polynomial operators $p_i^{(I)}, q_i^{(I)}$ given in Eq.(5.113) and then scale them by the averaged signal divided by the noise. Thus, we obtain after some algebra,

$$\begin{aligned} \vec{f_+} &= \rho_0 \frac{(1+\cos^2\theta)}{2}(-\sin\Phi, \cos\Phi, 0), \\ \vec{f_\times} &= -\rho_0 \cos\theta(\cos\Phi, \sin\Phi, 0), \end{aligned} \tag{5.140}$$

where,

$$\rho_0 = \frac{3}{\sqrt{5}}\frac{H}{n_1}(\Omega L)^2, \quad \Phi = 2\phi + \frac{\pi}{3}. \tag{5.141}$$

The vectors $\vec{f_+}$ and $\vec{f_\times}$ are expressed in the $Y^{(I)}$ basis and in this basis they have real components. We observe the following properties of the vectors:

- The vectors $\vec{f_+}$ and $\vec{f_\times}$ lie in the $(Y^{(1)}, Y^{(2)})$ plane and the $Y^{(3)}$ component is zero for both vectors. This can be understood if we recall that $Y^{(3)}$ is proportional to symmetric Sagnac combination [28] which is insensitive to GW at low frequency.

- The apparent motion of a GW source in the LISA frame can be optimally and continuously tracked by $\hat{f}_+$ and $\hat{f}_\times$ by rotating the pair $(\hat{f}_+, \hat{f}_\times)$ by Φ at each instant of time as follows:

$$\begin{pmatrix} \hat{f}_\times \\ \hat{f}_+ \end{pmatrix} = \begin{pmatrix} \cos\Phi & \sin\Phi \\ -\sin\Phi & \cos\Phi \end{pmatrix} \begin{pmatrix} Y^{(1)} \\ Y^{(2)} \end{pmatrix}. \tag{5.142}$$

  Here $\hat{f}_+$ and $\hat{f}_\times$ are unit vectors in the directions of $\vec{f_+}$ and $\vec{f_\times}$ respectively. Thus, optimally tracking a source amounts to orienting the data combinations along $\vec{f_+}$ and $\vec{f_\times}$.

- Moreover, the vectors are orthogonal: $\vec{f_+} \cdot \vec{f_\times}^* = 0$ in this low frequency limit. The orthogonality implies that these eigen-observables $\vec{f_+}$ and $\vec{f_\times}$ have zero response to $\times$ and $+$ polarisations of GW respectively. We use this fact to estimate the polarisation angles; namely (ϵ, ψ) at the end of this section.

The eigenvalues of the eigen-vectors $\vec{f_+}$ and $\vec{f_\times}$ are just $|\vec{f_+}|^2$ and $|\vec{f_\times}|^2$ and are explicitly given by,

$$\begin{aligned} \lambda_+ &= \rho_0^2 \left(\frac{1+\cos^2\theta}{2}\right)^2, \\ \lambda_\times &= \rho_0^2 \cos^2\theta. \end{aligned} \tag{5.143}$$

Figure 5.25: Instantaneous $SNR_{+,\times}$ and $\mathrm{SNR}_{\mathrm{network}}$ as functions of time for the source direction $(\theta_B = \frac{\pi}{2},\, \phi_B = 0\,)$ at the GW frequency of $f = 1$ mHz in units of ρ_0.

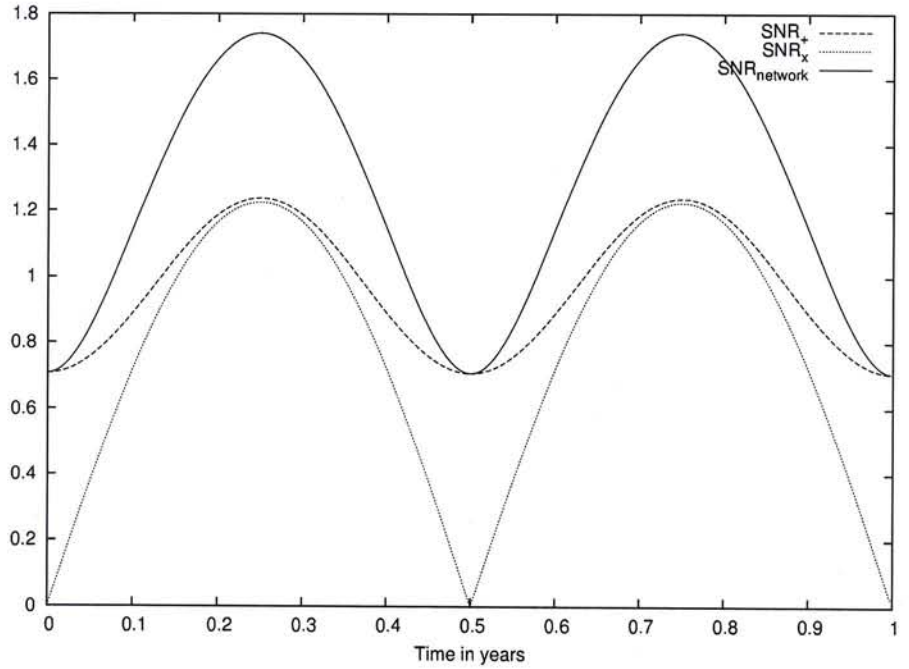

The eigenvalues are the squares of the instantaneous SNRs. We notice that ρ_0 is the maximum instantaneous SNR obtained when the source lies at the poles $\theta = 0$ or π in the LISA frame. If the source is observed over a period of an year, the eigenvalues must be integrated over this length of time. We notice that the eigenvalues do not depend on ϕ. Thus our next task of integrating the SNR becomes somewhat simplified.

5.6.2 The Integrated SNR

For a given source direction (θ_B, ϕ_B) the corresponding track $(\theta_L(t), \phi_L(t))$ of the source in LISA frame is given by Eq.(5.135). We may substitute these values into the integrals for the SNRs and the integrals yield simple analytical expressions for the SNRs if the integration is over an integral number of years. The instantaneous SNRs however change with time. In the Fig.5.25 we show how the SNRs change with time as LISA orbits the sun during the course of a year. The various SNRs are shown for a source lying in the ecliptic plane, $(\theta_B = \pi/2, \phi_B = 0)$ for the GW frequency of 1 mHz. We have chosen this direction because the SNRs show considerable variations during the course of a year.

Integration over a period of $T = T_\odot$ leads to the following results:

$$\begin{aligned} SNR_+(\theta_B, \phi_B) &= \mathrm{SNR}_0\; g_+(\cos\theta_B)\,, \\ SNR_\times(\theta_B, \phi_B) &= \mathrm{SNR}_0\; g_\times(\cos\theta_B)\,, \end{aligned} \tag{5.144}$$

where,

$$\mathrm{SNR}_0 = \rho_0\sqrt{T_\odot} = \frac{3}{\sqrt{5}}\frac{H}{n_1}(\Omega L)^2\sqrt{T_\odot}\,, \tag{5.145}$$

and

$$\begin{aligned} g_+^2(x) &= \frac{1}{T_\odot}\int_0^{T_\odot}\left(\frac{1+\cos^2\theta_L}{2}\right)^2 dt \\ &= \frac{1}{4}\left(1+\frac{x^2}{4}\right)^2 \\ &\quad +\frac{3}{16}(1-x^2)\left(1+\frac{3}{4}x^2+\frac{9}{32}\left(1-x^2\right)\right), \\ g_\times^2(x) &= \frac{1}{T_\odot}\int_0^{T_\odot}\cos^2\theta_L dt \\ &= \frac{1}{4}\left[x^2+\frac{3}{2}\left(1-x^2\right)\right]. \end{aligned} \tag{5.146}$$

We have purposely not 'simplified' the formulae in powers of x^2 because in this form it is easy to see the limits $x = \pm 1, 0$ corresponding to $\theta_B = 0, \pi, \pi/2$ respectively. Infact since only x^2 occurs in the expressions of $g_{+,\times}$ there is symmetry about the ecliptic plane. The network SNR is just the root mean square of the two SNRs:

$$\mathrm{SNR}_{\mathrm{network}}(\theta_B, \phi_B) = \mathrm{SNR}_0\; g_{\mathrm{network}}(\cos\theta_B)\,, \tag{5.147}$$

where, $g^2_{\mathrm{network}}(x) = g^2_+(x) + g^2_\times(x)$. In Fig.5.26 we plot the functions $g_{+,\times}$ and g_{network} as functions of θ_B between $0^o \leq \theta_B \leq 180^o$. The factors g are of the order of unity and the SNR_0 gives essentially the integrated SNR of a GW source. Recall that this is an SNR averaged over the polarisations.

We observe from Fig.5.26 that the maximum integrated SNR is obtained for sources lying in the ecliptic plane ($\theta_B = 90°$). This can be readily explained from Fig.5.24 where the trajectory of such a source is plotted. One observes that a large fraction of the orbit in the LISA frame is *away* from the LISA plane ($\theta_L = 90°$). As seen from Eq.(5.143) the sensitivity of LISA increases as we go away from the plane of LISA, that is, towards the poles. We also observe that the variations in the three curves are small; among these the network SNR shows the highest variation of $\approx 15\%$. This shows that LISA has a more or less uniform average response over the year as it moves in its orbit.

The above formulae are also more generally valid if the integration time T is taken to be in integral multiples of $T_\odot$; then the $T_\odot$ in Eq.(5.145) should be replaced by T. We compute the SNRs of six binaries in our galaxy which give high average SNR (averaged over polarisations) if we integrate the SNR optimally over the period of a year. The following table lists six binary systems which give the network SNRs ranging from about 3 to over 100. The SNRs have been computed assuming circular orbits for the binaries.

Figure 5.26: The functions $g_{+,\times}$ and g_{network} as functions of θ_B

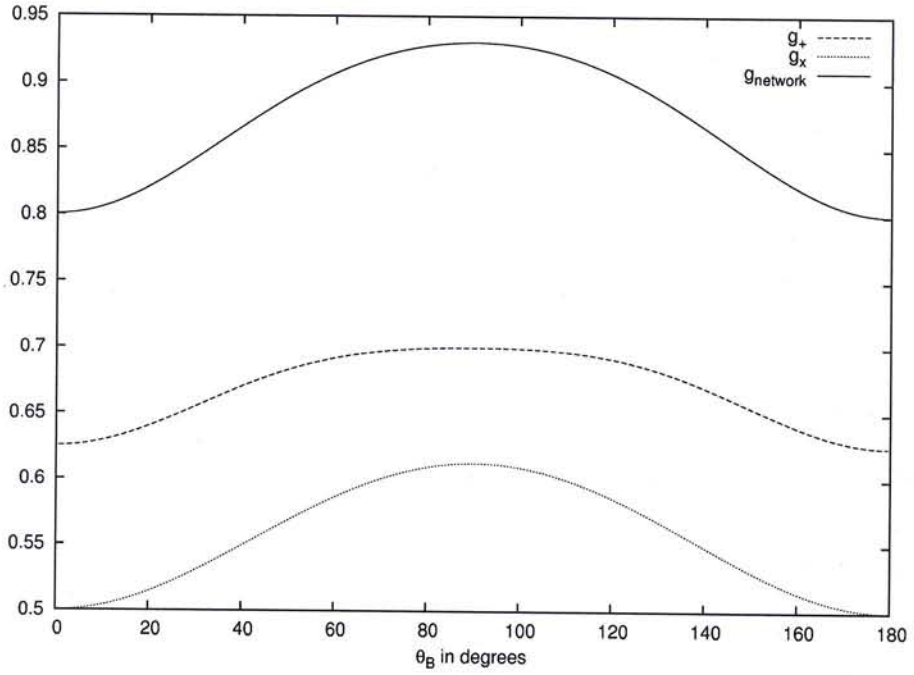

The information about the binaries has been obtained from [32]. We observe that the binary masses are small; $\sim .5M_\odot$ and companion mass $\sim .02M_\odot$. The reason for such small masses is that the orbital periods of the binaries must be short, in this case ranging from about .01 to .03 of a day. The GW quadrupole frequency f_{gw} is related to the orbital period by the equation:

$$f_{gw} = \frac{2}{P_{orb}} = 2.3 \left(\frac{P_{orb}}{.01\text{day}} \right)^{-1} \text{mHz}. \tag{5.148}$$

Thus the sources radiate GW at frequencies $\sim$ 1 or 2 mHz, the band in which LISA has maximum sensitivity. This yields the high SNRs. They are also close by; $R \sim 100$ or 200 pc which tends to increase the raw gravitational wave amplitude H. Note that the SNRs listed in the table are average and actual observations can yield different values depending on the orientation of the binary orbit. Also the observables used are optimal in the average sense. If the orientation of the binary is known then in general a better observable can be found.

Table 5.1: In this table we list six binaries in our galaxy whose parameters are known. For these we compute the optimum SNRs where the optimisation has been performed after averaging over the polarisations.

Name	P_{orb} in days	m_1	m_2	$\log(H)$	θ_B°	R in pc	SNR_+	$SNR_\times$	$SNR_{network}$
AM CVn	0.011907	0.5	0.03	-21.4	124.46	100	89.9	75.6	117.4
CP Eri	0.019950	0.6	0.02	-22.0	116.43	200	8.9	7.4	11.4
CR Boo	0.017029	0.6	0.02	-21.7	72.103	100	26.3	22.7	34.7
GP Com	0.032310	0.5	0.02	-22.2	66.997	200	2.2	1.8	2.8
HP Lib	0.012950	0.6	0.03	-21.4	85.040	100	77.6	67.8	103.0
V803 Cen	0.018650	0.6	0.02	-21.7	120.32	100	20.6	17.5	27.0

5.6.3 Estimation of Inclination Angle of the Orbital Plane

We showed in previous sections that if we do not have any prior information of the inclination angle ϵ of the binary orbit and the the angle ψ, then tracking the source with $\hat{f}_+$ and $\hat{f}_\times$ are optimal in the average sense. Typically, the orbital inclination is difficult to estimate from other astrophysical observational means. However, for binaries with known masses and distances (e.g. binaries in table-5.1), we can estimate (ϵ, ψ) from the output of eigen-observables $\vec{f_+}$ and $\vec{f_\times}$. The integrated SNRs over the period of one year of $\vec{f_+}$ and $\vec{f_\times}$, *without averaging over polarisations* are given by

$$\begin{aligned} SNR_+(\theta_B, \phi_B) &= \sqrt{\frac{5}{2}}\, \mathrm{SNR}_0\, g_+(\cos\theta_B)\, a_+ \,, \\ SNR_\times(\theta_B, \phi_B) &= \sqrt{\frac{5}{2}}\, \mathrm{SNR}_0\, g_\times(\cos\theta_B)\, a_\times, \end{aligned} \tag{5.149}$$

where $a_+ = |h_+(\Omega)/H|$ and $a_\times = |h_\times(\Omega)/H|$ (see Eq. (3.74)). We note that here the factor $\sqrt{5/2}$ appears, since there is no averaging over the polarisations. The $a_{+,\times}$ can be estimated, if the SNRs appearing on the LHS of Eq. (5.149) can be measured. Further, straightforward algebra shows that

$$a_+^2 + a_\times^2 = \left(\frac{1+\cos^2\epsilon}{2}\right)^2 + \cos^2\epsilon. \tag{5.150}$$

From the above equation, we can estimate ϵ. Substituting back in a_+, one can also estimate ψ if needed. This exercise can be carried out for the binaries listed in the table 5.1.

5.6.4 The General Case

In this section we relax the condition of dealing only with low frequencies and consider the entire band-width of LISA. We compare the sensitivities for LISA obtained by using the optimum SNR with the Michelson data combination usually denoted by X. As a

polynomial vector (p_i, q_i) it is given by:

$$X = (1 - E_2^2, 0, E_2(E_3^2 - 1), 1 - E_3^2, E_3(E_2^2 - 1), 0). \tag{5.151}$$

When we set all the E_i to be equal, the factor $(1 - E^2)$ factors out and one is left with a simple polynomial vector $(1, 0, -E, 1, -E, 0)$. This combination has been used to plot the standard LISA sensitivity curve. Two other Michelson observables are obtained by cyclic permutations called Y and Z in the literature [16]. In this section we will compare the sensitivities obtained by using the eigen-combination $\vec{v}_+$ and the network observable with the Michelson combination X and the observable $X_{\rm switch}$ obtained by 'switching' the Michelson's X, Y, Z optimally, that is, $SNR_{X_{\rm switch}} = \max(SNR_X, SNR_Y, SNR_Z)$. Extending the definition of sensitivity of a data combination given in Eq. (3.78) to an observable, we define the sensitivity of an observable W as,

$$\text{Sensitivity}_W(f) = \frac{5}{SNR_W(f)}, \tag{5.152}$$

where $SNR_W(f)$ is the integrated SNR over a observation period T. The number 5 has been chosen following earlier literature. Eq. (5.152) for a fixed data combination W_0 reduces to the standard one in literature:

$$\text{Sensitivity}_{W_0}(f) = 5\frac{\sqrt{S_{W_0}(f)B}}{|h_{W_0}|}, \tag{5.153}$$

where $B = 1/T$. As before we take $T = T_\odot$ for plotting the sensitivity curves in the figures below. The results of our findings are displayed in the plots. Fig.5.27 displays the sensitivity curves for the observables (a) Michelson - X (dotted curve), (b) Switched Michelson $X_{\rm switch}$ (dash-dotted curve), (c) Eigen-combination $\vec{v}_+$ (dashed curve) and (d) network observable (solid curve). We observe that the sensitivity over the band-width of LISA increases as we go from (a) to (d). We observe that the $X_{\rm switch}$ does not do much better than X. This is because for the source direction chosen X is reasonably well oriented and there is not much switching to Y and Z combinations. However, the network and $\vec{v}_+$ observables show significant improvement in sensitivity over both X and $X_{\rm switch}$. The sensitivity curves (except X) do not show much variations for other source directions and the plots are similar. The quantitative comparison of sensitivities is shown in Fig.5.28.

Here we have compared the network, and the eigen-combinations $\vec{v}_{+,\times}$ with $X_{\rm switch}$. Defining:

$$\kappa_a(f) = \frac{\text{SNR}_a(f)}{\text{SNR}_{X_{\rm switch}}(f)}, \tag{5.154}$$

where the subscript a stands for network or $+, \times$ and $\text{SNR}_{X_{\rm switch}}$ the SNR of the observable $X_{\rm switch}$, we plot these ratios of sensitivities over the LISA band-width. We notice from the $\kappa_{\rm network}$ curve that the improvement in sensitivity for the network observable is about

Figure 5.27: Sensitivity curves for the observables: Michelson, Switched Michelson, $\vec{v}_+$ and network for the source direction $\theta_B = 90°, \phi_B = 0°$.

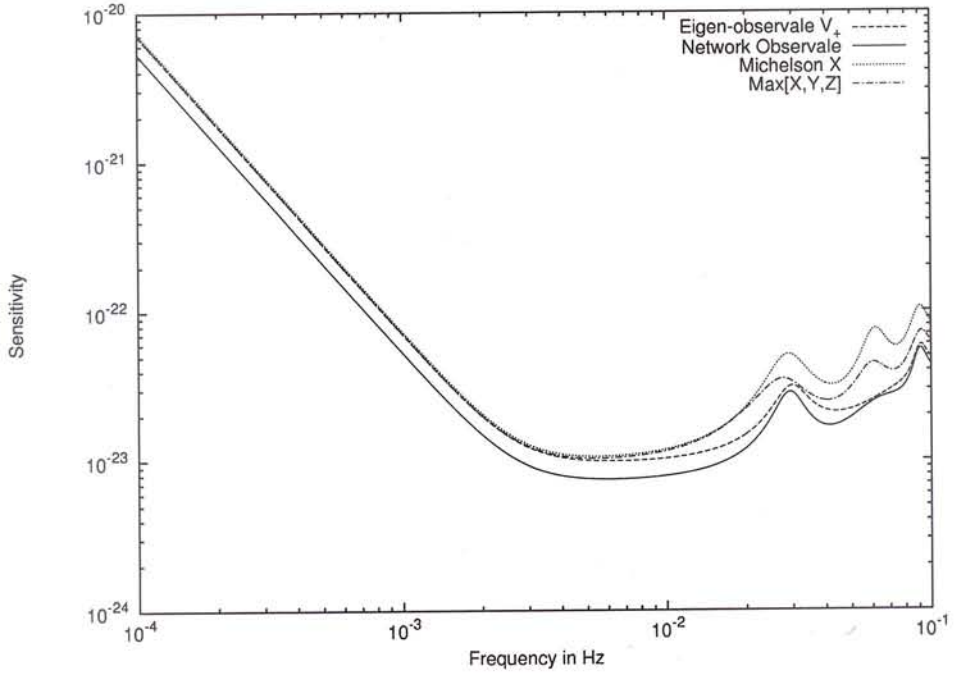

Figure 5.28: Ratios of the sensitivities of the observables network, $\vec{v}_{+,\times}$ with X_{switch} for the source direction $\theta_B = 90°, \phi_B = 0°$.

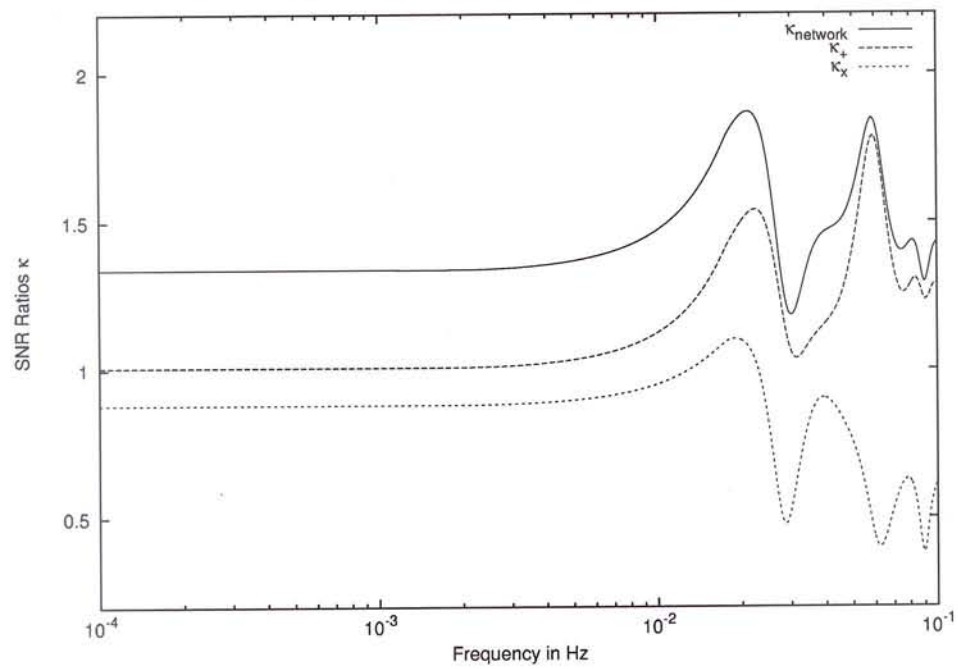

Figure 5.29: The sensitivity curves for the network observable for $\theta_B = 0°, 30°, 60°, 90°$

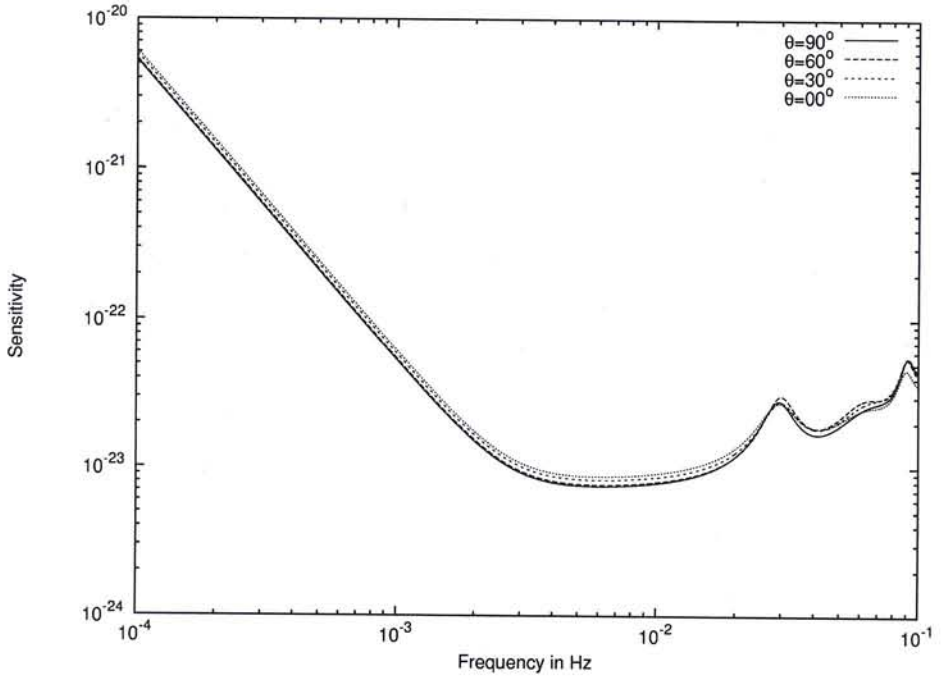

34% at low frequencies and rises to nearly 90 % at about 20 mHz, while at the same time the $\vec{v}_+$ combination shows improvement of 12 % at low frequencies rising to over 50 % at 20 mHz. Finally, Fig.5.29 exhibits the sensitivities of the network observable over various source directions. Since the sensitivity of this observable is independent of ϕ_B, we plot the curves for several values of $\theta_B = 0, 30, 60, 90$ degrees. Also since the network observable possesses reflection symmetry about the ecliptic plane $\theta_B = 90°$, we do not need to plot the curves θ_B between 90° and 180°. The important observation from this figure is that not much variation in sensitivity is seen as all source directions are scanned. Thus the network observable integrated over the year has essentially uniform sensitivity to all source directions over the frequency range $10^{-4} - 10^{-1}$ Hz.

5.7 Conclusion

We have shown how the SNR can be optimised for a GW source with known direction but with unknown polarisation. While obtaining the SNR the signal is averaged over the polarisations and then optimised. Because of this procedure we lose out to some extent on the SNR but on the otherhand it leads to robust results. The optimisation methods are algebraic in that one must solve an eigenvalue equation to determine the optimum SNRs. We have separately dealt with the low frequency case as it is of considerable astrophysical importance - a large fraction of GW sources are expected to belong to this

category. Secondly, it lends itself to simple analytical approximations which throw light on the results obtained. Lastly, we have dealt with the general case covering the full band-width of LISA. We have compared the sensitivities obtained with our strategy to those obtained in the standard way. We have found that the improvement in sensitivity of the network observable over X or $X_{\rm switch}$ ranges from about 34% to nearly 90% over the bandwidth of LISA for a source lying the ecliptic plane. Finally we have presented a list of few binaries in our galaxy for which the optimal SNRs and the network SNRs have been computed. We have also described a method of extracting information about the inclination angle of the orbit of the binary if $SNR_{+,\times}$ can be measured.

Conclusion of the Work

In this work, we have presented a rigorous and systematic procedure for obtaining data combinations which cancel the laser frequency noise, which is based on algebraic geometrical techniques and commutative algebra. The data combinations cancelling the laser noise have the structure of a module called the module of syzygies. The module is over a ring of polynomials in three variables, corresponding to the three time delays along the three arms of the interferometer. Our formalism can be extended in a straightforward way to include (cancel) the Doppler shifts due to the motion of the optical benches and the USO noise. This module provides us with a choice of data combinations which are in turn linear combinations of the generators of the module. This module has four generators which can reproduce all the data combinations cancelling laser phase noise. Telemetering just the four generators to Earth is sufficient for obtaining all the information about the GW signal. Moreover, the telemetering can be done at a reduced band-width saving on the total cost. This approach is general in that it can be extended to space-missions with more than three spacecraft with alternative geometric configurations.

The underlying mathematical structures for any time-delay data analysis should consist of rings and modules. Our work on LISA data analysis essentially establishes this link.

One of the important applications of this formalism is the extremisation of SNR. We use this formalism to maximise the SNR over frequency for one class of GW sources, namely, those that are monochromatic. We have considered binaries as GW sources whose frequencies change at most adiabatically (monochromatic sources are included), that is, even if the frequency changes during the observation time, the change in SNRs under consideration is insignificant. We observe that in the plot of sensitivity verses direction angles for the generators $X^{(A)}$, namely figures 3.10 (a)-(d), the sensitivity has several peaks. It may be possible to employ this property to optimally resolve binaries in the confusion noise regime by considering suitable data combinations which would be sensitive to specific directions in the sky.

We have investigated the following applications of the above formalism:

(i) We have shown that the optimisation of SNR/sensitivity can be carried out efficiently by algebraic techniques because of the special nature of the signal and noise ma-

trices. The signal matrix has been computed for which the signal is averaged over polarisations and directions. We have then computed the noise covariance matrix for LISA and obtained its eigenvectors and eigenvalues. This matrix has the same eigenvectors, resulting in calculational simplification. We have shown that the SNR for any data combination in the module, lies between the upper and lower bounds which are determined by the eigenvectors of both matrices. We have further shown that the bounding SNR curves of the eigenvectors have multiple intersections within the band-width of LISA - 10^{-4} - 1 Hz. We have obtained the following results for the improvement in SNR: The improvement of SNR of the upper-bound over the Michelson combination goes upto 70% , at high frequencies $\gtrsim$ 5 mHz, however, at low frequencies $\lesssim$ 5 mHz, both have the same sensitivity. Since the eigenvectors are independent random variables, a 'network' SNR of independent detectors [24] has been constructed from likelihood considerations which gives an improvement between $\sqrt{2}$ and $\sqrt{3}$ over the maximum of SNRs of the eigenvectors. The improvement of the network SNR over the Michelson combination is about 40% at low frequencies $\lesssim$ 3 mHz and rises above 100% at high frequencies.

(ii) The second application is a simple toy model of LISA rotating in its own plane. For this model we estimated the improvement of SNR by optimally switching from one data combination to another. We have shown that, if this strategy is used, it is possible to improve the SNR by about 55% on an average over the band-width of LISA. We also show that if we instead maximise over the module, the SNR improves by about 60% on an average over the LISA band-width. These improvements are obtained using just one data combination, namely, the eigenvector $Y^{(1)}$. The SNR improvement in both cases is larger at higher frequencies $\gtrsim$ 10 mHz than at low frequencies.

(iii) We have also shown that the SNR can be optimised for a GW source with known direction but with unknown polarisation. While obtaining the SNR the signal is averaged over the polarisations and then optimised. This is different from (i) where the averaging was also done over directions. Because of this procedure we lose out to some extent on the SNR but on the otherhand it leads to robust results. The optimisation methods are algebraic in that one must solve an eigenvalue equation to determine the optimum SNRs. We separately deal with the low frequency case as it is of considerable astrophysical importance - a large fraction of GW sources are expected to be of this category. Secondly, it lends itself to simple analytical approximations which throw light on the results obtained. Lastly, we deal with the general case covering the full band-width of LISA. We have compared the sensitivities obtained with our strategy to those obtained in the standard way. We have found

that the improvement in sensitivity of the network observable over the X or $X_{\rm switch}$ ranges from about 34% to nearly 90% over the bandwidth of LISA for a source lying the ecliptic plane. Finally we have presented a list of few binaries in our galaxy for which the optimal SNRs and the network SNRs have been computed. We have also described a method of extracting information about the inclination angle of the orbit of the binary if $SNR_{+,\times}$ can be measured. Although here we have investigated monochromatic GW sources, we believe that this formalism may also be applied successfully to other type of GW sources *eg.* stochastic GW background.

The following are the salient achievements of our work:

1. **We have given a general method based on commutative algebra for generating data combinations for cancelling laser phase noise in LISA:**

   (i) **The method can be applied to more general configurations, *eg.* LISA follow-on missions with more than three spacecraft. In fact the plan is to have four spacecraft in case of one of them fails.**

   (ii) **The mathematical theorems guarantee that *ALL* such data combinations are generated from a set of (four) generators.**

2. **Only four data streams (four generators) need to be telemetered to the earth instead of the six data streams.**

3. **The data needs to be sampled at lower rate; laser noise of higher frequency (~ 30 Hz/$\sqrt{\rm Hz}$) is eliminated, and the sampling rate is governed by the highest detectable GW frequency 1 Hz. This and the previous point implies *saving in the band-width* while telemetering the data to earth.**

4. **This formulation allows simple expressions/notations which is important for numerical coding.**

5. **The method can be extended in a straight forward way for bench motion noise, Ultra Stable Oscillator (USO) noise. The cancellation of USO noise is easily apparent from our formalism.**

6. **The SNR can be maximised for monochromatic sources by diagonalising the noise covariance matrix.**

7. **LISA can be viewed as a network of independent detectors. One can square and add the outputs to yield higher SNR - factor of $\sqrt{2}$ or $\sqrt{3}$ depending on the mode of operation.**

8. **The combinations can be switched optimally when tracking a source. We find that the SNR can be improved upto 60% because of the optimal tracking.**

6.1 List of Publications

1. S. V. Dhurandhar, K. Rajesh Nayak and J-Y. Vinet, "Algebraic approach to time-delay data analysis for LISA", *Phs Rev.* **D65**, 102002(2002).

2. K. Rajesh Nayak, A. Pai, S. V. Dhurandhar and J-Y. Vinet, "Improving the Sensitivity of LISA", *Class. Quantum. Grav.*, **20,** 1217(2003).

3. K. Rajesh Nayak, S. V. Dhurandhar, A. Pai and J-Y. Vinet, "Optimising the directional sensitivity of LISA", *Submitted to Phs Rev.* **D**, http://arxiv.org/gr-qc/0306057.

4. A. Pai, K. Rajesh Nayak, S. V. Dhurandhar and J-Y. Vinet, "Time Delay Interferometry and LISA Optimal Sensitivity", To appear in Proceedings of *XXXVIIIth Recontres de Moriond: Gravitational Waves and Experimental Gravity*, 2003.

6.2 Assessment of the Project

This project was initially conceived and proposed in the view of developing efficient data analysis tools for space based GW detector LISA. A major source of noise is the laser phase noise. The earlier method for cancellation of this noise was purely on the basis of trial and error. In the present work a rigorous and systematic formalism based on algebraic geometrical methods involving computational commutative algebra, which can generate *all* the data combinations cancelling the laser frequency noise was developed. The generality of this approach allows us to extend this method in a straight forward way for cancellation of bench motion noise and USO noise. Furthermore, this method can be applied to more general configurations – LISA follow-on missions.

An important application of this formalism is the maximisation of SNR, which is essential for the detection and parameter estimation of a GW source. The SNR maximised for monochromatic sources using algebraic techniques. The eigenvalue problem for the signal and noise matrices yields the optimal SNR. The algebraic method works because of the special nature of the matrices. The improvement in SNR can go over 100 % at

some frequencies over the Michelson combination. LISA can also be operated in a network mode where each of the eigenvectors behave as independent detectors. Thus the sum of the squares of the eigenvectors produces a 'network' statistic whose SNR is improved by a factor between $\sqrt{2}$ and $\sqrt{3}$ over the maximum of SNRs of the individual eigenvectors. We also show that a GW source with known direction can be *optimally* tracked by switching the data combinations so that the SNR at each moment remains maximum.

The above results will have a direct impact on future LISA data analysis strategies.

It is remarkable that the a field in pure mathematics, that of commutative algebra, has been successfully applied to obtain physically important results for LISA data analysis and in general in gravitational wave data analysis. The major contribution is that the link between the fields of commutative algebra and gravitational wave data analysis has been established. Rings and modules are the mathematical structures which underlie any time-delay data analysis. The time-delay data analysis need not be just restricted to gravitational waves. We emphasise that we have not only found interesting results, but also presented a general method which allows the systematic treatment for all potential problems involving the suppression of noise in LISA, and moreover in general, open a new way of considering digital data processing.

On the academic side, Dr. Rajesh Nayak from IUCAA and Dr. A. Pai from Observatoire de la Côte d'Azur, have strongly contributed to this project. The gravitational wave group at IUCAA and the Prof. Vinet's group have formed a close knit scientific group. This has led to the exchange of ideas, knowledge and skills which has resulted in innovative and original research and finally a successful completion of the project. The Indians found the French attitude welcoming, forthcoming and warm. The Virgo project contingencies did not allow the French side to visit Pune although they were keen on visiting, but the number of Indian visits to France allowed close contact, and each of these visits proved extremely fruitful.

We would like to thank Dr.(Ms) Himani Arjunwadkar for her invaluable help with commutative algebra and Groebner basis methods.

Both the French and the Indians found IFCPAR absolutely perfect in its dealings. There was no bureaucracy of any kind which hampered the functioning. Dr. P. G. S. Mony, the director, IFCPAR, deserves a special mention since he went out of his way several times to help us and thus ensured smooth functioning of the project.

Appendix A

Rings and Modules

Definition: A nonempty set R is said to be an *associative ring* if in R there are defined two binary operations, denoted by $+$ and $\cdot$ respectively, such that for all a, b, c in R:

1. $a + b$ is in R.
2. $a + b = b + a$.
3. $(a + b) + c = a + (b + c)$.
4. There is an element 0 in R such that $a + 0 = a$ (for every a in R).
5. There exists an element $-a$ in R such that $a + (-a) = 0$.
6. $a \cdot b$ is in R.
7. $a \cdot (b \cdot c) = (a \cdot b) \cdot c$.
8. $a \cdot (b + c) = a \cdot b + a \cdot c$ and $(b + c) \cdot a = b \cdot a + c \cdot a$ (the two distributive laws).

In addition if $a \cdot b = b \cdot a$ for every elemet a, b in R, then R is called a *commutative ring.*

Examples: The basic commutative rings in mathematics are the integers $\mathbb{Z}$, the rational numbers $\mathbb{Q}$, the real numbers $\mathbb{R}$, and the complex numbers $\mathbb{C}$.

Definition: If R is a commutative ring, then $a \neq 0 \in R$ is said to be a *zero-divisor* if there exisits a $b \in R$, $b \neq 0$, such that $a \cdot b = 0$.

Definition: A commutative ring is an *intergal domain* if it has no zero divisors. A commutative ring is a *filed* if its nonzero elements form a group under multiplication.

Definition: A subset I of a ring R is a *Ideal* provided it is a subgroup of the additive group R and if $a \in R$ and $b \in I$, then $a \cdot b$ and $b \cdot a \in I$.

Definition: Suppose R is a commutative ring and x is a "variable" or "symbol". The polynomial ring $R[x]$ is the collection of all polynomials $f = \sum_{i=0}^{n} a_i x^i$ where $a_i \in R$. Under the obvious addition and multiplication, $R[x]$ is a *commutative ring.* The degree of a non-zero polynomial f is the largest integer n such that an $a_n \neq 0$, and is denoted by $n = deg(f)$.

Definition: An integral domain R is said to be a *Euclidean Domain* if for every $a \neq 0$ in R there is defined a nonnegative integer $d(a)$ such that

1. For all $a,\ b\ \in R$, both nonzero, $d(a) \leq d(a \cdot b)$.
2. For all $a,\ b\ \in R$, both nonzero, there exist $t,\ r\ \in R$ such that $a = t \cdot b + r$ were either $r = 0$ or $d(r) < d(b)$.

Definition: Suppose x and y are "variables". If $a \in R$ and $n, m \geq 0$, then $ax^n y^m = ay^m x^n$ is called a *monomial.*

Definition: A domain T is a *principal ideal domain* (**PID**) if, given any ideal I, there exists a $t \in T$ such that $I = tT$. Note that $\mathbb{Z}$ PID and any field is PID.

Definition: Let R be any ring; a nonempty set M is said to be an *R-module* (or a module over R) if M is an abelian group under an operation $+$ such that for every $r \in R$ and $m \in M$ there exists an element rm im M subjected to

1. $r(a + b) = ra + rb$;
2. $r(sa) = (rs)a$;
3. $(r + s)a = ra + sa$ for all $a,\ b \in M$ and $r,\ s \in R$.

Definition: An module $M$is said to be finitely generated if there exist elements $a_1, \ldots, a_n \in M$ such that every m in M is of the form $m = r_1 a_1 + r_2 a_2 + \cdots + r_n a_n$.

Appendix B

Generators of the Module of Syzygies

We require the 4-tuple solutions (p_3, q_1, q_2, q_3) to the equation:

$$(xyz-1)p_3 + (xz-y)q_1 + x(1-z^2)q_2 + (1-x^2)q_3 = 0\,, \tag{B.1}$$

where for convenience we have substituted $x = E_1, y = E_2, z = E_3$. p_3, q_1, q_2, q_3 are polynomials in x, y, z with integral coefficients i.e. in Z[x,y,z].

We now follow the procedure in book by Becker et al. [18].

Consider the ideal in $Z[x, y, z]$ (or $Q[x, y, z]$ where Q denotes the field of rational numbers), formed by taking linear combinations of the coefficients in Eq.(B.1) $f_1 = xyz - 1, f_2 = xz - y, f_3 = x(1-z^2), f_4 = 1 - x^2$. A Groebner basis for this ideal is:

$$\mathcal{G} = \{g_1 = z^2 - 1, g_2 = y^2 - 1, g_3 = x - yz\}\,. \tag{B.2}$$

The above Groebner basis is obtained using the function GroebnerBasis in Mathematica. One can check that both the $f_i, i = 1, 2, 3, 4$ and $g_j, j = 1, 2, 3$ generate the same ideal because we can express one generating set in terms of the other and vice-versa:

$$f_i = d_{ij} g_j, \qquad g_j = c_{ji} f_i\,, \tag{B.3}$$

where d and c are 4×3 and 3×4 polynomial matrices respectively, and are given by,

$$d = \begin{pmatrix} 1 & z^2 & yz \\ y & 0 & z \\ -x & 0 & 0 \\ -1 & -z^2 & -(x+yz) \end{pmatrix}, \qquad c = \begin{pmatrix} 0 & 0 & -x & z^2-1 \\ 1 & -y & 0 & 0 \\ 0 & z & 1 & 0 \end{pmatrix}. \tag{B.4}$$

The generators of the 4-tuple module are given by the set $A \bigcup B^*$ where A and B^* are the sets described below:

A is the set of row vectors of the matrix $I - d.c$ where the dot denotes the matrix product and I is the identity matrix, 4×4 in our case. Thus,

$$\begin{aligned} a_1 &= (1-z^2, 0, x-yz, 1-z^2)\,, \\ a_2 &= (0, z(1-z^2), xy-z, y(1-z^2))\,, \\ a_3 &= (0, 0, 1-x^2, x(z^2-1))\,, \\ a_4 &= (z^2, xz, yz, z^2)\,. \end{aligned} \tag{B.5}$$

We thus first get 4 generators. The additional generators are obtained by computing the S-polynomials of the Groebner basis $\mathcal{G}$. The S-polynomial of two polynomials g_1, g_2 is obtained by multiplying g_1 and g_2 by suitable terms and then adding, so that the highest terms cancel. For example in our case $g_1 = z^2 - 1$ and $g_2 = y^2 - 1$ and the highest terms are z^2 for g_1 and y^2 for g_2 . Multiply g_1 by y^2 and g_2 by z^2 and subtract. Thus, the S-polynomial p_{12} of g_1 and g_2 is:

$$p_{12} = y^2 g_1 - z^2 g_2 = z^2 - y^2\,. \tag{B.6}$$

Note that order is defined ($x >> y >> z$) and the $y^2 z^2$ term cancels. For the Groebner basis of 3 elements we get 3 S-polynomials p_{12}, p_{13}, p_{23}. The p_{ij} must now be rexpressed in terms of the Groebner basis $\mathcal{G}$. This gives a 3×3 matrix b. The final step is to transform to 4-tuples by multiplying b by the matrix c to obtain $b^* = b.c$. The row vectors $b_i^*, i = 1, 2, 3$ of b^* form the set B^*:

$$\begin{aligned} b_1^* &= (1-z^2, y(z^2-1), x(1-y^2), (y^2-1)(z^2-1))\,, \\ b_2^* &= (0, z(1-z^2), 1-z^2-x(x-yz), (x-yz)(z^2-1))\,, \\ b_3^* &= (x-yz, z-xy, 1-y^2, 0). \end{aligned} \tag{B.7}$$

Thus we obtain 3 more generators which gives us a total of 7 generators of the required module of syzygies.

Appendix C

Matrices of Conversion between Generating Sets

In this appendix we list the three sets of generators and relations among them. We first list below $\alpha, \beta, \gamma, \zeta$:

$$\begin{aligned} \alpha &= (1, z, xz, 1, xy, y)\,, \\ \beta &= (xy, 1, x, z, 1, yz)\,, \\ \gamma &= (y, yz, 1, xz, x, 1)\,, \\ \zeta &= (x, y, z, x, y, z)\,. \end{aligned} \tag{C.1}$$

We now express the a_i and b_j^* in terms of $\alpha, \beta, \gamma, \zeta$:

$$\begin{aligned} a_1 &= \gamma - z\zeta\,, \\ a_2 &= \alpha - z\beta\,, \\ a_3 &= -z\alpha + \beta - x\gamma + xz\zeta\,, \\ a_4 &= z\zeta \\ b_1^* &= -y\alpha + yz\beta + \gamma - z\zeta\,, \\ b_2^* &= (1 - z^2)\beta - x\gamma + xz\zeta\,, \\ b_3^* &= \beta - y\zeta\,. \end{aligned} \tag{C.2}$$

Further we also list below $\alpha, \beta, \gamma, \zeta$ in terms of $X^{(A)}$:

$$\begin{aligned} \alpha &= X^{(3)}\,, \\ \beta &= X^{(4)}\,, \\ \gamma &= -X^{(1)} + zX^{(2)}\,, \\ \zeta &= X^{(2)}\,. \end{aligned} \tag{C.3}$$

This proves that since the a_i, b_j^* generate the required module, the $\alpha, \beta, \gamma, \zeta$ and $X^{(A)}, A = 1, 2, 3, 4$ also generate the same module.

The Groebner basis is given in terms of the above generators as follows: $G^{(1)} = \zeta, G^{(2)} = X^{(1)}, G^{(3)} = \beta, G^{(4)} = \alpha$ and $G^{(5)} = a_3$.

Bibliography

[1] P.L. Bender and D. Hils, *CQG*, **14**, 1439(1997).

[2] G. Nelemans, L.R. Yungelson and S.F. Portegies Zwart, *A & A*, **375**, 890(2001).

[3] W.A Hiscock, *Ap. J.*, **509**, L101(1998).

[4] K.A. Postnov and M.E. Prokhorov, *Ap.J*, **494**, 674(1998).

[5] D.I. Kosenko and K.A. Postnov, *A & A*, **336**, 786(1998).

[6] D. Hils and P.L. Bender, *Ap.J*, **537**, 334(2000).

[7] V.B. Ignatiev, A.G Kuranov, K.A Postnov and M.EÂ· Prokhorov, *MNRAS*, **327**, 531(2001).

[8] F. Verbunt and G. Nelemans, *CQG*, **18**, 4005(2001).

[9] RÂ· Schneider, *et. al* , *MNRAS*, **324**, 797(2001).

[10] K. Ioka, T. Tanaka, T. Nakamura, *Phys. Rev.* **D 60**, 083512(1999).

[11] W.A. Hiscock, *et. al*, *Ap. J*, **540**, L5(2000).

[12] M. Tinto, J.W. Armstrong and F.B. Estabrook, *Phys. Rev.* **D 63**, 021101(2000).

[13] C. Cutler, *Phys. Rev*, **D 57**, 7089(1998).

[14] R. Schilling, *CQG*, **14**, 1513(1997).

[15] M. Tinto, F.B. Estabrook, and J.W. Armstrong, *Phys. Rev.* **D 65**, 082003 (2002).

[16] J.W. Armstrong, F. B. Eastabrook and M. Tinto, *Ap. J.*, **527**, 814 (1999).

[17] F.B. Estabrook, M. Tinto and J.W. Armstrong, *Phys. Rev*, **D 62**, 042002(2000).

[18] T. Becker, *"Groebner Bases: A computational approach to commutative algebra"*, Volker Weispfenning in cooperation with Heinz Kredel, Graduate texts in Mathematics 141, Springer Verlag (1993).

[19] M. Kreuzer and L. Robbiano, *"Computational commutative algebra 1"*, Springer Verlag(2000).

[20] Macaulay2 software by D.R. Grayson and M.E. Stillman, http://www.math.uiuc.edu/Macaulay2/.

[21] M. Tinto and J.W. Armstrong, *Phys. Rev*, **D 59**, 102003(1999).

[22] M. Tinto, F. B. Estabrook, and J. W. Armstrong, *P*hys. Rev., **D 65**, 082003(2002).

[23] P. Bender *et al.* "LISA: A Cornerstone Mission f or the Observation of Gravitational Waves", System and Technology Study Report ESA-SCI(2000) 11, (2000).

[24] S. Bose, S. V. Dhurandhar and A. Pai, *Pramana*, **53**, 1125-1136 (1999).

[25] S. V. Dhurandhar, K. Rajesh Nayak, J-Y. Vinet, *Phys. Rev*, **D 65** , 102002(2002).

[26] W.H. Press, S.A. Teukolsky, W.T. Vetterling and B.P. Flannery, *" numerical recipes in C, The art of scientific computing*, Sec. ed., Cambridge University press(1999).

[27] T. Prince, M. Tinto, S. Larson and J. W. Armstrong Phys. Rev. **D 66**, 122002 (2002).

[28] K. Rajesh Nayak, A. Pai, S. V. Dhurandhar and J-Y. Vinet, *Class. Quantum Grav*, **20,** 1217(2003).

[29] The Michelson combination was first described in Schilling, *Class. Quantum Grav*, **14**, 1513 (1997).

[30] P. R. Brady, T. Creighton, C. Cutler and B. F. Schutz, *Phys.Rev*, **D57**, 2101(1998).

[31] B. F. Schutz, "Data Processing Analysis and Storage for Interferometric Antennas", in D. G. Blair, ed., *The Detection of Gravitational Waves*, Cambridge University Press, Cambridge England, 406(1991).

[32] M.T. Meliani, J.C.N. De Araujo and O.D Aguiar, Astron. Astrophys., 358, 417(2000); H. Ritter and U. Kolb, Astron. Astrophys, 129, 83(1998).